Reviews of Geophysics

REVIEW ARTICLE
10.1029/2019RG000665

Understanding Hail in the Earth System

John T. Allen[1], Ian M. Giammanco[2], Matthew R. Kumjian[3], Heinz Jurgen Punge[4], Qinghong Zhang[5], Pieter Groenemeijer[6], Michael Kunz[4], and Kiel Ortega[7]

[1]Department of Earth and Atmospheric Sciences, Central Michigan University, Mount Pleasant, MI, USA, [2]Insurance Institute for Business and Home Safety, Richburg, SC, USA, [3]Department of Meteorology and Atmospheric Science, The Pennsylvania State University, University Park, PA, USA, [4]Institute of Meteorology and Climate Research, Karlsruhe Institute of Technology, Karlsruhe, Germany, [5]Department of Atmospheric and Oceanic Sciences, Peking University, Beijing, China, [6]European Severe Storms Laboratory, Wessling, Germany, [7]Cooperative Institute for Mesoscale Meteorological Studies, University of Oklahoma and NOAA/OAR/National Severe Storms Laboratory, Norman, OK, USA

Key Points:
- Global hail research is reviewed, encompassing formation, occurrence, and impacts
- Much remains unknown about the growth processes and environmental controls
- Improved understanding of hail occurrence is needed to better anticipate the hazard

Correspondence to:
J. Allen,
JohnTerrAllen@gmail.com

Citation:
Allen, J. T., Giammanco, I. M., Kumjian, M. R., Punge, H. J., Zhang, Q., Groenemeijer, P., et al. (2020). Understanding hail in the Earth system. *Reviews of Geophysics*, *58*, e2019RG000665. https://doi.org/10.1029/2019RG000665

Received 12 JUL 2019
Accepted 18 NOV 2019
Accepted article online 22 NOV 2019

Abstract The processes leading to the development of hail and the distribution of these events worldwide are reviewed. Microphysical and physical characteristics of hail development are described to provide context of the notable gaps in our understanding of what drives hail to grow large, or what determines how it falls to the ground. Distributional characteristics of hail are explored, utilizing both surface observations of hailstones and remotely sensed observational data sets to identify opportunities and needs for new observations. These observational deficiencies contribute to our limited capacity to both forecast hail or its expected size and reduce the effectiveness of using favorable conditions for hail development as a proxy to frequency where observations are unavailable. Given the substantive influences of both climate variability and the changing Earth system on hail, the latest understanding of their contributions to risk are addressed. Applying this understanding of the distribution and physical characteristics of hail, the damage by hail to agriculture and insured property is assessed. Much remains unknown about the processes leading to hail growth and environmental controls on hail occurrence, size, and magnitude, particularly outside of the United States and Europe. A better understanding of the global occurrence of hail is also needed to better anticipate the hazard and associated impacts.

Plain Language Summary The processes leading to the development of hail and the resulting distribution of these events worldwide are reviewed. Hail forms from small frozen embryos that are lofted into the updraft of a thunderstorm, subsequently encountering a region of supercooled water, and growing by either riming or accumulation. Contrary to popular belief, the suggestion that hailstones that take multiple up-and-down excursions through an updraft are not observed. Hail can grow to large sizes on any continent, and stones as large as 200 mm have been recorded. Damages associated with hail reach more than 10 billion U.S. dollars a year in North America alone. In this review a range of topics are covered, including characteristics of hail growth and development, surface observations of hail, remotely sensed observations, the approaches to forecasting hail and estimating its frequency where observations are unavailable, the influences of climate variability and a warming earth system and the impacts on insured property. Much remains unknown about the processes leading to hail growth and environmental controls on hail occurrence, size, and magnitude, particularly outside of the United States and Europe. A better understanding of the global occurrence of hail is also needed to better anticipate the hazard and associated impacts.

1. Introduction

Hailstones associated with thunderstorms are a damaging phenomenon found in many areas of the world. They are much more frequent than tornadoes: In many locations hail occurs at a rate of more than one event per year. In this article, we define hail as any regular or irregular piece of ice falling from a thunderstorm exceeding a maximum diameter on any axis of 5 mm (American Meteorological Society, 2017). Storms producing large volumes of hail or hail of large axial diameters can result in significant damage to agriculture and property. These losses can range from the complete destruction to crops, to damage to vehicle paneling and windows, and in extreme cases, damage to roofing, windows, and side paneling of houses (Brown et al., 2015; Changnon, 1977; Yeo et al., 1999). Losses due to severe convective storms have consistently exceeded

©2019. American Geophysical Union. All Rights Reserved.

more than $10 billion USD per annum for the United States alone, and while records are incomplete, likely produce similar losses globally each year, with the vast majority due to the impacts of hail (Gunturi & Tippett, 2017; Munich, 2017).

To provide a context for this review, our understanding of hail has regularly been assessed (Foote & Knight, 1977; Knight & Knight, 2001; Souter & Emerson, 1952), though few of these evaluations have considered research contributions outside of North America (Punge & Kunz, 2016). The impacts of these events have led to numerous studies on each of the continents and, given this disparate body of research, have led to a limited picture of what is known about hail. This article approaches the topic of hail in the Earth system by providing a set of perspectives of the areas of research that have been used to inform our understanding. Motivation for this review is driven by recent workshops that have brought together the community in both Europe and North America, which have raised many of the limitations and advances in hail science (e.g Martius et al., 2018; Romppainen-Martius et al., 2015).

Hereafter, the paper is structured as follows: In section 2, the formative mechanisms for hailstone development and the associated understanding of microphysics are assessed. Readers who are already familiar with the basic formative mechanisms of hailstones may wish to skip to section 2.1.3. Next, the various observational sources to understand hail climatology and its characteristics are considered (section 3) from in situ surface measurements, while in section 4, remotely sensed approaches to detect hail using radar and satellites are examined. This context is then used in section 5 to discuss the current limitations of capacity to forecast hail, or proxy its historical frequency using the environments favorable to hail development. In section 6, the connection to the broader climate scale is considered, both in terms of the highs and lows of variability, and the projected impacts of a changing Earth system on these events. Finally in section 7, the implications of these events in terms of physical an economic impacts to the built environment will be discussed.

2. Hailstone Ingredients, Microphysics, Physical Characteristics, and Formation in Convective Storms

2.1. Microphysics

2.1.1. Ingredients

There are a number of ingredients needed for a storm to create hailstones. First, a small (<1 cm) particle is needed to serve as the nucleus for further growth. Any particle consisting of heavily rimed snow particles of diameters less than 5 mm is defined as graupel (American Meteorological Society, 2017). These particles are collectively known as "embryos" and typically take the form of graupel or frozen drops (e.g., Carte & Kidder, 1966; Federer et al., 1982; Heymsfield, 1982; Knight, 1981; Knight & Knight, 1970a, 1979; List & de Quervain, 1953, among others). More exotic embryos have been documented on occasion (e.g., Samenow, 2015), including fauna and flora of terrestrial origin. Storms can produce hailstones from either type of embryo; however, a climatology by Knight (1981) revealed that storms with warmer cloud bases tended to have higher fractions of frozen-drop embryos. These drops can be generated by coalescence as rain droplets at lower altitudes that are then lofted into the updraft. Alternatively, they can arise from melting of graupel, frozen drops, aggregates, or other ice particles that descend beneath the 0 °C level that are subsequently swept back into the updraft.

Once an embryo is formed, the second ingredient needed to create hailstones is an abundance of supercooled liquid water. Growth occurs when supercooled liquid water is collected by the embryo and freezes either immediately or at some later time (discussed further in section 2.1.2). The collection of supercooled liquid water is known as "riming" when it freezes immediately or "accretion" if it remains as a liquid. Supercooled liquid water is supplied by the convective storm's updraft through activation of cloud condensation nuclei (CCN), subsequent condensation, and coalescence growth of droplets, and through recirculation of melting/melted ice particles. Most studies have suggested that the majority of hail growth occurs at temperatures between about −10 and −25 °C (e.g., Knight et al., 1975; Nelson, 1983; Ziegler et al., 1983), although supercooled liquid water may exist until the temperature of homogeneous freezing (~ −38 °C).

Finally, the third ingredient for creating large hailstones is time. Appreciable growth is only attainable if particles remain in an environment conducive to growth for an extended period of time. Some studies suggest that large hailstones spend as much as 10–15 min or more in growth regions of storms (e.g., Nelson, 1983). The path or trajectory a hailstone takes through a storm's updraft dictates the time available for it to

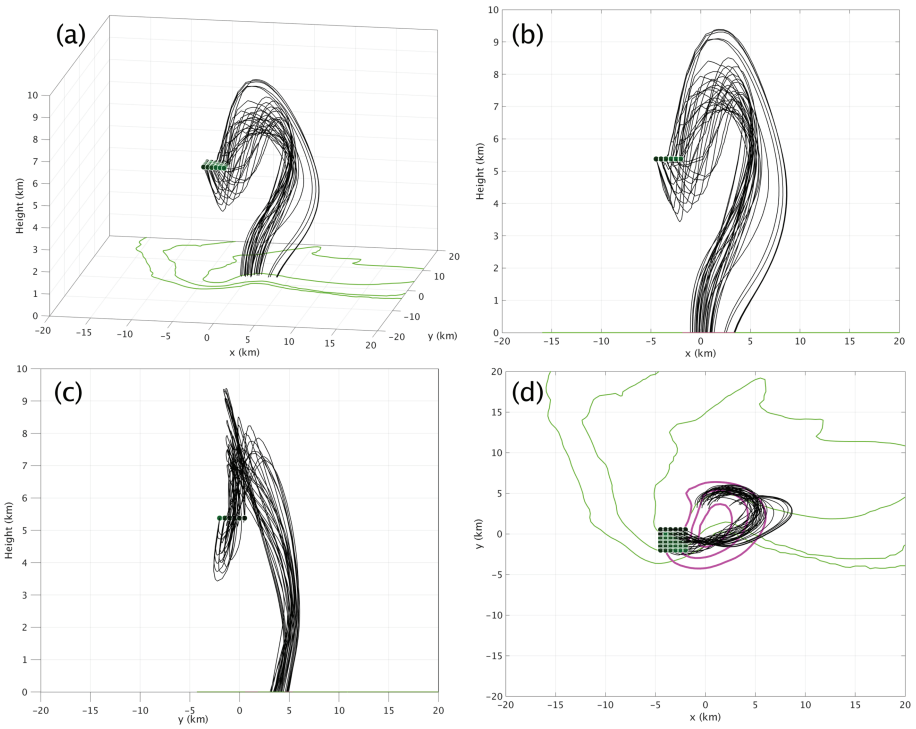

Figure 1. Example hail trajectories in a simulated supercell, based on Dennis and Kumjian (2017). Trajectories are shown by black lines and are initialized by a block of embryos aloft (circle markers). (a) Three-dimensional perspective view of the trajectories, with the simulated radar reflectivity factor at the lowest model level in green (10-, 30-, and 50-dBZ contours are shown). (b) Trajectories in the *x*-*z* plane. (c) Trajectories in the *y*-*z* plane. (d) Trajectories in the *x*-*y* plane. The magenta contours show the location of the midlevel updraft (5-, 10-, and 15-m/s contours shown).

grow. These trajectories are a complicated function of the hailstone's fall speed (which changes as it acquires mass), the local updraft speed, and the horizontal airflow patterns within the storm that advect particles through the updraft. Furthermore, updraft breadth (or width) has been implicated in being conducive to greater hail growth potential by providing both a larger embryo injection region(Nelson, 1983) and a larger volume through which trajectories may pass (Dennis & Kumjian, 2017). These trajectories, when projected onto a horizontal plane (e.g., see Figure 1) tend to trace out a cyclonic path through the updraft, with one main ascending and descending branch. More complicated paths, such as helical trajectories or multiple large vertical excursions (e.g. Browning, 1963; Morgan, 1972), are thought not to occur (discussed further in Section 2.4; Knight et al., 1975; Nelson, 1983; Ziegler et al., 1983; Heymsfield, 1983; Foote, 1984; Conway & Zrnić, 1993; Dennis & Kumjian, 2017).

2.1.2. Growth Processes

When these ingredients come together in severe convective storms, large hailstones may be formed. Hailstones grow mainly by collecting supercooled liquid cloud droplets and raindrops within the updrafts of convective storms (Pruppacher & Klett, 1997). In some cases, hailstones also grow via vapor deposition (Nelson, 1983; Rasmussen & Heymsfield, 1987a). Note that hailstone "aggregation" or coagulation of hailstones is not expected to occur in storms, nor is it typically observed or treated in numerical models of hailstone growth processes.

Traditionally, microphysicists have delineated different growth regimes to characterize the growth mechanisms and physical properties of the resulting hailstones. These different growth regimes are defined by the liquid water content available for growth, the ambient temperature, the hailstone's surface temperature, and the size of the hailstone. The two main regimes are called "dry growth" and "wet growth" (Ludlam, 1958; Lamb & Verlinde, 2011), which describe whether the hailstone surface during growth is ice or liquid, respectively. Note that other intermediate regimes have been identified (e.g., spongy growth, when the growing hailstone contains liquid trapped within ice structures; List, 1959; Knight, 1968; Lesins & List, 1986) but are omitted here for brevity.

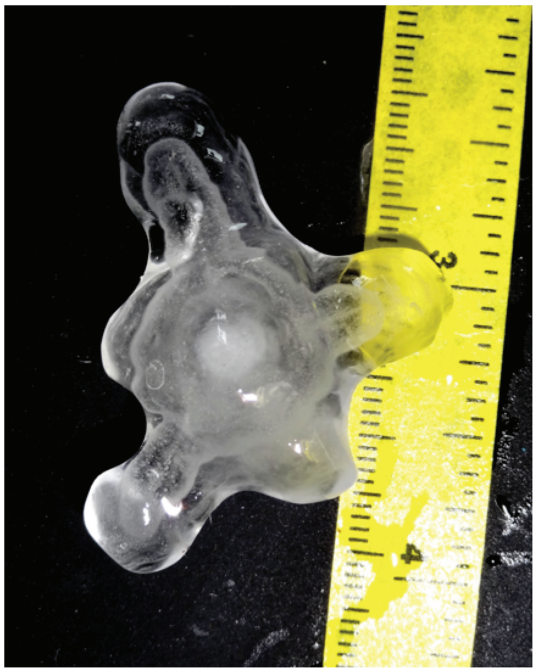

Figure 2. Photograph of a hailstone collected during the 2016 IBHS Hail Field Project showing prominent icicle lobes. Photograph by H. Pogorzelski.

Theoretical treatments of hailstone growth use an energy balance equation (e.g., Lamb & Verlinde, 2011; Pruppacher & Klett, 1997). The collected supercooled liquid water freezes, which heats the surface of the hailstone via the release of the enthalpy of fusion. In dry growth; this heating is balanced by three effects: (i) heating rate owing to vapor deposition, (ii) heating of the accreted cloud water to the surface temperature of the hailstone, and (iii) conduction of excess thermal energy to the air (Pruppacher & Klett, 1997). This raises the hailstone surface temperature above that of the ambient environment, which drives conduction of the excess thermal energy away from the stone (Rasmussen & Heymsfield, 1987a; Rasmussen & Heymsfield, 1987b). Depending on the temperature and water vapor concentration near the hailstone surface and in the ambient environment, sublimation or vapor deposition may occur, leading to cooling or heating of the hailstone surface, respectively.

In rapid growth conditions, the hailstone surface temperature may substantially exceed the ambient environmental temperature (Heymsfield, 1982, 1983). In such cases, sublimation may occur simultaneously with collection of supercooled liquid water, despite the environment being saturated with respect to liquid (e.g., Cober & List, 1993). During rapid growth, it is possible that the hailstone surface temperature warms to 0 °C, even if the ambient environmental temperature is much lower. If this occurs, the accreted liquid may remain on the stone's surface, and the stone is said to be undergoing wet growth. The thermal energy balance equation may be solved for the supercooled liquid water content threshold needed to attain wet growth (e.g., Lamb & Verlinde, 2011); this threshold is known as the Schumann-Ludlam limit (Ludlam, 1958; Schumann, 1938).

The presence of unfrozen liquid on the surface of the hailstone is important for a number of reasons. First, it changes the thermal energy balance equation: Now, energy must be transferred through liquid, changing the thermal conductivity. Additionally, liquid may evaporate from the hailstone surface, and accreted supercooled liquid drops must be warmed to 0 °C. Second, liquid on the hailstone surface possibly increases the hailstone's collection efficiency for small ice crystals, providing an additional pathway through which the hailstone may gain mass. Third, liquid may alter the hailstone's drag characteristics, affecting its fall behavior and speed. Finally, the presence of liquid on or within an ice particle significantly affects its electromagnetic scattering properties and thus its backscattering cross section, with implications for radar detection and sizing of hail (see section 4).

Most theoretical and numerical model treatments for hailstone formation, growth, and melting processes assume that hailstones are spherical or spheroidal. However, natural hailstones exhibit a plethora of irregular shapes and protuberances called “lobes.” Such irregularities can alter growth rates and the thermal energy balance, complicating the treatment of microphysical processes. Lobes observed in real hailstones are classified into two categories: cusp lobes and icicle lobes (Knight & Knight, 1970b). Small features such as cusp lobes are thought to form in dry growth conditions, and affect the collection efficiency of the hailstone. As hailstones tumble, any bump on the surface will preferentially collect supercooled liquid droplets from a wider range of impact angles, enhancing its growth. Concurrently, this bump will shield nearby regions, starving them of supercooled liquid drops and thus inhibiting growth. This nonlinear effect preferentially grows the cusp-like or scalloped lobes at the expense of adjacent regions (Browning, 1966; Knight & Knight, 1970b). Icicle lobes are always observed in clear ice, implying they form in wet growth conditions. Very thin growth layers observed in icicle lobes imply thin layers of liquid that freeze, similar to how icicles form (Knight & Knight, 1970b). Icicle lobes are thought to arise from liquid streaming across the hailstone surface to the tips of the protuberances under the influence of hydrodynamic effects imparted by the air stream as the hailstone falls. In extreme cases, icicle lobes can become quite prominent and extend surprising distances from the main hailstone body leading to highly axial stones (Figure 2), further than cusp lobes can extend (Knight & Knight, 1970b).

2.1.3. The Influence of Aerosols and Cloud Seeding

Another area of scientific interest in hail formation and growth involves the impacts of environmental aerosols on the resulting hail distribution. Conceptually, aerosols may be ingested into convective cloud updrafts, where they may serve as CCN, ice nuclei (IN), or remain interstitially and not participate further in microphysics (Lamb & Verlinde, 2011). Such particles are necessary to form hydrometeors like cloud droplets and ice particles critical for hail production. A recent laboratory study (Li et al., 2018) investigated 10 ions (Na^+, K^+, Mg^{2+}, Ca^{2+}, Cl^-, NO_3^-, SO_4^{2-}, NO^{2-}, $HCOO^-$, and CH_3COO^-) in 15 different hailstone samples collected from hailstorms in China and showed that ions in the ice likely originated from particulate matter ≤10 μm in diameter.

Ice may form at temperatures below −38 °C by homogeneous freezing of liquid drops. More commonly in the atmosphere, IN including mineral dusts, biological species (e.g., pollen, bacteria, fugal spores, and plankton), and volcanic ash trigger ice formation at much higher temperatures (e.g. Vali et al., 2015). For example, laboratory studies find mineral dust and volcanic ash are active IN below −10 °C, whereas biological species can be active above −10 °C, possibly even above −5 °C (Lamb & Verlinde, 2011). However, laboratory and in situ measurements of IN are difficult, and it is impossible to monitor IN concentrations or compositions in practice. Further, the natural variability of IN in the atmosphere is highly uncertain (Flossmann et al., 2018). Regardless of the source or type of IN, however, the ubiquitous presence of ice in deep convective storms demonstrates a sufficient amount of IN is available.

Because of the critical role of CCN and IN in hail production, many of the early hail research efforts and field campaigns were primarily motivated by the desire for hail suppression (C. Knight, personal communication, August 16, 2018, including those described by Barge & Isaac, 1973; Thams, 1966; Schmid et al., 1967; Knight, 1982; Knight & Squires, 1982; Squires & Knight, 1982; Federer et al., 1986). The concept behind this approach was to artificially introduce IN ("seeding" the clouds) to cause premature glaciation and shut down the collection of supercooled liquid water that is the main driver of hail growth. After no conclusive evidence for hail suppression was found, partly related to the limited understanding of the formative processes (e.g. Federer et al., 1986; Knight et al., 1979), these hopes faded, though research toward the goal of hail suppression has persisted both regionally and in many parts of the globe (e.g. Cazac et al., 2017; Dessens et al., 2016; Farley et al., 2004; Gavrilov et al., 2013; Makitov et al., 2017; Wieringa & Holleman, 2006). Further details on these efforts can be found in Wieringa and Holleman (2006) and Dessens et al. (2016). For prolific hail-producing storms such as supercells, simple physical and practical arguments suggest seeding would likely have a negligible impact on hail production.

The influence of CCN loading on hail production has drawn increased attention recently, given that CCN can have a substantial influence on the microphysical properties of water and ice clouds, which in turn may affect the processes that lead to the formation of hail (Andreae & Rosenfeld, 2008; Fan et al., 2013; Lebo & Morrison, 2014; Liu & Niu, 2010; Rosenfeld et al., 2008). A variety of numerical simulations have suggested potentially monotonically increasing effects of CCN on hail development. In these simulations a greater number of supercooled droplets are available for deposition and riming, leading to increased hail growth as CCN availability increases, in contrast to the more commonly accepted role of liquid water content (Khain et al., 2011; Noppel et al., 2010; Yang et al., 2011). However, other independent studies found a nonmonotonic response of hail to CCN (Carrió et al., 2014; Li et al., 2017; Loftus & Cotton, 2014). Lebo (2014) also found that low-level aerosol perturbations have little to no effect on midlevel microphysics in simulated storms, whereas entrained midlevel aerosol particles may play a more substantial role. As an added complication, simulations have shown that the relationships between CCN and hail production are dependent on model grid spacing, choice of microphysics scheme and scheme complexity, environmental conditions, and even the triggering mechanism for convection (see Fan et al., 2016, and references therein).

Many of the studies mentioned above are case study simulations; it is likely that the effect of CCN loading on hail varies with different input soundings under different environments. For example, Fan et al. (2009) and Lebo and Morrison (2014) found that CCN effects on simulated deep convective clouds change sign with increasing vertical wind shear. Further, Lebo (2018) demonstrated that the proposed aerosol-invigoration effect from increased latent heating for the larger number of droplets proposed by Rosenfeld et al. (2008) is small and likely unmeasurable. This is especially the case when compared to changes in updraft width and slope that may arise from small changes to the environmental wind shear (e.g., Dennis & Kumjian, 2017) across a variety of input thermodynamic profiles. However, an ongoing theme is that simulation results

Figure 3. Photographs of hailstones collected during the 2016–2017 IBHS Hail Field Project showing alternating layers of clear and cloudy ice. Photographs by M. Kumjian.

for these problems strongly depend on the model setup, the range of changes of the input parameters, and microphysics scheme choice, raising additional questions as to how this relationship manifests.

Thus, the detailed conducive or suppressive effects of CCN on hail and hailstorms remain largely inconclusive from the perspective of microphysics, as they are intimately linked with storm dynamics. The discrepancies between many of the studies mentioned above arise from the complexity of deep convective storm microphysics, the lack of sufficient observations of these characteristics, and the inability of the simplified parameterizations and models to adequately treat these processes. For example, important hail processes like melting, sedimentation, density of rimed material, and surface temperature are not well handled by two-moment bulk microphysics schemes that are commonly used in convective resolving models (e.g., Dennis & Kumjian, 2017; Loftus & Cotton, 2014; Ryzhkov et al., 2013). Lebo et al. (2012) showed that the saturation adjustment parameterization (all excess supersaturation with respect to water is converted to liquid water McDonald (1963)) in bulk schemes overestimates the extra heating derived from increased CCN. Even in studies with bin microphysics, use of a simplified two-dimensional framework does not accurately capture updraft dynamics (Morrison, 2016a; Morrison, 2016b) or hail growth trajectories (Nelson, 1983, among many others; Foote, 1984) that are inherently three-dimensional.

2.2. Hailstone Characteristics

The shapes, sizes, mass, and internal structure of hailstones are interconnected through the microphysical growth processes. In dry growth, in which supercooled liquid water is frozen immediately onto the surface of the stone, air bubbles may be trapped. Additionally, the rapid freezing may lead to cracks or fractures in the ice. These bubbles and irregularities in the ice structure scatter visible light in all directions, leading to a white or milky appearance to the ice. Because of these bubbles, nooks, and crannies, the ice incorporated during dry growth has a bulk density lower than that of pure ice. In contrast, during wet growth, liquid remains on the surface of the stone and can soak into any gaps in the ice structure. Soaking and subsequent freezing leads to an increased density of the ice (e.g., Rasmussen & Heymsfield, 1987a). Further, the slow freezing of liquid on the surface allows air bubbles to escape and for the liquid to spread more evenly across the surface of the stone, leading to a clearer ice with higher bulk density. Hailstones may alternate between these growth regimes, leading to rings of cloudy and clear ice (Figure 3). However, these alternating layers do not necessarily indicate multiple up-and-down excursions through the storm as popularly thought.

It is well understood that hailstones can exhibit a variety of shapes with large protuberances at times. Hailstone shape information is also applied toward understanding the aerodynamic properties of falling hail, particularly drag coefficients, tumbling characteristics, terminal velocities, and kinetic energies. Radar hail detection and numerical weather prediction parameterization schemes also have dependencies to these quantities and the underlying hailstone shapes that drive them. The physical measurements of hailstones after impacting the ground such as maximum diameter, mass, density, and basic shapes (e.g., axis ratios) have been well documented in the historical literature; however, the material properties of hailstones such as hardness or strength have been more difficult to quantify (Blair & Leighton, 2012; Browning, 1963; Browning, 1977; Browning & Foote, 1976; Foote & Knight, 1979; Giammanco et al., 2015; Heymsfield et al., 2014; Heymsfield et al., 2018; Knight et al., 2008; Knight & Knight, 2001; Macklin, 1977; Ziegler et al., 1983).

Hailstones are generally oblate spheroids with mean axis ratios (i.e., ratio of minimum and maximum diameters) near 0.8 (Barge & Isaac, 1973; Browning & Beimers, 1967; Knight, 1986; Matson & Huggins, 1980). The relationship between mass and maximum diameter follows a power law curve departing from that expected for pure ice spheres of the same diameter (Figure 4). Knight (1986) calculated axis ratios for

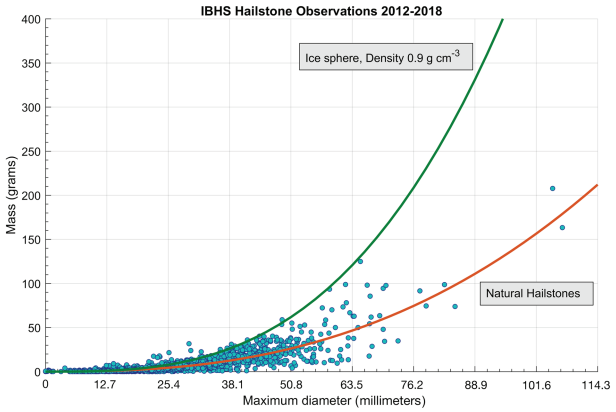

Figure 4. Relationship between hailstone mass and diameter based on samples collect by IBHS field campaigns described by Heymsfield et al. (2014), and during field operations 2015–2018 as compared to the power law relationship used for ice spheres, and a curve fitted for the observed natural hailstones.

6,208 hailstones collected from thunderstorms in Oklahoma, Colorado, and Alberta, Canada. The axis ratios were obtained through thinly sliced cross sections measured in a cold laboratory at the National Center for Atmospheric Research. The results identified the trend of decreasing sphericity with increasing maximum diameter, which was also supported by more recent results of Heymsfield et al. (2014), which used physical measurements of hail made at the ground. Axis ratios decrease from 0.95 for hail sizes near 5 mm to 0.6 for diameters of 50 mm. The trend is important when considering applications, which make assumptions that hailstones are spherical. Figure 5 provides an overview of the available observations of hail axis ratios and their relation to maximum diameters. In the historical literature, hailstone shapes have also been stratified into subjective categories based upon their appearance: conical, spheroidal, and irregular (including all with discernible protuberances) (Browning & Beimers, 1967; Carte & Kidder, 1966; Weickmann, 1953). In an effort to further quantify hailstone shapes Heymsfield et al. (2014) used digital photographs of hailstones to determine the ratio of the hailstone surface area to the area of a circle of the same diameter. The distribution of area ratios from several hundred hailstones was found to have a mean and median of 0.77 and 0.78, respectively, supporting a basic underlying oblate spheroidal shape (Heymsfield et al., 2014). It is noted that many of these studies relied on capturing hailstones at the ground after they have fallen such that melting or impact with the ground may round off protuberances. It is also unclear if differential melting may bias observations of hail at the ground toward a more oblate shape. New technologies have opened the door toward a more detailed examination of hailstone shapes. For example, Giammanco et al. (2017) successfully used a 3-D laser scanning system to produce high-resolution (0.008 cm) digital modeled hailstones of actual hailstones scanned in the field (Figure 6). The models allow for the ratio of the volume of a scanned hailstone to be compared with the volume of a sphere of the same maximum diameter. The pilot results of this approach confirmed as in previous studies that hailstones depart from spherical shapes as they increase in size (Heymsfield et al., 2014; Heymsfield et al., 2018; Knight, 1986).

The material properties of hailstones have received far less attention than the basic dimensional properties. Hail is often referred to as “hard,” “soft,” or “slushy” within the context of historical studies. The hardness or strength of hail is also often described as being explicitly tied to density. These statements were made with little supportive quantitative evidence. The damage that hail produces are likely influenced by the material properties. Knight et al. (2008), for example, documented a hailstorm in Colorado, which produced a large

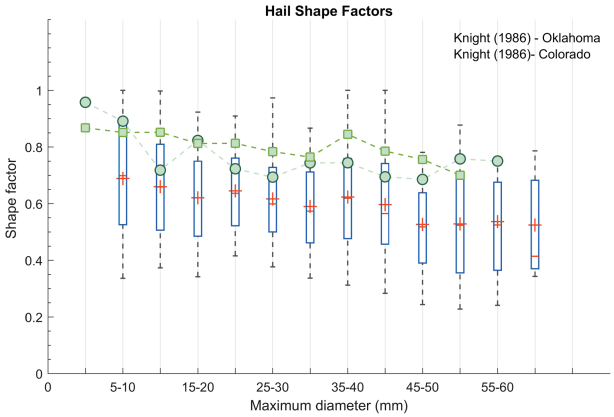

Figure 5. Box and whiskers plot, including the mean (red plus sign) and median (red line), of hail shape factors (axis ratios) for increasing hail size bins, based on data collected by IBHS. The whiskers represent the 95th percentile confidence intervals of the distribution. Also shown are historical hail shape factors from Knight (1986) from Oklahoma (dark green circles), and Colorado (light green squares).

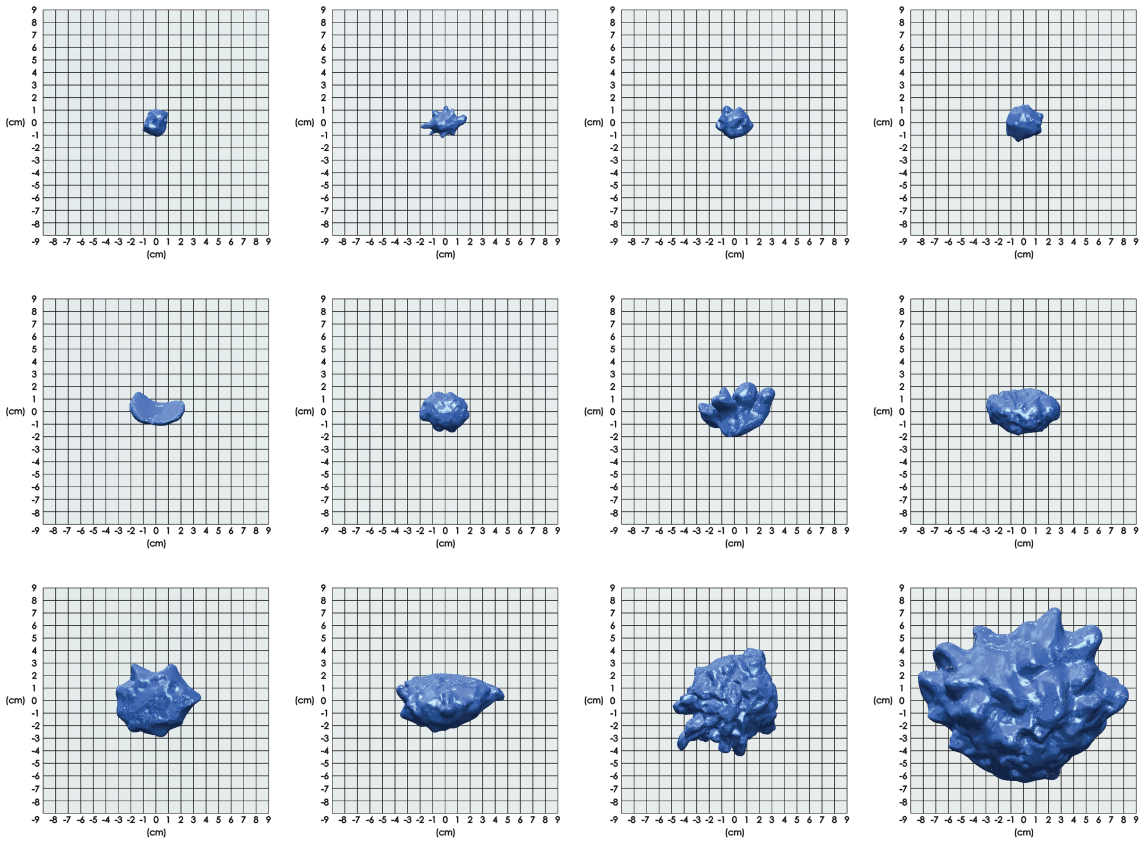

Figure 6. Three-dimensional hail scans from the IBHS field campaigns.

amount of low density, "soft" hail, speculating that little property damage would have occurred from the event.

The hardness property of any material is governed by its strength, both tensile and compressive among other factors (e.g., ductility, elastic stiffness, viscoelasticity etc.). For ice, the material strength is governed by the temperature at which the ice grains developed, their size, and the rate in which strain is applied (Kim & Kedward, 2000; Schulson & Duval, 2009; Silva, 2011; Swift, 2013). The ability to measure these properties of natural hail in the field has proven difficult given the logistical challenges of using standard laboratory test equipment in the field since the 1980s (M. Smith, personal communication, April 6, 2015). Giammanco et al. (2015) was able to develop a suitable field testing device to estimate the compressive stress, which is used as a proxy for the hardness of hailstones. The peak compressive force at the moment of failure was captured and then scaled by the cross-sectional area of the hailstone (an approximation for the plane of fracture). The calculated quantity yielded an estimate of uniaxial compressive strength. Over 900 hailstones were tested and analyzed in the study, with a large spread in compressive strength, ranging from unmeasurable (i.e., extremely soft) to over an order of magnitude stronger in compressive strength than laboratory pure ice spheres (Giammanco et al., 2015). The ability to measure hailstone strengths coupled with the emergence of 3-D laser scanning technology allowed for the exploration of the relationship between bulk density and strength. Throughout historical literature high density and high strength are often used in concert with little quantifiable evidence that a relationship exists. Analysis of 42 hailstones, which were scanned and subjected to a compressive strength test, showed no statistically significant relationship between bulk density and strength. It was speculated that the radial distribution of density, due to alternating growth regimes, may be more related to the compressive strength of hail along with the influence of temperature within the hail growth zone and is influence on ice grain size (Giammanco et al., 2015; Giammanco et al., 2017). Recent advances in this area have the potential to facilitate the development of testing protocols which adequately represent the properties of natural hail. Given the global financial impact of hailstorms each year, improved building product testing and ratings are sorely needed to foster a more resilient built environment.

2.3. Hail Terminal Velocities and Kinetic Energies

The accurate assessment of hailstone terminal velocities (V_t) and kinetic energies (*KE*) is vital to a wide range of meteorological and engineering applications, spanning numerical weather prediction parameterizations to material impact testing (e.g. Punge et al., 2014; Schuster et al., 2006; Waldvogel et al., 1978). These quantities relate to the size of hail, for example, the aerodynamic drag is influenced by hailstone size and shape as well as their orientation when tumbling. These properties bounds the possible velocity these stones can achieve upon reaching the ground. Subsequently, their kinetic energy, which is also a function of the mass of the stone, will increase with the square of the terminal velocity. Historical studies have often applied the aerodynamic properties of smooth and roughened spheres toward natural hailstones (Achenbach, 1972; Achenbach, 1974; Bilhelm & Relf, 1937; List et al., 1973; Millikan & Klein, 1933). This has produced widely used estimates of diameter based hailstone size-kinetic energy relationships that most engineering testing standards are based (Laurie, 1960).

Within existing literature there has been little consensus on the terminal velocities of graupel and hail as a function of their size. Graupel particles often form the growth embryos for hailstones. The methods for producing these results include theoretical calculations, idealized measurements, and flow tank studies. The differences across the historical literature arise from the methodology in assessing the aerodynamic drag coefficient (C_D). Observations have shown that the surface characteristics of hailstones or ice spheres (e.g., spikes, protuberances, and liquid water) have a large influence on C_D and therefore V_t and *KE*. Bilhelm and Relf (1937) developed a C_D to Reynolds Number (*Re*) relationship based on physical measurements from a previous study by (Millikan & Klein, 1933). The initial Millikan and Klein (1933) study was not acknowledged in their article (Heymsfield & Wright, 2014). In this experiment, ice spheres were towed behind an aircraft and direct measurements of C_D were made. The curve presented by Bilhelm and Relf (1937) contained a precipitous decrease in C_D as *Re* increased for more turbulent flow. The relative discontinuity is often referred to as the "supercritical Reynolds number." A relationship between terminal velocity and hail diameter based upon the C_D values was determined, which contained the increase in terminal velocity due to the rapid reduction in drag (Bilhelm & Relf, 1937). The effect on pure ice spheres was confirmed by (Achenbach, 1972); however, when nonsmooth ice was examined by List et al. (1973) and Achenbach (1974), the reduction in C_D was not found. The original results of Bilhelm and Relf (1937) were used by Laurie (1960) to describe the damage potential of hail impacts on buildings and are still contained within impact test standards (FM Approvals, 2005; Underwriters Laboratory, 2012).

Heymsfield and Wright (2014) reexamined the C_D to Reynolds number relationship to determine its applicability to natural hail. This study compiled a volume of graupel and hail observations from existing literature to derive Reynolds numbers and C_D. To investigate terminal velocities, a nondimensional Best Number (i.e., *Davies Number*) approach was used. The advantage to the method is that it can be calculated from quantifiable hailstone properties (e.g., mass and diameter) and environmental conditions (e.g., temperature and pressure). The results showed that natural hailstones likely do not reach a critical Reynolds number regime and the very low C_D values observed for smooth ice spheres are not common. Examining hail below the melting level, little response in C_D was found (Willis et al., 1967). Heymsfield et al. (2014) applied the relationships shown in Heymsfield and Wright (2014) to field observations of natural hailstones collected by the Insurance Institute for Business and Home Safety (IBHS). Simple power law relationships were able to capture the relationship between maximum hail diameters, V_t, and *KE*:

$$V_t = 12.43D^{0.4792} \tag{1}$$

and

$$KE = 0.0271D^{4.31} \tag{2}$$

where *D* is the maximum diameter of the hailstone (note this is not an equivalent diameter). The relationship is valid for hailstones larger than 1 cm at a pressure level of 1,000 hPa based on a sample of over 3,200 hailstones, though only 5.1% were for hailstones above 4 cm and 1.07% for hailstones above 5 cm diameter, and thus, values are extrapolated for the largest hail diameters. The large observational data set also allowed for power law curves for different percentile groups providing an estimate of the range of possible terminal velocities and kinetic energies (Table 1). Heymsfield et al. (2018) built upon this work through the use of a larger catalog of natural hailstones and provided detailed comparisons to historical research on hailstone aerodynamics. In addition, experimental testing was conducted in a vertical wind tunnel using 3-D

Table 1
Hailstone Terminal Velocities and Kinetic Energies According to Heymsfield et al. (2014; Mean, Median, and Distributional Characteristics) and Laurie (1960) for Selected Hailstone Maximum Diameters (KE)

Hail D (cm)	Hail D (in.)	Vt Mean	KE KE	KE Median	KE Mean	KE 10–30th%	KE 30-+50th%	KE 50–70th%	KE 70–90th%
1	0.39	15.69	0.04	0.02	0.02	0.01	0.03	0.03	0.04
1.5	0.59	18.08	0.21	0.12	0.12	0.07	0.12	0.17	0.23
2	0.79	20.00	0.67	0.42	0.43	0.23	0.37	0.55	0.81
2.5	0.98	21.62	1.67	1.16	1.13	0.57	0.86	1.38	2.11
2.54	1.00	21.74	1.78	1.24	1.21	0.61	0.92	1.48	2.26
3	1.18	23.05	3.52	2.62	2.47	1.20	1.73	2.92	4.62
3.18	1.25	23.52	4.47	3.41	3.18	1.52	2.16	3.72	5.93
3.81	1.50	25.06	9.38	7.67	6.92	3.15	4.31	7.81	12.91
4	1.57	25.49	11.45	9.54	8.54	3.84	5.19	9.54	15.91
4.45	1.75	26.46	17.71	15.40	13.52	5.92	7.79	14.79	25.16
4.5	1.77	26.56	18.54	16.20	14.18	6.19	8.13	15.48	26.40
5	1.97	27.56	28.55	25.99	22.34	9.48	12.16	23.87	41.53
5.08	2.00	27.71	30.47	27.91	23.92	10.11	12.92	25.48	44.46
5.5	2.17	28.49	42.19	39.87	33.68	13.95	17.50	35.32	62.57
6	2.36	29.37	60.26	58.93	49.01	19.84	24.41	50.51	90.96
6.5	2.56	30.21	83.64	84.42	69.20	27.44	33.14	70.18	128.33
7	2.76	31.00	113.32	117.75	95.24	37.05	43.98	95.17	176.48
8	3.15	32.49	195.82	214.45	169.35	63.63	73.24	164.76	313.38
9	3.54	33.85	317.26	363.92	281.35	102.52	114.86	267.35	520.03
10	3.94	35.13	488.51	584.07	443.06	157.08	171.78	412.24	818.06

Note. Kinetic energies by percentile group from Heymsfield et al. (2014) are also provided; however, samples sizes above 5 cm are small.

printed hailstones from digital models of natural hail (digital models of natural hailstones were captured using a laser scanning system). While the sample of hailstone shapes was limited, these results confirmed the assumptions of Heymsfield and Wright (2014) were well founded. These results suggest that the analysis of Bilhelm and Relf (1937) is likely an overestimate of damage potential from natural hail, in non-wind-driven conditions. However, the underlying aerodynamic drag coefficient, which these quantities rely on, remains an approximation based on idealized studies that do not take into account factors such as the tumbling of hailstones. We reiterate here that the influence of complex thunderstorm outflow wind profiles on hail trajectories is not well understood, which adds to this uncertainty. Strong winds within thunderstorm outflows may act to increase the probability of hailstones to exceed the terminal velocities and expected kinetic energies. Direct in situ measurements of hailstone terminal velocities and kinetic energies remain sparse. While photogrammetry-based instrumentation exists, such systems are often not rugged enough to survive repeated exposure to impacts from large hail. New technologies such as 3-D scanning and printing has fostered new experimental research using printed hailstones placed in a vertical wind tunnel to evaluate the aerodynamics and tumbling of hail in such situations (Heymsfield et al., 2018).

2.4. Hail Formation in Convective Storms

The basic mechanisms behind hail formation and growth are reasonably well understood. This is particularly the case in the form of conceptual models of hail formation in rotating supercell storms (Browning & Foote, 1976; Heymsfield & Musil, 1982; Morgan, 1972). The first step is embryo production during ascent in an updraft. These embryos may be formed in flanking line convection or "feeder cells" (e.g., Dennis et al., 1970; Heymsfield & Musil, 1982) or grown entirely within the main updraft. For the latter pathway, this likely occurs in the weaker periphery of the main updraft; particles in the strongest parts of the updraft are lofted too quickly for appreciable growth and ejected into the anvil, barring their participation in subsequent hail growth.

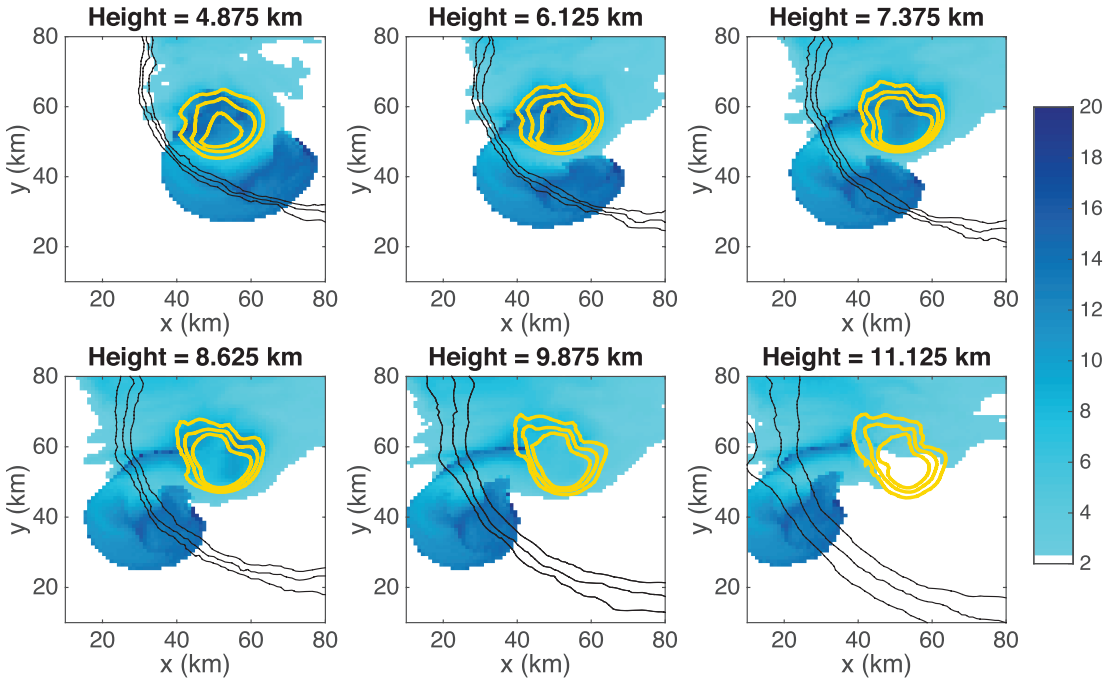

Figure 7. Optimal embryo injection regions for a simulated supercell storm. The blue shading represents the final size of a hailstone (mm) grown by seeding a 2-mm embryo at that location. Black contours are 0-, 10-, and 20-dBz simulated reflectivity factor. Goldenrod shows the 10-, 20-, and 30-m s^{-1} updraft contours. Each panel shows a different altitude. The deep-layer shear vector is approximately west-to-east. Adapted from Dennis and Kumjian (2017). Copyright American Meteorological Society, used with permission of the author.

In the next step, embryos are injected into the updraft via environmental storm-relative flow or the storm's inflow. For archetypical Northern Hemisphere supercells in westerly deep-layer shear, the embryo source region at midlevels is found on the right (southern) flank of the updraft relative to storm motion. Called the "embryo curtain" by Browning and Foote (1976), this optimal embryo injection region wraps around to the rear of the storm with altitude (Dennis & Kumjian, 2017, Fig. [fig:embryocurtain]). Embryos in this curtain fall and get swept into the updraft by southerly winds and/or inflow at lower altitudes (again, in the case of westerly deep-layer shear). Additional embryo sources can be frozen drops within the updraft (Figure 7) or alternatively graupel from nearby feeder cells or cumulus congestus clouds.

In the third stage, embryos swept into the updraft experience rapid growth in the liquid-rich updraft in trajectories that start with an upward section followed by a downward section. The commonly invoked "recycling" of hailstones that take multiple up-and-down excursions is not expected based on airflow patterns in typical hailstorms nor has it been found in hail growth trajectory calculations (e.g., Conway & Zrnić, 1993; Dennis & Kumjian, 2017; Foote, 1984; Heymsfield, 1983; Nelson, 1983; Ziegler et al., 1983). Further, isotope analysis by Knight et al. (1975) suggested "major recirculation at larger-than-embryo size is not a necessary condition for the formation of giant hail," despite the complex ring-like structure often observed in large hailstones.

Rather, key to maximizing residence time in the updraft is a balance between hailstone fall speed and the updraft speed (Browning, 1964, among many others; Morgan, 1972; Heymsfield, 1983; Miller & Fankhauser, 1983; Foote, 1984; Musil et al., 1986). If the updraft speed is greater than the fall speed, then the particle is lofted quickly out of the growth region and further growth ceases. If the particle fall speed is larger than the updraft speed, then the particle may fall out of the growth region. In contrast, when the fall speed and updraft speed are matched, the particle may remain suspended at a roughly constant altitude within the hail growth region, with only lateral movement by the horizontal components of the velocity field within the updraft. Previous studies have suggested large hailstones acquire most of their mass on such trajectories (e.g., Nelson, 1983). Because the hailstone is continuously growing via collection of supercooled liquid, the hailstone must be advected into regions of stronger updraft to maintain this balance. This implies horizontal trajectories passing from the updraft periphery into its core. Frequently, the mesocyclone of supercell storms

serves as a conduit for such a pathway (e.g., Tessendorf et al., 2005). Thus, it is no surprise that supercells are known to be prolific producers of large hail in both the northern and southern hemispheres (Blair et al., 2011; Blair et al., 2017; Dennis & Kumjian, 2017; Thompson et al., 2003; Witt et al., 2018; Yeo et al., 1999).

An example of simulated hailstone trajectories is shown in Figure 1. A 2-mm diameter embryo was placed in the embryo corridor region on the right flank of the supercell. It advects forward as it descends, until it is swept into the updraft by lower-level southerly inflow. The particle initially rises quickly, then approximately levels out as it grows rapidly, until it becomes too heavy and falls out of the updraft. The projection of this trajectory onto the horizontal plane (green line on the lower boundary of the image in Figure 1) shows a cyclonically curved trajectory across the updraft, consistent with previous studies (e.g., Foote, 1984; Nelson, 1983) and demonstrating the role of the mesocyclone in creating optimal hail growth trajectories.

3. Surface Observations of Hail

Having discussed the formative mechanisms of hail, next, the in situ observations that bound much of our understanding of the characteristics and underlying occurrence of hail are explored. These observed quantities vary from country-to-country and between continents, and thus, here we address the major known data sets currently available, predominantly over North America, Europe, Australia, and China. Sporadic climatologies of hail observations have also been conducted for a number of countries, based on either newspaper or media-sourced reports, local hailpad networks or national data sets. Several early studies explored distributions over a number of countries and over the tropics to identify the distribution of hail occurrence (e.g. Admirat et al., 1985;Frisby & Sansom, 1967 ; Gokhale, 1975). These reveal that hail has been reported on every continent other than Antarctica and occurs at most latitudes where convective instability is more readily available (Frisby & Sansom, 1967; Gokhale, 1975). Owing to the nature and volume of these small scale records and the sources describing these historically, here we briefly cover the available data of the most recent representative studies and illustrate the known spatial climatologies.

3.1. North American Surface Observations

The prevalence of hail in the United States has made the observational records of this phenomenon commonplace (Allen & Tippett, 2015; Blair et al., 2017; Blair & Leighton, 2012; Changnon, 1999; Ortega et al., 2009; Schaefer & Edwards, 1999), and yet from a perspective of analysis of the climatology of hail, researchers have predominantly explored the spatial distribution of tornadoes, at least in the past decade. These data range from station data (e.g. Changnon, 1999) to hailpad networks and volunteer spotter derived Storm Data (Schaefer & Edwards, 1999), or can be inferred from loss data (Changnon & Changnon, 1997). For an overview of the legacy station data sets, readers are directed to Changnon (1999), which describes in detail the nondigitized station hail occurrence record (1901–1996), and cooperative station hail size observations (1920–1950) that include observations of hail size, particularly those less than 19 mm (0.75 in.).

The largest single archive is the National Centers for Environmental Information Storm Data, a record of hail observations equal to or greater than 19 mm (0.75 in.) collated from reports by both trained and untrained observers (Schaefer & Edwards, 1999). This record, while voluminous and reflecting a useful source of observed and climatological information between 1955 and the present (Figures 8 and 9), is also a record beset with a number of limitations and challenges. Spatial coverage of observers is nonuniform with greater concentrations proximal to areas of higher population, a factor that is extremely important given that hail must be observed in situ, rather than from a distance (Allen et al., 2015a; Allen & Tippett, 2015; Doswell et al., 2005; Kelly et al., 1985). The measurement of hail size is also fraught with errors and challenges, as the limited spatial coverage of large hail events can mean that the extreme hail sizes are missed (Allen et al., 2017; Allen & Tippett, 2015; Blair & Leighton, 2012; Changnon, 1966; Changnon, 1977; Witt et al., 2018). This is further exacerbated by the single dimension measurement recording system based around the use of reference objects of similar dimension to any hailstone, which can result in variations in dimension of an inch or more compared to reality (Allen et al., 2017; Blair et al., 2017). An example of the distribution of hail size over the United States can be seen in Figure 9. In addition to Storm Data, since 2005 the Community Collaborative Rain, Hail and Snow Network has provided another source of in situ hail observations (Reges et al., 2016). These reports reflect volunteer maintained stations that are spatially confined to a few states but include a growing record of hailpad measurements for size and occurrence over a small predefined area, and can also include subsevere reports. As the Community Collaborative Rain, Hail and Snow

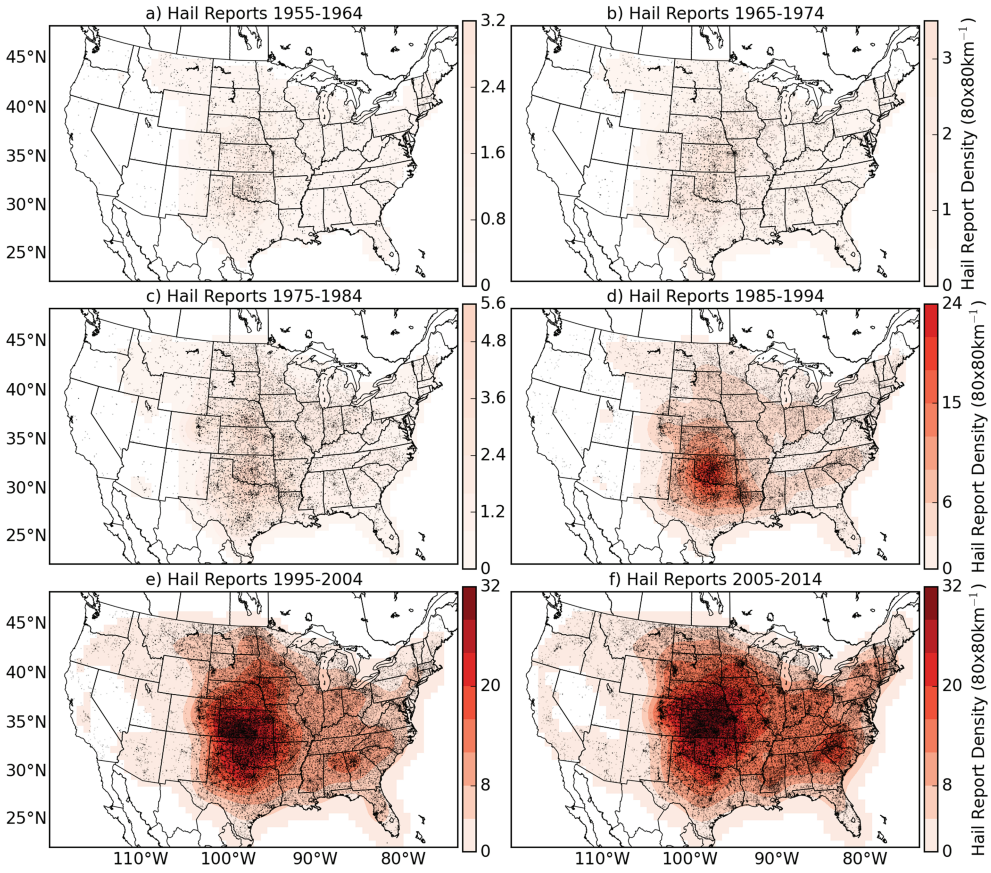

Figure 8. (a–f) Mean annual U.S. Gaussian kernel-smoothed subsevere (≥0.75 in. or 1.9 cm) hail report density for decade intervals for 1955–2014. Overlaid are point reports of hail diameter for the corresponding decades, illustrating the growth in report spatial frequency through time. Density contours are scaled by the peak density of the 2005–2014 period, such that the color scales are equivalent to the 0–32 report density per 80 × 80-km^{-1} range used in panel (f). Adopted from (Allen & Tippett, 2015), their Figure 6), used with the permission of the author.

Network hailpads record diameter, fall density and multiple stone impacts, they provide a more complete viewpoint of hail occurrence than Storm Data reports. However, the short record duration, together with the cost and painstaking nature of maintenance of this type of measurement and sensitivity to the large spatial variations in hail size (Changnon, 1977; Changnon, 1999) mean that potential applications of the record are somewhat limited.

The Canadian hail record extends from 1955 to the present but is beset by inconsistencies associated with the source of reported occurrences and is an order of magnitude smaller in terms of report numbers than the U.S. record (Etkin & Brun, 1999). Between 1977 and 1993, Environment Canada mandated recording of hail at manned weather stations across the country leading to high-quality observed data, which contrasts field campaign-related (e.g., the Alberta Hail Project; Barge and Isaac (1973)) or spotter reports for the remainder of the record, which are mostly concentrated in Ontario, Alberta, Manitoba, and Saskatchewan around centers of population (Figure 10). Mexico is also no stranger to significant hailstorms, particularly over the northern parts of the country, though there are few publications discussing these events (e.g. Creel et al., 2001).

The uncertainties present in Storm Data for both hail size and event location led the National Severe Storms Laboratory to conduct two different verification efforts: the Severe Hazards Analysis and Verification Experiment (SHAVE; Ortega et al., 2009) and the Meteorological Phenomena Identification Near the Ground project (mPING; Elmore et al., 2014). The mPING began as a website interface for crowd-sourced submission of observations of precipitation to validate the National Severe Storms Laboratory's polarimetric research radar, including hail reports. The increase in popularity of "apps" on mobile smartphones led to a transition of the mPING to a smartphone app, where users can report a number of precipitation related phenomena,

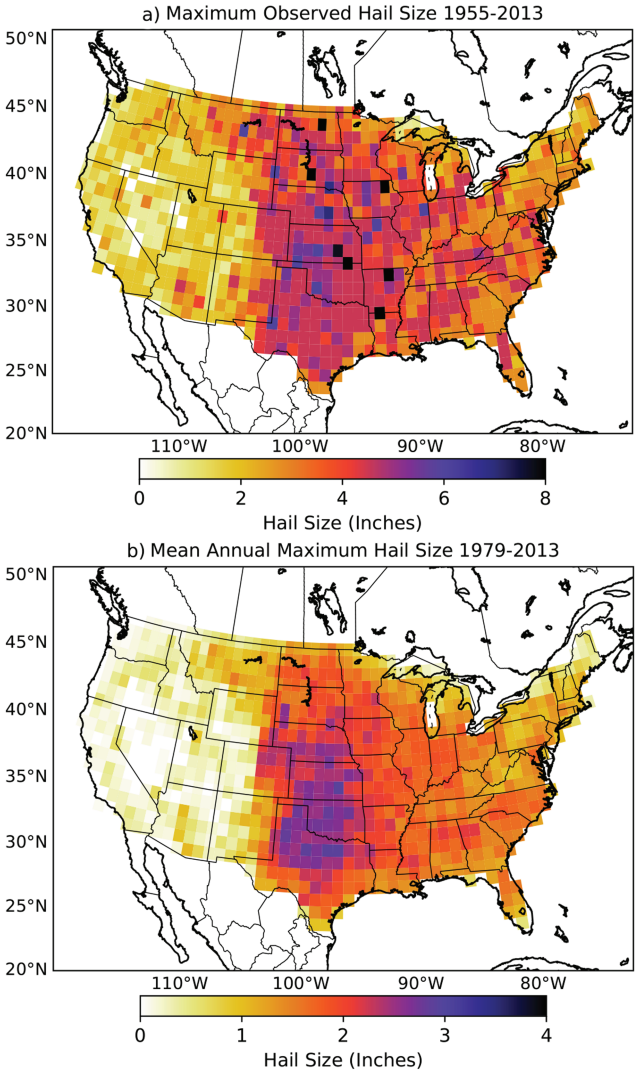

Figure 9. Maximum observed U.S. hail size from the NCEI data set for the period (a) 1955–2013. (b) Mean annual maximum hail size 1979–2013. Adapted from (Allen et al., 2017), their Figure 1). Copyright American Meteorological Society. Used with permission of the author.

including hail. Work has just begun to explore the mPING hail database and shows that a very small percentage of reports associated with thunderstorms are of hail exceeding 25 mm in diameter, contrasting the Storm Data record. Nearly 20% of thunderstorms documented in mPING were also documented as having at least some hail occurrence (Noll et al., 2018).

SHAVE in contrast pursued an active approach to collect hail reports from the general public. The project leveraged phone operators and an internet-based map that combined phone records and proxy radar-derived hail swaths from the multiradar, multisensor (MRMS; Smith et al., 2016) data set. The goal was to collect reports at high spatial density and provide a source of reports of "no hail" and of smaller hail sizes not typically recorded in Storm Data. Records included the most common hail size, hailfall timing, and ground coverage after the hailfall. The project ran from 2006 through 2015, primarily in the summer months, and random calls were placed after thunderstorms in every state in the contiguous United States, collecting 54,299 hail reports of predominantly no hail or less than 25 mm. Applications of SHAVE have shown utility in providing higher-resolution hail swaths for evaluating remotely sense metrics, with significant advantages over Storm Data (Ortega, 2018; Ortega et al., 2016). These include better identification of local variations in maximum diameter compared to Storm Data reports (Ortega, 2018), consistent with prior observations of narrow hail swaths for larger hail diameters (Blair et al., 2017; Blair & Leighton, 2012; Changnon, 1977).

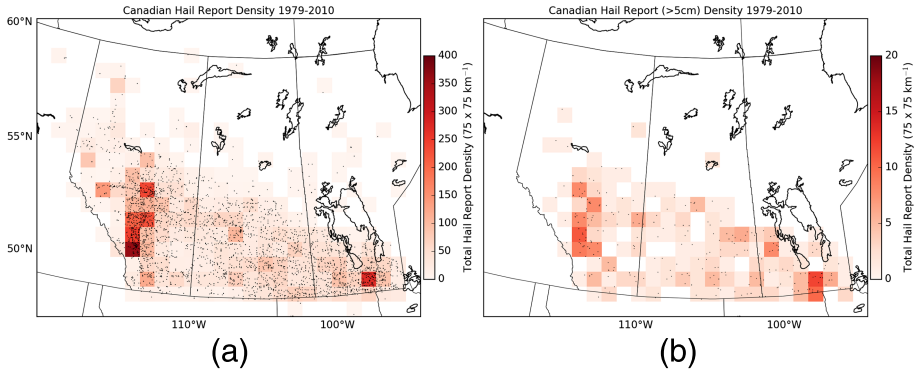

Figure 10. Hail observations over Canada from the Environment Canada plains hail data set 1979–2010 for (a) Total density aggregated on a 75 × 75-km grid and overlaid with point report locations. (b) As for panel (a), except greater than 5-cm hail reports. Data and code to reproduce this figure are available from Allen (2019).

3.1.1. Field Campaigns and Aerial Observations

From the 1950s through the middle 1980s several field research campaigns were conducted with a focus on hail. The Alberta Hail Studies project, which began in Canada in the early 1950s was followed by the better known Alberta Hail Project (1974–1985 Barge & Isaac, 1973; Brimelow et al., 2002), which consisted of both ground-based and aerial observations. The primary goal of the subsequent five large-scale dedicated field campaigns was to determine if cloud seeding could reduce the occurrence of damaging hail within thunderstorms. The National Hail Research Experiment (NHRE) in 1972–1976 remains the last, large-scale, coordinated field effort for both ground and aerial observations explicitly dedicated toward hail and hailstorms (Foote & Knight, 1979;Knight & Squires, 1982 ; Squires & Knight, 1982). NHRE operated in the high plains of Colorado, Kansas, Nebraska, and Wyoming. The program focused on understanding microphysical processes within thunderstorms and its application toward cloud seeding. While the influence of cloud seeding proved difficult to quantify, the program and campaigns like it helped advance the understanding of hail microphysical growth processes, hail size distributions, hailstone characteristics, and radar detection of hail (Knight & Squires, 1982; Squires & Knight, 1982) as summarized by Knight and Knight (2001). Since the conclusion of NHRE, attention in the United Stats has turned away from weather modification toward forecasting, detection, and mitigation through improved building product resiliency. Subsequently, the Cooperative Convective Precipitation Experiment (CCOPE; Knight, 1982) aimed to continue to fill this gap by collecting observations of convective storms through several Doppler radar installations, upper air soundings, and 14 research aircraft in an effort to better quantify precipitation processes including hail. However, research dedicated toward hail over the past three decades has lagged behind other thunderstorm related hazards and has been relatively stagnant.

Observations in field campaigns have also not solely been confined to the ground. The T-28 Trojan Storm Penetrating Aircraft was a 1949 U.S. military propeller-driven, training aircraft equipped with reinforced wing leading edges and a polycarbonate canopy (Sand, 1976). The aircraft was configured to penetrate thunderstorms with hail impact design criteria of a 3-in. hail impact at a speed of 100 $m \quad s^{-1}$. The aircraft was also designed to be able to withstand direct lightning strikes. Its instrumentation was primarily focused on making in situ measurements of particle sizes, electric fields, and wind flow characteristics (Sand, 1976; Johnson & Smith, 1980; Detwiler et al., 2012). The aircraft made its first flights into hail-producing thunderstorms in 1970 during the Joint Hail Research Project (Goyer, 1970). The T-28 subsequently flew during the NHRE making 110 thunderstorm penetrations (Sand, 1976; Sand & Schleusener, 1974). Since its development, the T-28 participated in over 25 different field campaigns, including the original Verification of the Origin of Rotation in Tornadoes Experiment (VORTEX) project and most recently the Thunderstorm Electrification Experiment (TELEX) in 2003, before it was retired in 2005. It completed its career with over 2,000 in-storm hours logged (P. Smith, personal communication, August 14, 2018). Archived data collected by the T-28 can be found online (https://archive.eol.ucar.edu/projects/t28/).

The data sets collected by the T-28, and other aircraft (e.g., Cooperative Convective Precipitation Experiment), have been used extensively and continue to be used to improve our understanding of microphysical processes within thunderstorms, including particle size distributions, thunderstorm electrification, and

wind flow characteristics. The foundational research behind our current state of knowledge regarding hail growth processes, trajectories, and size distributions are rooted in observations that were collected by the T-28. These have included recent use of in cloud observations to establish that hail particle size distributions are exponential, and the distributions can be inferred from hail water content within the cloud with implications for model and radar inferred hail characteristics (Field et al., 2019). The breadth of data sets and research contributions are well summarized by Foote and Knight (1979), Knight and Knight (2001), Detwiler et al. (2012), Brimelow (2018) and Field et al. (2019). With the retirement of the T-28, there remains no operational aircraft that can safely penetrate intense land-based convection to obtain such measurements.

The need for more detailed surface measurements of hailstones has fostered a new interest in field research experiments in the Unites States from nontraditional groups. The hail spatial and temporal observation network effort (HailSTONE) began as a grassroots program to collect high spatial and temporal resolution, in situ observations of maximum hail sizes at the ground (Blair et al., 2017). The program successfully sampled 73 hail-producing thunderstorms from 2011–2015 in an effort to improve operational forecasting for large hail (Blair et al., 2014; Blair et al., 2017). Four to seven vehicles with specialized hail guards intercepted hail-producing thunderstorms, making transects through target storms. High spatial resolution observations of hailstones were collected and measured in situ as part of multiple spatial and temporal samples, focusing on measuring maximum diameters. Over 1,400 severe hailstones in supercell thunderstorms over the Great Plains were measured during the project. Based on these data, Blair et al. (2014) showed that storm data hail reports underestimate the maximum hail size produced by a given thunderstorm by nearly a factor of 2, with differences increasing with storm maximum hail size. In the context of warning decision making, the maximum forecast hail size was often less than that observed, especially for events with very large hail (Blair et al., 2014).

In parallel, in 2012 the IBHS began an annual field research campaign as a part of their multifaceted hail research program. The overarching goal of the broad research agenda focused on mitigating impacts on the built environment (Brown & Giammanco, 2013). The IBHS program assembled photographs and physical measurements (maximum diameter, intermediate dimension, minimum diameter, and mass) of over 3,000 hailstones from 60 different thunderstorms. Similar to HailSTONE, hailstones were collected off the ground after the passage of a thunderstorm using multiple measurement teams working across the swath of hail. Compressive strength tests were performed on a subset of these hailstones (Giammanco et al., 2015). The observations contained in the database are primarily from United States Great Plains supercells. The program also pioneered the use of hand-held laser scanners to collect detailed digital models of hailstones. IBHS has also developed an adaptive network of 18, rapidly deployable hail impact disdrometers based on the design of Lane et al. (2006). Adaptive networks are ideal for studying hailstone size sorting, radar hail detection techniques, and can provide validation for storm-scale modeling efforts. The field campaigns of HailSTONE and IBHS succeeded in collecting a very robust collection of hail observations. When viewed together, the resulting data sets likely surpass hailstone records collected at the ground during NHRE, despite the nontraditional research groups involved (Blair et al., 2014; Brown & Giammanco, 2013).

3.1.2. Commercial Hail Detection Networks

Mesoscale automated observing networks have been in existence for some time (Brock et al., 1995; Mahmood, 2017; Schroeder et al., 2005). However, there has been little advancement regarding in situ automated hail detection. Historically, hailpads have been relied upon to obtain information beyond reports of maximum hail size. Advances in in situ measurements has led to a new commercial urban hail detection network in the Unites Stats. One of example of this type of network was developed by Understory Weather Inc. to detect hail, rain, and wind within urban and suburban environments (Bussmann et al., 2017). The Understory sensors operate using a similar principal to the IBHS disdrometers by applying a momentum to hail size relationship. The instruments are calibrated using laboratory ice impacts to develop an impact signal to momentum or kinetic energy curve. The instrument uses a configuration of multiple load cells within a metallic sphere. The load cells sense impacts anywhere on the surface of the sphere which enable a slightly higher degree of precision than an acoustic-based sensor and the ability to estimate impact angle. Similar to the IBHS instruments, there is some degree of inherent error due to the reliance on momentum/kinetic energy to hail diameter relationships such as those found in Heymsfield et al. (2018) and Heymsfield et al. (2014). Over time, the data collected from these networks may offer a more detailed climatology of the characteristics of hailstorms and provide another data set for comparisons with other hail sensing applications (i.e., radar-based, satellite, etc.); however, these networks are in their infancy.

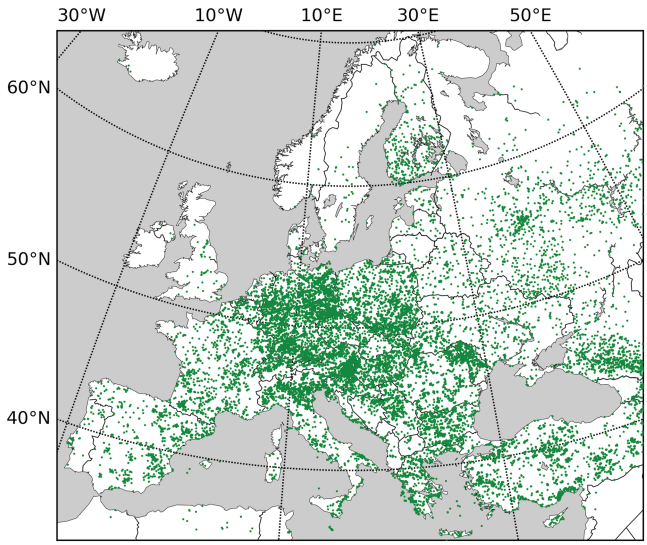

Figure 11. Hail observations over Europe from the ESSL ESWD database for the period 2008–2017.

3.2. European Surface Observations

Hail climatologies for individual countries and regions in Europe have been established using a variety of methods. Some use direct observations of hail by voluntary observers or extract such information from media sources (e.g., Tuovinen et al. (2009) for Finland; Kahraman et al. (2016) for Turkey), while others are exclusively based on synoptic station data (e.g. Abshaev et al., 2009; Suwala & Bednorz, 2013), or data collected using regional hailpad networks (e.g. Berthet et al., 2011; Manzato, 2012; Pocakal, 2011; Vinet, 2001). For further details of these country-based records, readers are directed to the comprehensive review of nationally and regionally collected data sets in Europe performed by Punge and Kunz (2016) and Michaelides et al. (2018).

Systematic observation of hail in weather station networks began in the late nineteenth century (*Karlinski, F.*, 1867; Prohaska, 1902; Hamberg, 1919). Hail frequency estimations from these studies are often biased high due to the lack of distinction from the more frequently encountered graupel. Hailstone size is still not generally recorded at weather stations, with the notable exception of Romania (Burcea et al., 2016). Independent surface hail detection networks with focus on crop protection have been installed in Europe since the 1970s, in particular in hail-prone areas around the Mediterranean (Federer et al., 1986; Michaelides et al., 2018; Morgan, 1973; Sánchez et al., 2009; Simeonov, 1996; Svabik, 1989). Consisting of hailpads distributed over several hundreds to several thousands of square kilometers, they offer the possibility to measure hailstone spectra, hailstreak dimensions, and event frequency (Berthet et al., 2011; Fraile et al., 2003; Michaelides et al., 2018; Sánchez, Gil-Robles, et al., 2009). Network-scale hail frequency estimates have been compared by Giaiotti et al. (2003), but a comparison of local hail frequencies accounting for varying measurement standards remains missing. In some regions, observer networks often consisting of farmers exist (e.g, the Ebro valley, García-Ortega et al., 2014) or have existed in the past (e.g., Poland, Kolkowska & Lorenc, 2012). An automated hail detection network is also currently being installed in Switzerland.

A pan-European collection of severe weather reports, including hail, is coordinated by the European Severe Storms Laboratory (Figure 11). Individuals, and networks of volunteers as well as a number of weather services relay such reports to the European Severe Weather Database (ESWD; Dotzek et al., 2009; Groenemeijer et al., 2017). The annual number of hail reports has strongly risen since ESSL's founding in 2006 as the networks of observers has expanded (Groenemeijer et al., 2017). More recently, the ESWD has also expanded to additional reports from the general public using a mobile app, the European Weather Observer (EWOB; Holzer et al., 2017), which includes the possibility to upload photographs of the hailstones and/or the damage that was caused. It is important to note that ESWD reports in this figure disproportionately favor central Europe, where the most active voluntary observer networks are located and climatological frequency of severe hail is high. However, many impactful hailstorms also occur through the Mediterranean regions and in areas from where reports are not regularly received by the ESWD (Punge & Kunz, 2016). In addition to

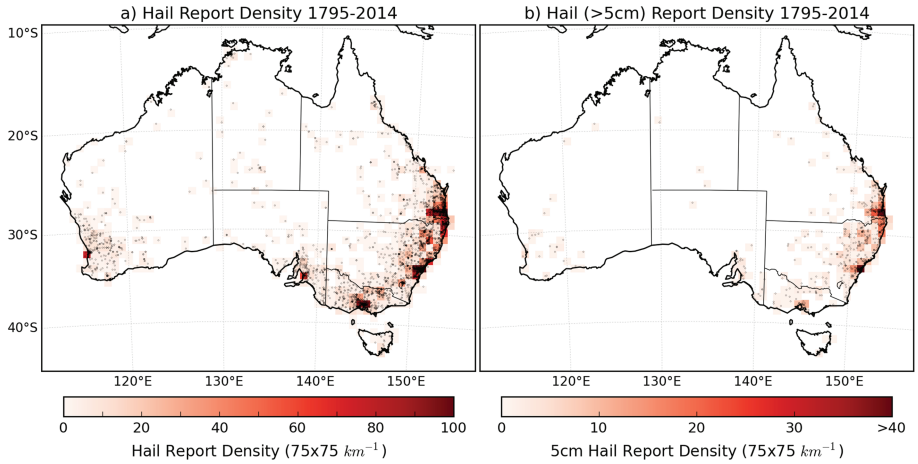

Figure 12. Hail observations over Australia from the Bureau of Meteorology Severe Thunderstorm Archive 1795–2014 for (a) total density aggregated on a 75 by 75-km grid and overlaid with point report locations. (b) As for panel (a), except greater than 5-cm hail reports. Adopted from (Allen & Allen, 2016), their Figure 7). Used with permission of the author and Elsevier.

real-time collection of hail events, historical reports have been added to the ESWD, which were collected from newspaper archives and nationally operated disaster databases. Despite these efforts, the report frequency is affected by motivation and awareness in the population, meaning that further proxy information is needed to derive hail frequency estimates from this data (see sections 4.2 and 5.1).

3.2.1. Field Campaigns

In Europe, coordinated field campaigns on hail observations have taken place in Switzerland. These experiments were primarily designed to evaluate hail suppression methods. Grossversuch III (Schmid et al., 1967; Thams, 1966) took place in the Ticino region of Switzerland between 1957 and 1963. The most recent campaign from 1977 to 1981, and the largest of its kind, was the *Grossversuch IV* (Federer et al., 1986), which included the use of a dense network of 330 hailpads to test the efficacy of hail prevention by using rockets to inject clouds with silver iodide. Grossversuch III showed that hailfall increased after seeding, but at a very low level of significance, whereas Grossversuch IV showed that the difference in hail kinetic energy was not significantly different (at the 5% significance level) on days with seeding versus those without seeding. Nonetheless, efforts to mitigate the impacts of hail continue to motivate a significant portion of hail research in southern and southeastern Europe (e.g. Cazac et al., 2017; Dessens et al., 2016; Gavrilov et al., 2013; Makitov et al., 2017; Wieringa & Holleman, 2006).

3.3. Australian Surface Observations

The Bureau of Meteorology maintains the Severe Thunderstorm Archive (BOM, 2017), a record spanning 1795 to the present that includes hail, though scientific documentation did not really begin until after 1893 (Russell, 1893). This record is limited by observational biases related to primarily the coastal concentration of population, together with the sparse network of trained individuals who make the vast majority of these reports (Figure 12). Until recently there has also been a lack of integration of active methods for identifying hail such as the use of social media or application-based reporting as seen in both Europe and the United States (Allen & Allen, 2016). Despite these limitations, this data set has seen several applications for evaluating environmental forecast parameters or climatological frequency (e.g. Allen et al., 2011; Allen & Allen, 2016; Allen & Karoly, 2014; Griffiths et al., 1993; Mills & Colquhoun, 1998; Niall & Walsh, 2005). The primary factor driving expansion of hail observations has been the impacts of the 1999 Sydney hailstorm, and thus, most analyses are regionally specific (Schuster et al., 2005). This growth in record using archived digital newspapers and crop hail records has focused on New South Wales (McMaster, 2001; Schuster et al., 2005); however, such reports can be limited in quantity or subject to interpretive biases. Nevertheless, there is a need to expand these efforts for the national record, and this process is underway.

3.4. Surface Observations in Asia

Hail observations over Asia are relatively uncommon outside of China, India, and Bangladesh (Frisby & Sansom, 1967). Although hail was recorded as early as in 877 BC in China, systematic observations did not begin until the start of the nineteenth century. From this point onward, hailstorms in China have routinely

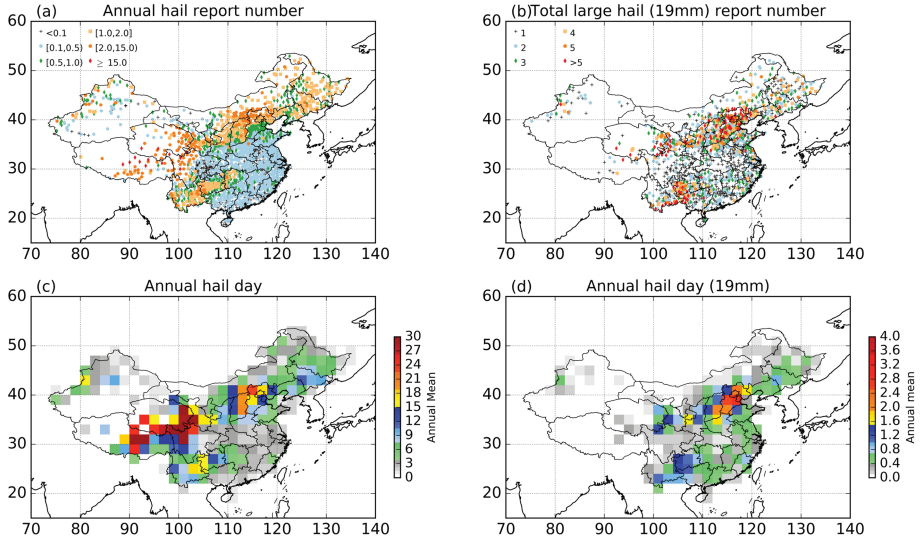

Figure 13. (a) Annual mean hail reports (2 mm) at 2,265 stations in China from 1980 to 2015 adapted from Figure 1 of Ni, Zhang, et al. (2017). (b) Total weather station reports with large size hail (19 mm) at 1,459 stations from 1980 to 2015, adapted from Figure 7 of Li, Zhang, Zou, et al. (2018). (c) Annual hail day counted in 2° by 2° grid box from 1980 to 2015, gridded from data used for Figure 1 of Ni, Zhang, et al. (2017). (d) Annual hail day with large size hail counted in 2° by 2° grid box from 1980 to 2015 gridded from Figure 7 of Li, Zhang, Zou, et al. (2018).

been reported at meteorological stations. Hail occurrence is recorded by trained meteorological observers, who note the start and end time of the hailfall at each station. At some stations, the largest hailstones' diameter and weight were measured occasionally, until 1980 when the maximum hail diameter measurement was included in standard reports (Ni et al., 2017). Climatological studies of observed hail began with Liu and Tang (1966), who explored spatial and temporal distributions of 811 stations in China. Readers are directed to Xu (1983) for a discussion of many of these earlier climatologies. A subsequent gap in the literature occurred until 2008, with no national hail studies published. A hail day climatology of long-term hail observations (1961 to 2005) from 753 meteorological stations (Xie et al., 2008; Zhang et al., 2008) is the first recent effort toward understanding these events over China. Li et al. (2016) built on this hail day climatology, extending it to 2012. Recently, manually observed hail data from 2442 stations were released by the National Meteorological Information Center of China for the period 1954–2015 (Figure 13), producing one of the most complete and uniform surface hail data sets currently available in the world (Ni, Zhang, et al., 2017). Subsequent analysis of this data set also yielded historical hail sizes and frequencies and have allowed assessment of the climatology of hail size (Li et al., 2018). It must be pointed out that hailstones in China are defined as precipitation in the form of balls or irregular lumps of ice with diameters that are larger than 2 mm (China Meteorological Administration, 2003). This is smaller than the 5-mm threshold of the World Meteorological Organization and 19 mm used in the Unites Stats and thus can overlap with sleet, snow, or graupel (2 and 5 mm). Sleet and hail are distinguished by hardness, for small hail of this diameter is hard, while sleet or snow is loose in shape and fragile (China Meteorological Administration, 2003).

In other parts of Asia recent climatologies have been derived for South Korea (1972-2013; Jin et al., 2017) using data from 32 observation stations for hail 5 mm or greater, and for Mongolia using a similar approach (1984-2013; Lkhamjav et al., 2017). While these records reflect important parts of the global understanding, the uneven distribution of stations in these countries means that these climatological frequencies may not be representative of the surrounding region. In Bangladesh and India there are also smaller archives of hail reports, drawn from local meteorological agencies in the form of station records or collated from historical newspaper reports, though there have been few such climatological studies in recent years (e.g. Frisby & Sansom, 1967; Gokhale, 1975; Nizamuddin, 1993; Yamane et al., 2010). For Iran, 118 stations were used to assess the risk posed by hail to crops for the period 1985–2004 (Jamli, 2014).

3.5. South America

Early studies for South America were mainly station derived or small-scale climatologies as part of assessing global distributions (e.g. Frisby & Sansom, 1967; Gokhale, 1975). Analyses have shown hail occurring from

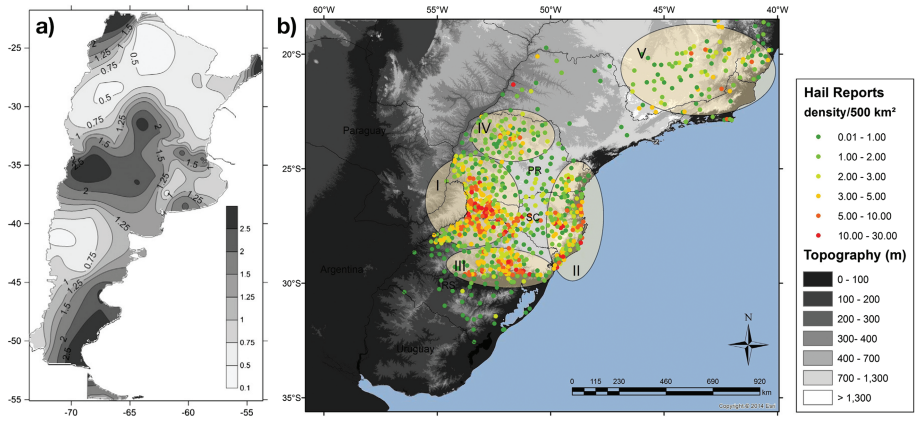

Figure 14. (a) Station recorded hail occurrence over Argentina 1960–2008. Adopted from (Mezher et al., 2012). (b) Hail observations over Brazil 1991–2012. Adopted from (Martins et al., 2017). Both figures are used with permission of Elsevier on behalf of the respective authors.

the north in Venezuela and Columbia to southern regions into Patagonia, predominantly east of the Andes. In Columbia, Arias et al. (2010) identified 231 hail events that occurred near Bogotá from 1939–2008. Mezher et al. (2012) used data from 93 weather stations to explore hail climatology over Argentina over the period 1960–2008 (Figure 14a). This revealed a high clustering of reports toward elevated topography, over the far south, close to the foothills of the Andes and the region around Mendoza and Cordoba, and over the far northwest. Subsequent analysis over Argentina and Uruguay noted a consistent distribution, with the frequent occurrence of large hail close to the foothills necessitating hail netting to mitigate risk at wineries (Rasmussen et al., 2014). To validate a satellite-derived climatology produced in that study, a small number of hail reports were identified from newspaper articles. Martins et al. (2017) explored the climatology of hail over Brazil between 1991 and 2012 using a data set derived from national disaster responses and as such focused on the most destructive hailstorms during the period. This data set of over 1,500 reports illustrated clustering toward population but noted significant increases in report density to the lee of topography in the region (Figure 14b). Hail in the region is predominantly a spring phenomenon, with declining frequency into the summer months.

3.6. Africa

Comparatively few studies exist for the African continent, which illustrate that hail events are predominantly found in the southern half of the continent (Frisby & Sansom, 1967; Gokhale, 1975). The majority of recent studies have focused on occurrence in South Africa (Le Roux & Olivier, 1996), including efforts to enhance or suppress precipitation (Mather et al., 1997). Much of the research stemming for South Africa stems from a historic record of hail occurrence maintained by the Council for Scientific and Industrial Research for the period 1980–1995, and other small locally compiled data sets from newspaper archives, which have some measure of size (e.g Pyle, 2006). Admirat et al. (1985) explored a limited set of hail observations and compared the occurrence to both Switzerland and Canada using data sets of up to 20 years. Subsequent analysis has suggested that convective storms favorable to hail development occur with some regularity (Blamey et al., 2017; Brooks et al., 2003) and can produce hail in excess of golf ball in diameter, and these are accompanied by sporadic reports in the region (Pyle, 2006). More recently, efforts are underway to derive an improved baseline understanding of hail occurrence in South Africa (Dyson & Pienaar, 2017). Other records of hail occurrence have been documented for Tunisia (Latrach, 2013), and there have been some evidence of hail causing impacts over the tea-producing regions of Kenya (e.g., Sansom, 1966).

4. Remote Sensing of Hail

4.1. Radar

Weather radar is the most powerful remote sensing tool for the detection and sizing of hail. Most weather radars operate by transmitting bursts or pulses of electromagnetic waves, which propagate through the atmosphere and scatter off cloud and precipitation particles. Analysis of the backscattered radiation received by the radar after each pulse provides information about these scatterers, including their location, motion parallel to the wave propagation path, size, shape, orientation, and physical composition (for

more details, see Doviak & Zrnić, 1993; Bringi & Chandrasekar, 2001; Fabry, 2015; Kumjian, 2018). In particular, dual-polarization Doppler radars have been a popular choice for operational radar networks at meteorological services around the world.

Dual-polarization Doppler weather radars can provide a suite of measurements that provide information on scatterers in the radar pulse volume. For a detailed review of these variables and their physical interpretation, see Kumjian (2013a), Kumjian (2013b), Kumjian (2013c). The most familiar is the equivalent reflectivity factor at horizontal polarization, hereafter "reflectivity" (Z_H), which provides information on precipitation size and concentration. The difference in reflectivity at horizontal and vertical polarizations is known as the differential reflectivity (Z_{DR}), which provides the reflectivity-weighted shape of particles in the pulse volume. The specific differential phase (K_{DP}) gives information about the mass concentration of nonspherical particles in the pulse volume. The copolar correlation coefficient (ρ_{hv}) provides a measure of the diversity of Z_{DR} within a sampling volume. An application of this parameter is use as a proxy for frozen-drop embryo supply based on the identification of differential reflectivity (Z_{DR}) columns observed with dual-polarization radar Kumjian et al. (2014). Some radars may provide the linear depolarization ratio (*LDR*), which is enhanced in the presence of wet, nonspherical, or irregular, wobbling particles. Kinematic information is also available, including the Z_H-weighted mean velocity component projected onto the beam propagation path (called the "radial velocity" or "Doppler velocity"), and a measure of the variance of radial velocities within the pulse volume (the "Doppler spectrum width").

Another method for radar-based hail detection and sizing has been simultaneously transmitting radiation at two or more frequency bands (e.g.,Bringi et al., 1996; Carbone et al., 1973; Jameson & Heymsfield, 1980; Jameson & Srivastava, 1978; Kaltenboeck & Ryzhkov, 2013; Picca & Ryzhkov, 2012; Tuttle et al., 1989). The premise behind such dual-frequency measurements is that radiation of different wavelengths will scatter differently from hailstones, particularly when the hailstone maximum dimension is comparable to one of the radar wavelengths. A major limitation of this approach is the difficulties in matching beams in space and time, as well as difficulties in correcting for differential attenuation (e.g. Rinehart & Tuttle, 1982; Tuttle & Rinehart, 1983). More recently, Melnikov et al. (2010) and Melnikov et al. (2014) have proposed using two closely spaced frequencies in the same band to detect large particles like hailstones. However, their study is limited by the use of two different radars without careful spatiotemporal beam matching, as both the timing between scans and differences in distance-dependent beam width can cause issues. Kumjian et al. (2018) has extended this idea with the dual-X-band-frequency Doppler on Wheels radar, which has better matched beams and minimal attenuation differences, and has found success in detecting hail within narrow size bands. Because most operational radar networks do not employ multiple frequencies, however, these approaches have limited broader applicability.

Armed with information available from dual-polarization or multiple-frequency radar observations, there are several approaches to detection and sizing of hail: direct measurements of backscattering from hail, indirect hail-related signatures, and overall storm intensity measures.

To directly detect backscattered radiation from hail, particles' backscattering properties need to be understood. It is widely stated that Z_H is proportional to the particle equivalent spherical diameter to the 6th power. This is only true for particles that are small relative to the radar wavelength; unfortunately, large hail does not fall into this category for most weather radar wavelengths (S, C, and X bands). As has been known for several decades, the backscattering properties of large hail are complicated functions of radar wavelength and hailstone size, owing to so-called resonance scattering effects (e.g., Herman & Battan, 1961; Atlas & Wexler, 1963; Bohren & Battan, 1982; Aydin et al., 1984, among many others). Thus, *there is no direct relationship between hail size and observed* Z_H. However, because rain tends to not produce Z_H in excess of ~55 dBz, any Z_H values exceeding this (and especially >60 dBz) are a reliable indicator of the presence of hail (though this hail may be of any size). The addition of dual-polarization information has aided in the detection of large (>2 cm) hail through the combination of high Z_H and low Z_{DR} and/or some combined measure of the two like "hail differential reflectivity" (H_{DR}), indicating large (and/or numerous) isotropically scattering particles like tumbling hail (e.g., Aydin et al., 1986; Bringi et al., 1984; Depue et al., 2007; Hubbert et al., 1998; Kumjian & Ryzhkov, 2008; Picca & Ryzhkov, 2012). Heinselman and Ryzhkov (2006) have found this large-hail signature in Z_H and Z_{DR} to be reliable. Additionally, reduced ρ_{hv} either near the surface (e.g., Balakrishnan & Zrnić, 1990) and/or aloft (e.g., Kumjian et al., 2010; Kumjian & Ryzhkov, 2008) has been suggested for detection of large hail. Analogously, enhanced *LDR* aloft has been implicated in the

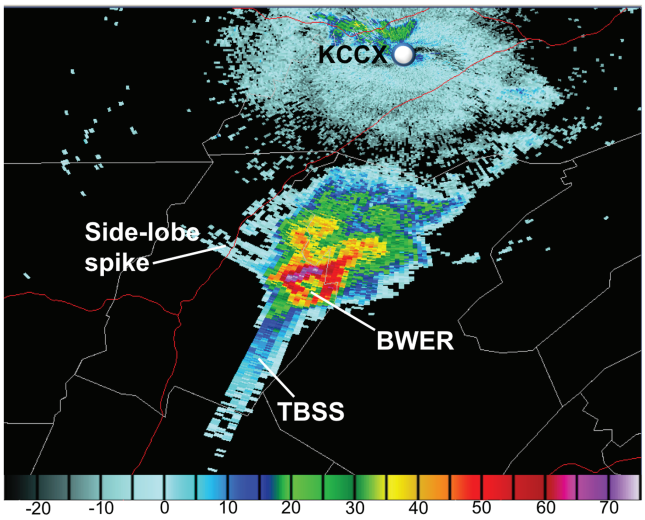

Figure 15. Example Z_H image (in dBz, shaded according to scale) from a hailstorm in central Pennsylvania, featuring a three-body scattering signature (TBSS), sidelobe spikes, and a bounded weak echo region (BWER). Data from KCCX radar near State College, PA, on 30 April 2017 at 2215 UTC. The KCCX radar location is shown by the white circle.

growth of large hail Kennedy et al. (2001). However, there is a lack of validating in situ or surface observations to evaluate the reliability of such signatures. More recently, Ryzhkov, Kumjian, Ganson, and Khain (2013), Ryzhkov et al. (2013) have investigated the use of melting hail signatures for hail sizing, with limited success (Ortega et al., 2016).

A major limitation of many of these studies is their reliance on the assumption of spherical or spheroidal models of hail for electromagnetic scattering properties. Recently, 3-D scans of real hailstones Giammanco et al. (2017) have been used for scattering calculations by Jiang et al. (2018), who found that departures from spheroidal shapes and lobes/protuberances in real hail lead to enormous variations in backscattering properties relative to spheroids. Jiang et al. (2018) conclude that unambiguous hail sizing from direct backscatter measurements alone likely is impossible.

Indirect signatures caused by hail have also been investigated for their use in detection and sizing of hail. Zrnić (1987) first explained the appearance of a "three-body scattering signature" (TBSS), also called the "flare echo" by Wilson and Reum (1988). The signature appears as a spike-shaped echo in Z_H extending downrange from a heavy-precipitation core (Figure 15) and originates when radiation scatters off (i) hydrometeors to the (ii) ground, which scatters it back to the (iii) hydrometeors, which finally scatter it back to the radar. Its polarimetric characteristics were documented and described in subsequent studies by Hubbert and Bringi (2000),Picca and Ryzhkov (2012),Kumjian (2013c). Though initially thought to be a reliable indicator of large hail (e.g., Lemon, 1998), follow-up studies have concluded that the TBSS in Z_H has an ambiguous relationship with hail size (Lindley & Lemon, 2007; Zrnić et al., 2010). A comprehensive study of the relationship between the TBSS manifestation in all polarimetric and Doppler measurements and hail size is needed. Scattering of radar sidelobe radiation off hail cores (Figure 15) as an indicator of large hail have also been explored and showed some promise Manross et al. (2010); however, more detailed and comprehensive studies of the reliability of this signature have yet to be undertaken.

Finally, radar-detected indicators of storm intensity have been used for hail detection and sizing efforts. These include measures of integrated Z_H throughout a storm-like vertically integrated liquid (e.g., Amburn & Wolf, 1997; Billet et al., 1997; Kitzmiller et al., 1995). Although storms with high VIL or VIL density (VIL divided by echo top height) are more prone to producing large hail, Edwards and Thompson (1998) Blair et al. (2011), and Wapler et al. (2016) found that VIL had little skill in estimating maximum hail size. Another integrated measure of Z_H is the Maximum Estimated Size of Hail (MESH; Witt et al., 1998), which is used in the U.S. operationally (see the subsection below). Similarly, maximum altitudes of certain Z_H thresholds have shown some predictive skill for hail size (Blair et al., 2011; Donavon & Jungbluth, 2007). Indicators of storm severity in the radial velocity field have also shown some correlation with hail size, including storm-top divergence magnitude (Witt & Nelson, 1991) and maximum rotation velocity (Blair et al., 2011; Witt et al., 2018). Large storm-top divergence implies an intense updraft, a necessary (but not sufficient) condition for large hail, whereas a strong mesocyclone is thought to be important for providing optimal hail trajectories, as described above. Other signatures associated with convective storm updrafts, including the bounded weak echo region (BWER (Figure 15); Marwitz, 1972) in Z_H or Z_{DR} columns (Kumjian et al., 2014) may provide some skill for diagnosing hail size but have yet to be thoroughly investigated for such applications. A major limiting factor of all of these indirect diagnoses of hail size based on storm intensity is that they are necessarily empirical; as such, empirical relationships developed in one part of the world may not be applicable globally or even regionally depending on the sample used in development. Additionally, detection and quantification of features aloft in storms are often limited by operational sampling strategies, which tend to prioritize scanning at lower levels, and distance from the radar to the storm, which affects the resolution of the observations.

4.1.1. U.S. Radar

The algorithm described by Witt et al. (1998) (the Hail Detection Algorithm; HDA) uses two-dimensional reflectivity components identified by a storm identification algorithm (Johnson et al., 1998) and weighted

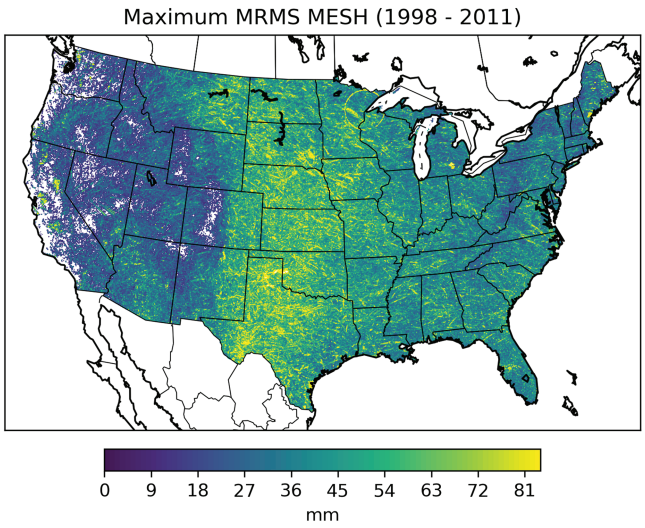

Figure 16. Maximum value MESH for the period 1998 through 2011 from the MRMS climatology (Smith et al., 2016), as determined using the 75th percentile threshold of Witt et al. (1998). Image and analysis courtesy of Skylar Williams (CIMMS/NSSL). Data archived at Allen et al. (2019).

vertical integrations to generate several hail related products, including MESH. In general, the HDA takes a vertical profile of reflectivity and weighs the reflectivity values by the relative location to a lower (40 dBZ) and upper (50 dBZ) bound, where values less than 40 dBZ are ignored, values between the bounds are weighted between 0 and 1 using linear interpolation, and values greater than 50 dBZ are given full weight. The reflectivity values and weights are used to transform the reflectivity values to flux values of hail kinetic energy (Federer et al., 1986; Waldvogel et al., 1978). These flux values are then weighted by the height of the reflectivity relative to the 0 and −20 °C heights. Any flux value below 0 °C height is ignored, flux values between 0 and −20 °C heights are weighted between 0 and 1 using linear interpolation, and all flux values above the −20 °C height is fully weighted. These weighted flux values are then vertically integrated to produce the Severe Hail Index (SHI), and SHI is then used to calculate MESH. Witt et al. (1998) calibrated the SHI/MESH relationship such that 75% of the observed hail reports should be less than the MESH value output by the algorithm. The logic for using such a relationship is that MESH is a *maximum* forecast of hail size and by overestimating the size, an inherent lead time for hail was built into the algorithm for use by an operational warning forecaster. Anecdotal evidence suggests this engineering of MESH is largely unknown or ignored, and the MESH value is used as an actual hail size to be expected from a thunderstorm. The HDA has served as the only operational algorithm for hail sizing within the United States' NWS since its deployment.

The performance of the HDA can be dependent on range, especially close to the radar where the radar volume may not extend above the melting level. In order to alleviate problems due to gaps in radar coverage, Lakshmanan et al. (2006) developed a merger technique for combining multiple single-radar data (i.e., the radar scan volume), which is collected in polar coordinates, onto a common latitude-longitude-height grid. The merged radar data can be easily combined with other data, such as near-storm environment data, to produce derived products, like MESH, on a spatial grid. The individual software to process single-radar and model analyses to create the merged radar and derived products was compiled into the Warning Decision Support System-Integrated Information (WDSSII; Lakshmanan et al., 2007) and was recently deployed operationally within the NWS as the MRMS system (Smith et al., 2016) giving forecasters the ability to use the MESH spatial grids for severe-weather warning operations. The ability of the MRMS grids to discriminate between different hail sizes was evaluated by Ortega (2018). That study showed for modest skill using the MRMS grids to discriminate where general hail size categories fell (e.g., “no hail”/any-sized hail). The MRMS MESH product was found to be larger than 79% of the paired hail observations, which is close the 75% as designed by (Witt et al., 1998). The modest skill and overall lack of specificity in the MRMS MESH values was explained by large amounts of overlap in the vertical reflectivity profiles for different hail size categories. Comparing MESH to VIL, both have similar skill in discriminating hail size categories as the parameters are highly correlated; however, MESH is advantageous as it is only related to convective echoes, while VIL can instead be present for any echo (Ortega, 2018). Recent analyses have also suggested that recalibration of MESH thresholds using a larger sample size of hailstorms than the original (Witt et al., 1998) sample can result in increases to overall skill in identifying severe hail (Murillo & Homeyer, 2019).

Leveraging these methods the use of radar-based hail detections to develop spatial climatologies for hail has been explored. Basara et al. (2007) assessed the advantages of using a proprietary algorithm in depicting severe hail swaths as compared to reports from Storm Data. Cintineo et al. (2012) used the MRMS MESH output to generate a 4.5-year hail climatology for the entire contiguous United States. The study found areas where the MESH-based climatology and the Storm Data reports-based climatology differed the most were areas of low population density, and over the southeast of the country. Work has continued to develop a MRMS MESH-based hail climatology with the Multi-Year Reanalysis of Remotely Sensed Storms (MYRORSS; Ortega, 2015). A particular focus on the recent efforts has been radar quality-control as poor radar data leads to a number of false “hot spots” for hail occurrence, especially for some coastal locations (Rosseau et al., 2017). Multi-Year Reanalysis of Remotely Sensed Storms has currently completed reflectivity

and reflectivity-based derivatives for the years 1998 through 2011. An example of the derived hail climatology is shown in Figure 16. This climatology, despite its limitations, stands to provide the most complete record of proxy hail observations in the years to come.

4.1.2. European Radar

Europe has the world's most dense weather radar coverage provided by 234 radars operated by national weather services (170 C-band, 45 S-band, and 19 X-band; 126 are dual-polarization radars; as of February 2018). Because dual-polarization radars have only been in operation in recent years, long-term studies aiming to assess hail frequency from radar have usually relied on reflectivity Z_H from conventional single polarization radars.

Several studies conducted in different regions across Europe have shown that hail detection algorithms using volumetric (3-D) radar reflectivity Z_H, sometimes combined with other observations, produce reliable estimates for hail on the ground (Delobbe & Holleman, 2006; Holleman, 2001; Holleman et al., 2000; Kunz & Kugel, 2015; Skripniková & Řezáčová, 2014; Stržinar & Skok, 2018). Modifications of these algorithm to prevailing conditions and specific user needs have also helped to increase the prediction skill. A potential source of error in these evaluations is the inadequacy of available ground truth data, such as spotter observations, reliable media reports, insurance loss data, or hailpad measurements, as each of these sources is fragmentary and heterogeneously distributed in space and time.

A pan-European radar composite based on radars from 30 national weather services is created by the Operational Program for Exchange of Weather Radar Information (OPERA; www.eumetnet.eu/opera; Huuskonen et al., 2014). Unfortunately, the 2-D reflectivity data that compose it have low spatial and temporal resolution and does not allow estimation of reliable hail signals. Thus, radar-based hail frequency assessments, usually expressed by the number of hail days per year, have mostly been generated on a regional to national scale (Fluck, 2018; Junghänel et al., 2016; Kunz & Puskeiler, 2010; Nisi et al., 2016; Puskeiler et al., 2016; Stržinar & Skok, 2018; Svabik et al., 2013). The use of different hail detection algorithms, varying radar sites, and inconsistent study periods hampers quantitative comparison. Holleman et al. (2000), for example, assessed the prediction skill of five different hail detection criteria on 15 days with severe weather in the Netherlands and found the Waldvogel et al. (1978) criteria to perform best compared to VIL, SHI, Auer, or Mason criteria. In a subsequent study, Holleman (2001) further improved the hail detection by adjusting the thresholds of the Waldvogel method to their specific situation. This was later confirmed in a comprehensive study by Skripniková and Řezáčová (2014), who tested and adjusted seven algorithms from Czechia and southwest Germany from 2002 to 2011. They proposed a combination of the Waldvogel technique and the HDA, which performed best. Kunz and Kugel (2015) found the best performance for HDA and POSH for hail detection over a 15-year period by verification against comprehensive insurance data. More recently, Stržinar and Skok (2018) found significant differences when comparing four different hail detection algorithms for Slovenia and found the best performance for the classic (Waldvogel et al., 1978) method and the SHI (SHI Witt et al., 1998) compared to commonly applied maximum reflectivity threshold and VIL (Edwards & Thompson, 1998) methods. The impacts of using different spatial resolution, frequency band, radar station density, storm tracking algorithm, and interference filters in the various national and regional networks all contribute to uncertainty and may affect the best algorithm choice. Nevertheless, common findings of these studies are a large spatial variability of hail frequency as a result of both large-scale atmospheric conditions and local-scale orography, the latter primarily due to the triggering or invigoration of convection.

Germany has been the focus of several regional studies of up to 7 years, obtaining similar results by applying the Waldvogel et al. (1978) algorithm to either 3-D Z_H (Puskeiler et al., 2016), or 2-D reflectivity (Junghänel et al., 2016; Fluck, 2018), filtering using coindicative cell tracking, station observations or insurance data. These studies reveal a substantial increase of radar-derived hail days from north to south toward mountainous regions that is not as apparent from limited observational data sets (Kunz & Puskeiler, 2010). Similar results have been found over the edges of the Alpine regions of Switzerland and Austria (Nisi et al., 2016; Svabik et al., 2013). In contrast, over the main Alpine chains hail is relatively infrequent, which can be plausibly explained by lower temperatures at higher elevations leading to reduced moisture content. Radar-derived hail days show several maxima over the foothills north and south of the Alps in Switzerland, based on a climatology of Probability of Hail and MESH between 2002 and 2014 (Nisi et al., 2016). Belgium and its neighboring countries has also been assessed using Probability of Hail for a 10-year period, with a gradual increase in the number of hail days from NW to SE, and the highest number of events over NE France and West Germany (Goudenhoofdt & Delobbe, 2013; Lukach et al., 2017).

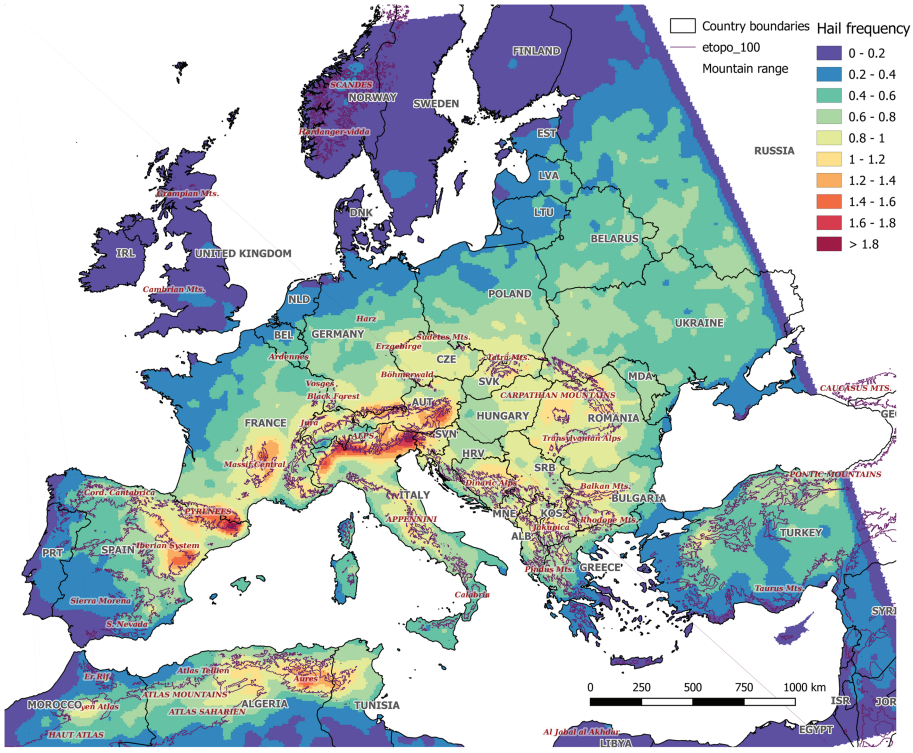

Figure 17. Hail frequency estimate for Europe based on overshooting top detection with Meteosat imagery (2004–2014), accounting for hail conditions as determined from ESWD hail reports with the ERA-INTERIM reanalysis (Punge et al., 2017), adapted from their Figure 6. Used with permission of Elsevier and the author.

For many other regions, radar-based hail climatologies are still lacking. In order to develop a pan-European radar-based climatology of hail occurrence and to monitor hailfall operationally, international exchange of radar data must be expanded to include volumetric data of all relevant parameters.

4.1.3. Other Radar Studies

In Australia, Doppler radar has only been recently implemented for a wide array of sites, and hence, the nationwide availability of climatological length records is limited. Given the propensity for hailstorms in southeast Queensland, analysis using radar data and MESH-derived climatology for 18-years has been developed over the Brisbane region (Soderholm et al., 2016; Soderholm et al., 2017a), with work ongoing to expand these studies to Sydney and Melbourne. These climatologies have illustrated the importance of sea breeze fronts for initiating the development of organized storm updrafts in this region (Soderholm et al., 2017b). Upcoming upgrades of the network to dual-polarization and expansion of the coverage of Doppler S-band radars will likely improve coverage over the continent to provide reliable climatological quality records on a wider basis in the future.

4.2. Satellites

Satellite observations are capable of sampling large regions of the globe with similar sensitivity. It therefore stands to reason that satellite-derived proxies of hail can be used to construct homogeneous estimates of hail frequency on a continental scale. Satellite-based hailstorm detection methods rely either on passive instruments measuring outgoing electromagnetic radiation to determine brightness temperature or patterns in the visible, or active radar measurements, or combinations thereof.

A prominent method in this field was developed by Bedka et al. (2010) based on geostationary satellite imagery. The method consists in identifying the overshooting cloud tops (OTs) that generally penetrate into the lower stratosphere associated with severe convective updrafts. These features are visible as cold anomalies consisting of several pixels over the convective anvil cloud and can be detected using a dedicated algorithm. Typical OT temperatures range from 190 to 215 K. Relatively frequent scans from these satellites have enabled an OT-derived climatology of relatively high detail for Europe (Punge et al., 2014). With further filtering for conditions favorable to hail derived from ERA-Interim reanalysis, reliable hail proxies have

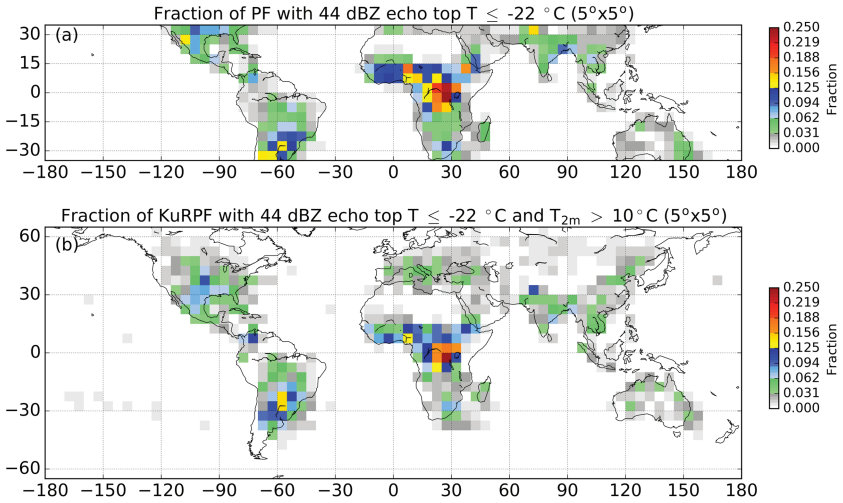

Figure 18. (a) Fraction of TRMM overpasses from 1998 to 2013 for each 5 × 5 grid box that have a PF satisfying the 44-dBZ echo top temperature criteria of −22 °C. (b) As in (a), but for GPM overpasses from March 2014 to February 2017, and with the restriction that the surface air temperature is greater than 10 °C. (Ni, Liu, et al., 2017), their Figure 4). Copyright American Meteorological Society. Used with permission of the authors.

been established for both Europe and Australia (Punge et al., 2017; Bedka, Allen, et al., 2018). In Europe, hail frequency is elevated in the vicinity of the Alps and lesser mountain ranges, similar to results identified by radar data and to a lesser extent observations and generally decreases toward the North (Figure 17). The highest proxy values occur in the northeastern parts of both Italy and Spain. In Australia, hailstorms are most frequent in the south-east in the area between the Australian Alps mountain chain and the Pacific coast. The highest frequencies were concentrated in northeastern New South Wales, south of Brisbane. A secondary maximum region was also found over central Western Australia. In a similar approach, Merino et al. (2014) and Melcón et al. (2016) identified methods to detect hailstorms from geostationary satellite bands, claiming Heidke skill scores between 0.37 and 0.62, but argued methods should be optimized by region rather than applied to larger domains.

Another method of hail detection from satellite data was first proposed by Cecil (2009). The approach relies on passive microwave imagery obtained from polar orbiting satellites. Zones of low apparent brightness temperature are the consequence of scattering by ice hydrometeors and can therefore be used as a proxy for hail on the ground. There is hence a potentially more direct link to hail than for the OT proxy; however, less frequent overpasses mean a higher degree of uncertainty compared to geostationary satellite approach. Combining with a further satellite data set, Cecil and Blankenship (2012) found the highest proxy values on a global scale in Central North America, Southern Brazil, Bangladesh, and Central Africa. Using a similar method but a different data set, Ferraro et al., 2015 found good agreement with the hail report frequency in the United States. However, Ferraro et al. (2015) and Allen et al. (2015a) both noted a tendency for the algorithm to overly detect occurrence for tropical regions, where such hail is rarely observed, even in populated areas. More recently, Mroz et al. (2017) combined microwave imagery and Ka- and Ku-band radar limb scans from the Global Precipitation Measurement (GPM) Core Observatory to identify the areas with highest hail probability in a range from 65°S to 65°N. The 3.25-year data set, calibrated used North American radar data, reveals further regional maxima in Northern Pakistan, Eastern South Africa, North Western South America, Eastern India, Northeast China, and parts of Southeast Asia. Adding further confidence to the accuracy of the data set, there is also reasonable agreement with the OT-based estimates for Europe and Australia. Detections are most frequent in spring and summer over land in both hemispheres, and in fall and winter over adjacent seas such as the Mediterranean, the Tasman Sea, and East of South Africa. In a similar approach, Ni et al. (2017) combined the 16-year record from precipitation radar and microwave imager aboard the Tropical Rainfall Measuring Mission with the GPM data set and confirmed the overall pattern (Figure 18). The generally high hail frequency estimates found in these data sets for the tropics, particularly for Central Africa, could not be verified with ground hail reports, and hail in these areas is likely to melt on its way to the ground, except for locations at altitude. Recently, Bang and Cecil (2019) produced a new climatology that attempted to address a number of the limitations of the original Cecil and Blankenship (2012)

algorithm, using a combination of GPM and Tropical Rainfall Measuring Mission and environmental data over a 5-year period to constrain occurrence to regions that experience hail. However, it is not clear that this has addressed the issues in overrepresenting tropical frequency as compared to favorable environments (e.g Prein & Holland, 2018) and satellite/environment hybrid approaches (Bedka, Allen, et al., 2018). Two contributions to this problem may be the low number of scans in tropical regions (200 per year) and the short time series of the record used to develop and train the algorithm.

As there are very few studies of hail occurrence in tropical regions, it is difficult to validate these results with surface hail reports and distinguish between hail in clouds and at the surface from these detections. Different formats and regulations for hail reporting in different regions also make it more difficult to conduct regional comparisons. Nevertheless, the ability to apply uniform standards across national boundaries is a strength of satellite-based approaches. Further validation using regional surface hail reports, especially over tropics, is still essential to verify the methods developed from satellite-based proxies. An ongoing issue is the differences between different satellite platforms, as systems age and retire. These discontinuities are the primary limitation of long-term reliable climatologies of hail proxies. As more GPM observations become available, the methodology developed by Ni, Liu, et al. (2017) could be further validated. In addition, cross validation using dual-frequency precipitation radar in the detection of hailstorms is also a useful avenue (Mroz et al., 2017). Another future application of satellite-derived hail detection might be estimation of crop damage using vegetation indices (Bell & Molthan, 2016; Gallo et al., 2019). Recent launches of the GOES–17 and 18 satellites over the Americas, Himawari over Asia, and new generation EUMETSAT will also likely lead to increasing utilization of satellite-derived hail frequency estimates.

5. Environmental Forecasting Parameters and Climatology

5.1. Forecast Parameters

The majority of forecast parameters for hail development have originated from operational forecasters seeking to improve their predictions. These parameters are derived by relating direct or indirect hail observations to proximal soundings, whether from rawinsonde or model data (e.g. Johnson & Sugden, 2014; Smith et al., 2012; Tuovinen et al., 2015). The relationship between suitable meteorological variables and hail observations can then by extracted based on observations for a limited region and/or a limited time period. The derived parameter or composite can then be transferred to forecast the likelihood of hail for other regions or periods where direct observations are not available. Typical operational forecast parameters for hail have focused on predicting the likelihood of organized severe thunderstorms or using hail as a null case for tornadoes, rather than explicitly trying to forecast the characteristics favorable to hail development (Allen et al., 2011; Brooks et al., 2003; Rasmussen & Blanchard, 1998; Thompson et al., 2003). Hail size is one of the more challenging predictions of severe thunderstorm features owing to the previously described complexity of hail formation, and our limited understanding of associated processes. Adding to this challenge, relationships between hail size and environment have proven particularly difficult to determine with certainty due to comparatively small sample sizes of reliable hail observations, and regional variations in the necessary parameters (e.g. Brimelow et al., 2006; Edwards & Thompson, 1998; Groenemeijer & van Delden, 2007; Jewell & Brimelow, 2009; Johnson & Sugden, 2014; Manzato, 2012; Púčik et al., 2015; Smith et al., 2012; Tuovinen et al., 2015). The issues limiting this type of approach arise partly because of the microphysical impacts on the growth rate of hail and the role of storm mode (Gagne et al., 2019; Grams et al., 2012; Smith et al., 2012), both of which cannot be inferred solely from proximity soundings with a reasonable level of confidence. It is also likely that the imprecise measurement techniques for hailstone magnitude also play a significant role.

Early work globally saw limited success with small samples of observed sizes used to develop empirical relationships between hail size and CAPE or temperature data at various levels (e.g. Fawbush & Miller, 1953; Foote & Knight, 1977; Foster & Bates, 1956; Miller, 1972; Moore & Pino, 1990), which tended to produce unrealistic hail sizes or show little skill distinguishing between large and small hail (e.g. Doswell, 1982). Parameters that relate to updraft strength have proven to be popular candidates in both Europe and the US owing to the propensity of strong updrafts being necessary for hail growth (e.g. CAPE, mid-level vertical lapse rate of temperature, Huntrieser et al., 1997; Manzato, 2005; Groenemeijer & van Delden, 2007; Kunz, 2007; Sánchez et al., 2009; Smith et al., 2012; Mohr & Kunz, 2013; Johnson & Sugden, 2014; Merino et al., 2014; Púčik et al., 2015; Tuovinen et al., 2015; Sanchez et al., 2017; Lkhamjav et al., 2017). Over Europe, for general hail occurrence, the fixed-layer lifted index has also proven to be useful (Mohr & Kunz, 2013).

Other factors with skillful predictability include contributions to vertical pressure gradient forces to strong updrafts, as organized storms produce the largest hail events. These contributions are most commonly seen in supercells which produce the vast majority of the largest hailstones, in particular as parameterized by vertical bulk wind shear over between the surface and 6 km (S06), or 0- to 3-km storm relative helicity (SRH) (e.g. Dennis & Kumjian, 2017; Johnson & Sugden, 2014; Kumjian et al., 2019; Kunz et al., 2017; Púčik et al., 2015; Rasmussen & Blanchard, 1998; Smith et al., 2012; Thompson et al., 2003; Tuovinen et al., 2015; Weisman & Klemp, 1982). Johnson and Sugden (2014) showed over the United Stats that there was strong dependence on shear characteristics for large hail sizes, in particular for SRH and storm relative winds above 6 km, which is consistent with recent modeling results (Dennis & Kumjian, 2017; Gagne et al., 2019), and analysis of smaller hail has shown it is generally favored in weaker shear environments (Kumjian et al., 2019). In a recent study, Kunz et al. (2017) identified during an 11-year period over France and Germany that both S06 and SRH are important quantities for large hail (≥5 cm), but only in combination with long duration storms with long storm tracks (≥100 km).

Other potential predictors come from leveraging depth of the optimal hail growth layer above the freezing level, or its minimum height (parameterized as freezing level or depth of the hail growth zone) (Allen et al., 2015a; Edwards & Thompson, 1998; Johnson & Sugden, 2014; Prein & Holland, 2018). The amount of moisture available below the freezing level or in the boundary layer also has an influence on hydrometeor density and potentially on the growth rates of larger hail (Allen et al., 2015a; Johnson & Sugden, 2014). Recent research in Europe has suggested that the lifted condensation level may also provide a useful predictor (Púčik et al., 2015), which may be related to broader updrafts, cloud base temperature, distance of cloud base from the ground, or perhaps higher cloud bases enhancing updraft speed (McCaul & Cohen, 2002). This result may also be similar to undiscussed characteristics in U.S. studies (e.g. Grams et al., 2012; Rasmussen & Blanchard, 1998). Numerous other candidate variables have also been proposed for identifying the forecast conditions favorable to large hail development (Brooks, 2013; Jewell & Brimelow, 2009; Johnson & Sugden, 2014; Rasmussen & Straka, 1998; Thompson et al., 2003; Witt et al., 1998), though few of these indices have proven to be useful in the operational setting (Edwards & Thompson, 1998; Johnson & Sugden, 2014). Like all environmental parameters characterizing conditions favorable to the development of severe thunderstorms, the aforementioned parameters are conditional on the initiation of a storm. A number of authors have addressed this limitation by leveraging the presence of synoptic features such as cold fronts, though this approach has been predominantly applied in Europe (Berthet et al., 2013; Michaelides et al., 2018). Indeed, several studies suggested that convective storms are more likely to occur (or not to occur) during specific large-scale weather types (Aran et al., 2011; García-Ortega et al., 2011; Kapsch et al., 2012a; Piper & Kunz, 2017). Other approaches to address this problem involve the use of satellite OT proxies or radar indicated storms (e.g. Bedka, Allen, et al., 2018; Smith et al., 2012; Punge et al., 2017).

Composite parameters have also seen applications to forecasting of hail, though in many cases little evaluation of their performance has been conducted. For example, the Significant Hail Parameter is a calibrated function of CAPE, the mixing ratio of a parcel, environmental midlevel lapse rate, 500-hPa temperature, and S06 and notionally provides an indication of higher likelihood of hail in excess of 2 in.. Yet despite the tailored nature of this parameter, no evaluation of its performance in a forecast context has been described in the literature. In a recent study by Johnson and Sugden (2014), a set of 500 large hail reports was used to evaluate near proximity soundings from the Rapid Update Cycle model for hail prediction. Considering a CAPE and S06 product similar to that of Brooks et al. (2003) they identified considerable overlaps for various hail sizes, suggesting that the predictive skill of a such a parameter for hail may be limited. Instead, they derived the large hail parameter (LHP), which includes a conditional requirement for S06 and most unstable CAPE, and in two terms combines MUCAPE with the 700- to 500-hPa lapse rate, and hail growth zone thickness, surface to equilibrium level bulk vertical shear, the angle between the ground relative equilibrium level wind direction and the ground relative 3- to 6-km wind direction, and the difference in wind direction between the 3- to 6-km storm relative wind and the 0- to 1-km storm relative wind. While a complex and calibrated parameter, evaluation of its performance suggested that it has a superior capability to discriminate between 5 cm and greater hail, and smaller hail sizes as compared to simpler CAPE-S06 products. It is important to note that calibrated parameters tend to be problematic when applied outside of their regional calibration domain, and thus, while parameters such as the LHP or Significant Hail Parameter may be effective in the United States, there is no guarantee they will be appropriate for cases elsewhere.

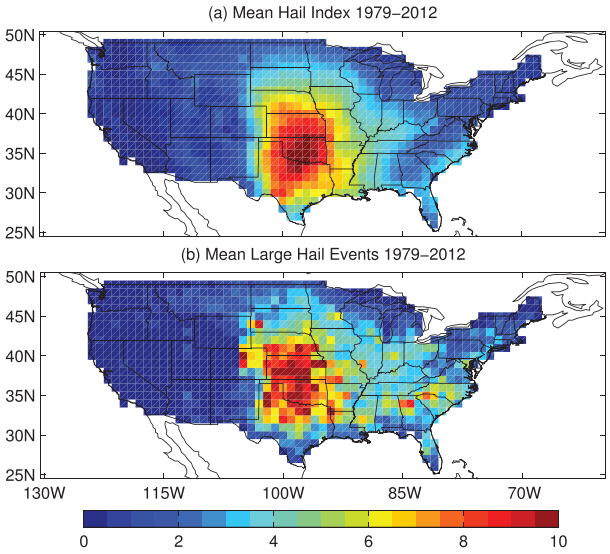

Figure 19. (a) Mean annual number of 3-hourly periods with large hail events as predicted by the four-parameter index 1979–2012. (b) As for (a) except the mean annual occurrence of observed large hail events. Adopted from (Allen et al., 2015a), their Figure 8). Used with permission of the author.

Alternate techniques to hail forecasting have used one-dimensional coupled hail and cloud models such as HAILCAST to estimate potential hail size based on the atmospheric profile (e.g. Brimelow et al., 2002; Brimelow et al., 2006; Jewell & Brimelow, 2009), or alternatively using explicit microphysics to forecast graupel or hail size from simulated updrafts (e.g. Gagne et al., 2019; Labriola et al., 2019). While not yet widely applied operationally, both approaches do appear to provide a reasonable predictions of hail size (Gagne et al., 2019; Jewell & Brimelow, 2009; Labriola et al., 2019). One example is the application of HAILCAST that has been implemented in high-resolution WRF model output based on simulated storms (Adams-Selin & Ziegler, 2016). This approach was found to produce high-resolution hail size estimates that are within 0.5 in. 66% of the time for two evaluation periods in May 2014 and 2015, providing a new tool for operational forecast applications (e.g. Gallo et al., 2017). Nonetheless, further evaluation and operational testing is underway to ensure these estimate provide appropriate guidance, and testing of simulated hail sizes has shown considerable sensitivity to the parent weather model.

A direction of growth for analysis of the parameters useful to forecasts of hail has been applications of machine learning. These approaches have tackled the problem by allowing a greater number of variables to be considered, including model simulated updrafts and derived microphysical representations of hail, environmental parameters and observed radar data (e.g. Czernecki et al., 2019; Gagne et al., 2017; Gagne et al., 2019; McGovern et al., 2017). Such approaches are intended to provide operational guidance for hail forecasting and allow greater dimensionality within forecast parameters, though have proven computationally expensive during testing for operational implementations.

5.2. Environmental Proxies and Climatology

The lack of comprehensive hail observations in both the United States and Europe has spurred development of techniques to estimate hail probability from hail-favoring environments using either proximity soundings or reanalyses (e.g. Allen et al., 2015a; Mohr et al., 2015; Mohr et al., 2015; Púčik et al., 2017; Rädler et al., 2018; Madonna et al., 2018). This method functions by applying developed forecasting parameters retrospectively to estimate spatiotemporal frequency; however, ideal conditions are not a guarantee of hailstorm occurrence. The majority of such approaches have been applied to climatological likelihood of environments favorable to severe thunderstorms in general rather than specifically hail (e.g. Allen & Karoly, 2014; Blamey et al., 2017; Brooks et al., 2003; Gensini & Ashley, 2011; Taszarek et al., 2019). Recently, several hail-specific environment-derived climatologies have been developed. For example, the mean annual occurrence of hail over 1 in. has been proxied using the climatogical monthly mean atmospheric parameters from reanalysis (Allen et al., 2015a). These parameters, while significantly removed from those used operationally, rely on the spatial likelihood of instability, 0- to 3-km SRH, boundary layer moisture and the occurrence of a thunderstorm as derived from convective precipitation. Even on a monthly scale, these parameters provide a useful rendition of the frequency of occurrence that corrects for biases that originate in hail observations (Figure 19). This illustrates the propensity of these favorable environments to occur east of the Rocky Mountains with a maximum over the Great Plains. The methodology is not without limitations however, as it relies on the weighted sampling of hail events, which may mean that events over the southeast Unites States are underestimated owing to hail occurring in predominantly thermodynamically driven environments.

Following a similar methodology, Madonna et al. (2018) modeled the monthly number of hail days over northern Switzerland with a combination of monthly anomalies of 2-m temperature, logarithm of CAPE, deep-layer shear, and the month itself. Applied to ERA-Interim reanalysis (Dee et al., 2011), the model captured the intra-annual variability of hail well, but slightly underestimated interannual variability. Logistic regression has also been successfully applied in different study regions to assess hail frequency as it allows to quantify the discriminating power of single variables gradually included in the model. Sánchez, Marcos, et al. (2009), for example, built a logistic model based on sounding data for four different areas, three of them in Europe, found that Showalter Index and 850-hPa dewpoint temperature exhibit the highest prediction

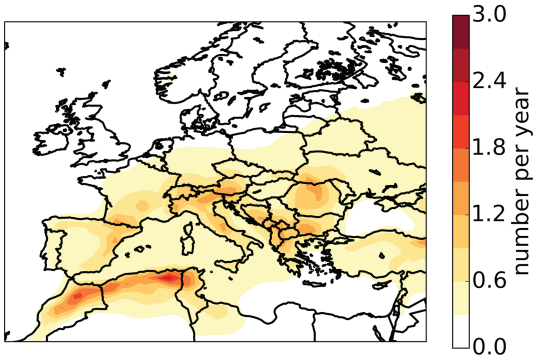

Figure 20. Modeled annual number of large hail events (diameter ≥2 cm) per 0.75 × 0.75 grid box across Europe, according to the statistical model AR-CHaMo (Rädler et al., 2018), their Figure 8b). Copyright American Meteorological Society. Used with permission of the authors.

skill for hail irrespective of the area considered. Over Germany Mohr, Kunz, and Keuler (2015) found high predictive skill for a linear logistic hail model applied to Germany using Lifted Index, large-scale weather types, 2-m temperature (all three parameters at 12 UTC), and 2-m minimum temperature in the morning. Applied to 20-year hindcast model runs initialized by ERA-Interim, the resulting potential hail index shows a high relation to both building insurance data and hail signals derived from radar reflectivity in Germany, and was similar effective for a 60-year period of downscaled data derived from the National Center for Atmospheric Research/NCEP reanalysis over Europe (Mohr, Kunz, & Geyer, 2015).

Combining this environmental estimation of frequency with short-term changes of ambient conditions and circulations associated with cold fronts allows a better estimation of the frequency (Kunz et al., 2017). Schemm et al. (2014) combined radar-based hail statistics for Switzerland between 2002 and 2013 with cold front detections and used this to identify that up to 45% of all hail events in NE and South Switzerland are associated with a cold front (Schemm et al., 2016). Applying the same front detection algorithm to Germany and France, Kunz et al. (2017) showed that in Northern Germany up to 50% of all radar-detected hailstorm tracks are prefrontal events, whereas in SW Germany only between 10% and 15% are prefrontal, presumably due to the complex terrain, where convection is frequently triggered by convergence zones developing over and around the mountains.

A common difficulty of modeling hail occurrence is that the microscale processes that govern the initiation of storms are difficult to model using data sets that are much larger than the scale of the storm. Rädler et al. (2018) developed a suite of generalized additive models (AR-CHaMo) that modeled the probability of hail as the product of the probability of storm initiation and the probability of a hazard given that a storm had occurred. This method only used three environmental parameters: 850- to 500-hPa relative humidity, LI, and 10 m- to 500-hPa wind shear derived from ERA-Interim reanalysis to model the climatology of hail larger than 2 cm over Europe. The resulting frequency corresponds rather well with other proxies for hail occurrence (Figure 20), such as the occurrence of overshooting tops detected by satellite, combined with favorable environments Punge et al. (2017).

The success of these methods in estimating the frequency of hail independent of other phenomena suggests opportunity to further explore the characteristics of the global hail distribution beyond that inferred from the known distribution of severe thunderstorm environments (Allen & Karoly, 2014; Blamey et al., 2017; Brooks et al., 2003; Gensini & Ashley, 2011). An effort in this direction can be seen in the recent study by Prein and Holland (2018), which applied a synthetic hail model developed using U.S. observations to environmental data from the ERA-Interim reanalysis to estimate global frequency, and cross validated the model against observations from Europe and Australia (Figure 21). Again, parameters common to those found in other studies were found to be effective in modeling proxy hail frequency (atmospheric instability, freezing level height, and 0- to 3-km wind shear and storm relative helicity). Efforts to better understand the climatology of hail should focus on the probability of a storm environment occurring, the relationship of incidence to hail size, and application of other statistical and machine learning methods to estimate climatological frequency. Another promising avenue of development is application of these techniques to reanalyses of increasingly higher spatial and temporal resolution.

6. Climate Interactions

6.1. Variability

The understanding of climate interactions with hailstorm occurrence is a relatively young field and has received far less attention to date than tornadoes (Tippett et al., 2015). Teleconnections to the El Niño–Southern Oscillation over Australia using severe thunderstorm frequency (e.g. Allen & Karoly, 2014; Yeo, 2005) and the United States with hail (e.g. Allen et al., 2015b) have shown a substantial influence in modulating frequency. These teleconnections alter the frequency of severe thunderstorms by either reducing or enhancing the frequency with which formation of ingredients (Doswell et al., 1996) favorable to

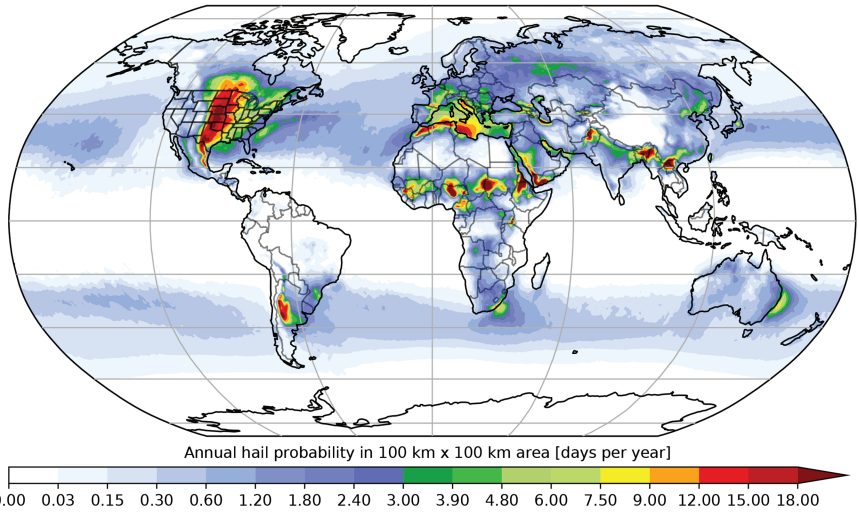

Figure 21. Global annual average large hail probability normalized to a 100 × 100 km area from 1979 to 2015, according to the statistical model of Prein and Holland (2018), their Figure 11a). Used with permission of the authors.

severe thunderstorms and hail occur, leading to changes in variability. Other seasonal driving patterns have been identified for sea surface temperature anomalies in the Gulf of Mexico for the United States (Molina et al., 2016). On the subseasonal scale, there are responses in the variability of hail to the Madden-Julian Oscillation (Barrett & Henley, 2015; Tippett, 2018), and more recently, the Global Wind Oscillation that encapsulates subseasonal modulations to the jet stream driven by equatorial convection and mountain torques (Gensini & Allen, 2018). The majority of these mechanisms function by modulating the storm track (e.g. ENSO Allen et al., 2015b; Cook et al., 2017), positioning or meridional wave breaking of the jet stream (Gensini & Allen, 2018; Gensini & Marinaro, 2016), or the passage of other factors related to thunderstorms activity.

Over Europe, there has been recent examination on the variations in thunderstorm frequency induced by the North Atlantic Oscillation (NAO) and sea surface temperatures in the Mediterranean or the North Atlantic Ocean (e.g. Miglietta et al., 2017; Piper & Kunz, 2017). The NAO was found to have a significant impact on lightning probability with its negative (positive) phases generally favoring (reducing) convective activity (e.g. Piper & Kunz, 2017). This relation is primarily caused by variations in the synoptic scale sources of lift (e.g., fronts, surface convergence, and upper-level troughing), relevant for convection initiation over larger areas, during the two NAO phases, but partly compensated by thermodynamic modifications toward higher stability of the preconvective environment.

Given that interannual variability in tornadoes and severe thunderstorm frequency has been demonstrated or indicated for a range of oscillatory climate scale patterns it stands to reason that year-to-year variability in hailstorms can be at least partially explained by the modulation of the frequency of favorable environments for hail, or the factors leading to the initiation of such storms (Allen et al., 2015b; Barrett & Gensini, 2013; Cook et al., 2017; Cook & Schaefer, 2008; Lee et al., 2012; Lee et al., 2016; Lepore et al., 2017; Weaver et al., 2012). For a more comprehensive listing of research on the topic, readers are directed to the review by Tippett et al. (2015).

6.2. Climate Change

A large number of studies have begun to focus on the question of the impact of global warming on severe thunderstorms (Diffenbaugh et al., 2013; Gensini et al., 2014; Gensini & Mote, 2014; Trapp & Hoogewind, 2016; Púčik et al., 2017; Rädler et al., 2018; Hoogewind et al., 2017); however, there have been comparatively few that have looked specifically at the implications for hail occurrence or intensity (e.g. Brimelow et al., 2017; Mahoney et al., 2012; Trapp et al., 2019). For a more complete review of the broader implications of climate change for severe thunderstorms, readers are directed to Allen (2018).

The limitations of hail observations present their greatest challenges when considering whether there have been observed increases to hailstorm frequency or intensity (Allen & Tippett, 2015; Groenemeijer et al., 2017). Despite this limitation, the increasing trends in severe thunderstorm losses (e.g., Eccel et al., 2012;

Sander et al., 2013) and perceived increases in the frequency of damage-causing hail events (Kunz et al., 2009) have prompted a large number of studies considering trends in hail frequency. Over Europe, these results have suggested a mixture of trends that vary considerably from region to region, predominantly for smaller hailstones (e.g. Dessens et al., 2015; Eccel et al., 2012; Hermida et al., 2015; Punge & Kunz, 2016). The most consistent signals appear to be a reduction in the frequency of smaller hail diameters, presumably in response to an increasing freezing level. Such a result is consistent with other observations worldwide, which suggest emerging declining trends in hail frequency, including the potential that these changes are influenced by aerosols (e.g. China, Li, Zhang, Zou, et al., 2018; Xie et al., 2008; Zhang et al., 2008; Zhang et al., 2017; Ni, Zhang, et al., 2017). The decreases in small hail frequency is consistent with the expected changes seen in future projections under a warmed climate (Brimelow et al., 2017; Mahoney et al., 2012; Trapp et al., 2019). These are contrasted by a general lack of trends in severe or larger hailstones (Allen, 2018), where the thermal impacts of a warmer lower troposphere contribute little to melting large bodies of ice (Brimelow et al., 2017; Mahoney et al., 2012; Trapp et al., 2019). Using the indirect methods described in section 5, similar analyses of environments have been used to explore long-term trends in hail frequency. Again, there is inconsistency depending on the regions considered, for example Kunz et al. (2009) and Mohr and Kunz (2013) found positive trends for various convective parameters and indices across Germany and Europe, respectively, mainly due to an increase in moisture content at lower levels. Several statistical analyses based on hail-favoring environments quantified from reanalysis suggests an increase in the convective potential over most areas during the past decades (e.g., García-Ortega et al., 2014; Mohr, Kunz, & Geyer, 2015; Rädler et al., 2018). However, long-term trend analyses indicate that a high annual and multiannual variability dominates the trend signal in the past, resulting in nonsignificant trends for several grid points (Mohr, Kunz, & Geyer, 2015). This is contrasted by a decrease in the frequency of hail favorable environments over China, related to increases in freezing level height and increasing convective inhibition (Li et al., 2016). Over the U.S. the incidence of large hail appears relatively flat (Allen et al., 2015a), consistent with no real evidence for shifts in favorable storm environments (Gensini & Ashley, 2011; Robinson et al., 2013).

Numerical modeling offers an alternative to using observational records for detecting hailfall trends. The limitations of the coarse scale of climate models, while already challenging for severe thunderstorms, are magnified when considering the small scales on which microphysical processes associated with hail growth occur. These processes are parameterized with the aim of minimizing errors in long-term climate means, rather than handling all storm-scale processes accurately. Thus, two approaches are available: (1) Consider environments favorable to hail development (which as discussed in section 5 are relatively poorly understood) or (2) direct simulation of the storms themselves (less than 4-km horizontal resolution), and searching for intense storms capable of large hail production. Both of these methods have been explored over North America and Europe, though the computational expense of direct simulation has prohibited anything beyond regional analyses (Brimelow et al., 2017; Mahoney et al., 2012; Trapp et al., 2019). Over North America these studies have suggested increases to larger hailstone frequency and decreasing small hail frequency both through hail graupel proxies and simulation of hail growth using HAILCAST. Over Europe only a relative few studies attempted to estimate future changes in the environmental conditions favorable for severe convective storms such as large-scale weather patterns (Kapsch et al., 2012b) or a combination of thermodynamic and dynamic proxies (Mohr, Kunz, & Keuler, 2015; Púčik et al., 2017; Sanderson et al., 2015). In summary, all those studies estimated a further increase of the potential for severe convective storms over future decades in Europe. Púčik et al. (2017), for example, estimated relative increases of up to 100% (50%) in severe thunderstorm occurrence until 2100 in a 14-member ensemble of downscaled general circulation models under a business-as-usual (moderate climate-change mitigation) scenario, modeled by instability, deep-layer shear and convective precipitation.

A number of fundamental questions related to the application of numerical modeling for hail frequency and size remain. These include whether the discrete supercell storm modes that favor large hailstones will continue to occur, as increasing hydrometeor loading and instability more often lead to stronger cold pools leading to more clustered storms regenerating along gust fronts that do not favor large hail growth. It also remains unknown whether there is likely to be microphysical responses to changes to this hydrometeor loading, or the ice condensation nuclei critical to the formation process. Trapp and Hoogewind (2016) have already shown that much of the buoyancy contributions to updraft intensity under pseudo-simulated storms will be offset by condensate loading. The argument that updraft intensity increases because of growing buoyancy thus may not hold in general. This is further compounded by the dependence of hail on vertical wind

shear (e.g. Dennis & Kumjian, 2017), which Trapp and Hoogewind (2016) show to undergo little change for future simulated events.

7. Impacts and Insurance

In the United States, the property and agricultural insurance industries, and their policy holders bear the brunt of the financial impacts of hail. Hail damage represents a high percentage of the overall loss for severe convective storm perils (i.e., *tornado*, *outflow wind, and hail*). Annual mean property losses have begun to exceed 10 billion U.S. dollars and severe hail events that impact large cities routinely reach 1 billion U.S. dollars in losses (Gunturi & Tippett, 2017), though these losses do not include the impacts to agriculture. The industry relies on a proper assessment of the annual hail risk to aid in developing financial underwriting tools to help develop risk transfer tools and manage the financial burden of hailstorms. Unfortunately, losses have outpaced advances in detection, forecasting, and mitigation.

Agricultural crop losses are typically related inversely to increasing hailstone size, experiencing greater impact with increased density of hailfall, and depend directly on the length and width of a hail swath (Changnon, 1977; Changnon, 1999; Sánchez et al., 1996). Complicating this different relationship between losses and hail, storms are likely to produce fewer large stones, or large volumes of hail, but tend not to produce both concurrently (Cheng et al., 1985; Fraile et al., 1992; Kumjian et al., 2019). A further issue is posed by the relative importance of the size of hailstones to different areas of exposed risk. To agriculture, a hail stone of 12.5 mm (0.5 in.) or larger could be extremely damaging (Changnon, 1977; Changnon, 1999; Changnon et al., 2002; McMaster, 2001), while typically for structures or vehicles, hailstones of 45 mm (1.75 in.) or greater are necessary to cause large amounts of damage (Cox & Armstrong, 1981; Heymsfield et al., 2014). Agricultural losses have received less attention than property losses, though a extended record of these events is maintained by the USDA (Changnon & Changnon, 2000) and where insurance data is not available can be inferred using proxies (Changnon et al., 2002; Changnon & Changnon, 1997).

Property insurance underwriting for both the wind and hail perils in the United States relies on an assessment of risk and vulnerability. The growth of catastrophe modeling firms have helped provide a science-based approach to understanding risk and determining estimates of annual average loss by peril. Through stochastic simulations, catastrophe models are able to account for basic hazard characteristics, occurrence intervals, and damage severity relationships to examine the long-term probabilistic loss. Severe convective storm catastrophe modeling is relatively young, when compared to tropical cyclones or earthquakes. Models must make use of the historical record of hail observations which are more prone to inherent biases (e.g. Allen et al., 2017; Allen & Allen, 2016; Allen & Tippett, 2015; Groenemeijer et al., 2017). The perils are also much smaller in spatial scale relative to other hazards considered by insurers. Some firms have taken a novel approach of using supplemental data sets (i.e., National Lightning Detection Network, satellite- and radar-based algorithms, etc.) as a proxy for the true occurrence of severe weather to overcome the observational limits and spatial biases of the historical record. The combination of hazard functions to estimate damage probabilities and severities, and property insurance claims are applied to tune the model output and account for knowledge gaps.

The loss statistics provide a financial risk management tool to determine how to appropriately price hail risk. Individual companies may evaluate this based upon their own respective portfolios. In the United States, regulatory controls on pricing are often determined at the state government level, which can places limits on pricing relative to the true nature of the risk. However, credits or incentives for the use of enhanced building materials to help mitigate loss can be mandated through regulatory controls. In some instances, primary property insurance carriers may offer credits beyond those mandated or offer incentives in locations that do not require them. There is wide variability in these programs, the amount of incentivization, and the ability to help offset the added cost of more impact resistant materials. The lack of quality data that describes building attributes and performance from real-world events makes it difficult to accurately assess the cost benefit of more resilient materials compared to the annual probability of hail occurrence.

The property losses, resulting from hailstorms in the United States, are driven in the majority by automobiles and roof cover replacements. While hail mitigation guidance has lagged behind loss trends, the advance of forecasting for severe storms should help reduce auto loss. Additional lead time, through improved forecasting, could allow people to take steps to protect their vehicles. This can already be seen by a recent trend in lower event automobile losses for nocturnal hail events compared to daytime storms. For nocturnal events a

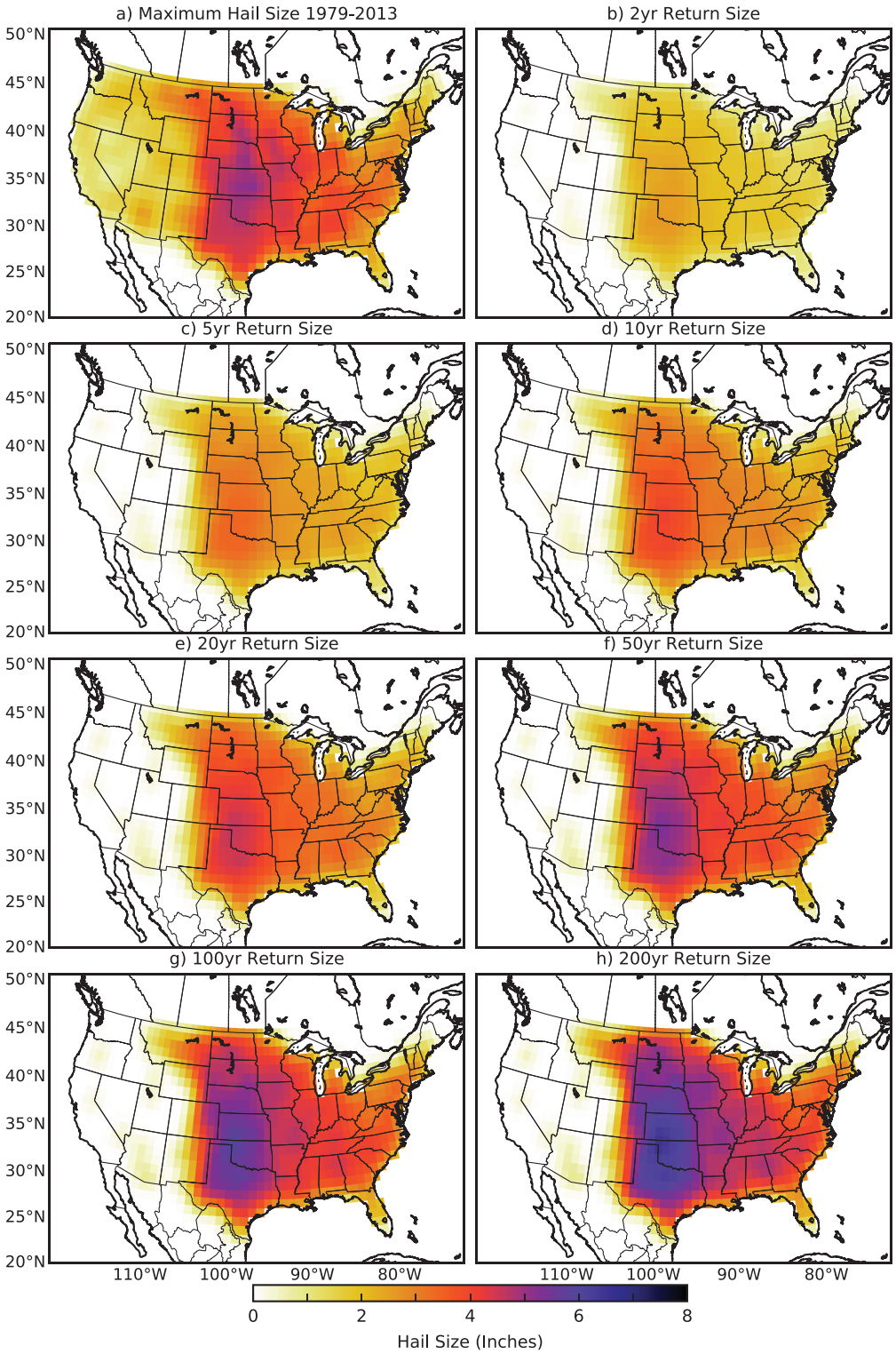

Figure 22. Hail return sizes as derived from Gaussian kernel smoothing of the raw Gumbel return values using a 1.00 sigma bandwidth. (a) Maximum observed hail size for each grid point during 1979–2013. Modeled return hail sizes are shown at the (b) 2-, (c) 5-, (d) 10-, (e) 20-, (f) 50-, (g) 100-, and (h) 200-year intervals, for points with at least 30 annual maxima on the 1 × 1 grid. Adopted from (Allen et al., 2017), their Figure 9). Copyright American Meteorological Society. Used with permission of the author.

statistically significant percentage of vehicles are protected in garages (B. Wood, personal communication, May 19, 2017).

Damage to building roof cover in the United States represents nearly 70% of property insurance claims (excluding automobile) in a typical hail event and is the dominant loss driver (Brown et al., 2015). While damage to wall cover, components, and cladding, and other attached features (i.e., HVAC units, vents, and carports) certainly occurs, it represents a much smaller fraction of total loss. In the United States, asphalt composition shingles make up over 75% of the residential roof cover market (National Association of Home Builders 2016). Asphalt shingles are highly susceptible to damage from hailstone impacts. The asphalt compounds, which make up the shingle mat can also degrade, sometimes rapidly, as the material ages. If the underlying materials are exposed to ultraviolet radiation this degradation will occur more rapidly making the material more brittle and increasing the potential for hail damage in a future event and/or water intrusion (Barth, 1962; Greenfeld, 1969; Morrison, 1999). Hail impacts are efficient at removing surface granules and exposing the underlying asphalt compound, which combined with the aging and weathering of shingles reduces the hail size threshold at which damage occurs. In general, hail begins to causes sensible damage to asphalt singles at sizes between 25 and 38 mm (1–1.5 in.) (Koonz, 1991; Morrison, 1999; Noon, 2000). While impact-resistant asphalt shingle products are available in most U.S. markets, there are large concerns regarding the test protocols that determine their ratings. In addition, their real-world performance capability is questionable relative to event frequencies (Brown et al., 2015). In other regions of the world, where different roof cover materials are more prevalent, (i.e., concrete tile, clay tile, wood shake, etc.) damage to wall components and cladding contribute to a larger percentage of the total loss.

Understanding the frequency of the underlying hail hazard is a critical element of appreciating overall insured risk and exposure. Recently, Allen et al. (2017) assessed the characteristics of hail size over the United States and used this data set to extrapolate return levels for hail size over the continent. These estimates reliably suggested that assuming stationarity within hail climatology, the central Unites States experiences golf ball hail (45 mm/1.75 in. or greater) every 1 to 2 years and 75 mm (3 in.) hail every 10 years, while the eastern United States is exposed to 75 mm (3 in.) hail on a 20 to 50 year interval (Figure 22). An implication of this result is that the threat of damaging hail may be to some extent underestimated when considered for business decisions, as the modeling approach was conservative.

In Europe, the situation is similar to the Unites States, and the insurance industry has shown growing interest in hail research in the context of regulatory requirements in form of the EU solvency II directive of 2009. Insurance intermediaries, catastrophe-modeling firms and (re)insurers themselves have hence cooperated with academic institutions in order to quantify their risk (e.g., Punge et al., 2014; Puskeiler et al., 2016). Key components of resulting hail risk models are the spatial extent (length, width, and angle) and severity (hailstone size and energy) of individual hailstorms that are important for the event loss (Hohl et al., 2002; Hohl et al., 2002). Events are often delimited as aggregated loss over 72 hr for each insurer, which can be important for reinsurance contracting conditions, and hence, clusters of hailstorms should be taken into account. Severe hail events in 2013 (Andreas, 27–28 July) and 2014 (Ela/Pentecost storm, 7–11 June) caused damage of several billion Euros, further increasing awareness of hail risk in the insurance market. In some regions of Central Europe, hail is the costliest natural hazard (e.g., Schemm et al., 2016). A large part of hail damage occurs to residential buildings. Since their vulnerability has been found to increase over recent decades, the federation of Swiss fire insurers has started *Hagelregister.ch*, a database of certified hail resistant building materials and seeks to coordinate these prevention efforts with the construction sector across the Alpine region.

8. Discussion and Future Directions

Though the basic mechanisms of hail formation and growth in convective storms are understood, there still remain many questions about formation of extreme hail occurrences (e.g., Knight & Knight, 2001). For example, the reasons that some storms produce large amounts of smaller hail (Kalina et al., 2016; Kumjian et al., 2019; Kumjian & Lebo, 2016), whereas others produce gigantic hail (Blair et al., 2011; Knight & Knight, 2005; Witt et al., 2018) are unknown. Furthermore, environmental controls on storm structures and behaviors that lead to hail formation are only recently starting to be explored (Dennis & Kumjian, 2017; Grant & van den Heever, 2014). The importance of aerosol loading effects on hail production and growth are highly uncertain (Lebo, 2018; Lebo et al., 2012).

One of the limiting factors in understanding the mechanisms of hailstorms is the sparsity of direct in situ measurements of hailstone properties and hail size both within the cloud and at the ground, as well as hailstone terminal velocities and kinetic energies. New technologies such as 3-D scanning and printing have fostered new experimental research using printed hailstones placed in a vertical wind tunnel to evaluate the aerodynamics of hail, and similar opportunities exist for the use of techniques such as 3-D photogrammetry (e.g. Seimon et al., 2016). The relative infrequency of quality hail observations also affects our understanding of climatological hail occurrence. There is a growing need to expand observational records for example, either via community involvement (Reges et al., 2016), or using crowd-sourced observations (Barras et al., 2019; Elmore et al., 2014; Holzer et al., 2017; Seimon et al., 2016; Witt et al., 2018). This accompanied by a growing demand for improving the quality of existing hail observations to include multiple attributes beyond the current solely text comma separated variable format of storm data and including visual records (Allen et al., 2017; Allen & Tippett, 2015; Blair et al., 2017). This includes moving forward and expanding efforts to sample hailstones in the field (e.g. Giammanco et al., 2017) and capturing comprehensive analyses of their dimensional properties to provide guidance for theoretical studies, developments in numerical modeling, and radar detection along with contributing toward improving building materials.

Given the rising costs of hailstorms, and the significant hail research questions related to microphysics and hail growth that remain, there is the need for the next generation of storm-penetrating aircraft to be developed following the retirement of the T28. Such aircraft will be critical for quantification of particle size distributions, thunderstorm electrification, and wind flow characteristics in storms to better understand how hail develops. A retired military A-10 Warthog was identified and acquired several years ago by the United States Naval Post-Graduate School, with funding support also from the National Science Foundation. However, the outfit of this aircraft for storm-penetration has been recently canceled due to funding constraints to outfit the aircraft with a better de-icing system (A. Heymsfield, personal communication, November 8, 2018). This lack of a suitable aircraft platform leaves a significant gap in our observational capabilities of hail-producing thunderstorms, and one that is not simple to resolve.

Many opportunities exist to better leverage remote sensing techniques from both a forecast and a climatological record perspective. How we estimate hail size from radar data remains a challenging problem. A comprehensive study of the relationship between the TBSS manifestation in all polarimetric and Doppler measurements and hail size is needed. For example, a scattering of radar sidelobe radiation off hail cores also requires comprehensive studies of the reliability of this signature have yet to be undertaken. Other features with potential to provide skill for diagnosing hail size include the bounded weak echo region (BWER (Figure, 15); Marwitz, 1972) in Z_H or Z_{DR} columns (Kumjian et al., 2014); however, more research is needed. A major limiting factor of all of these indirect diagnoses of hail size based on storm intensity is that they are necessarily empirical. Thus, empirical relationships developed in one region may not be applicable outside the region of development, or indeed globally without also including physical quantities that do not vary. Additionally, detection and quantification of features aloft in storms are often limited by operational sampling strategies, which tend to prioritize scanning at lower levels, and distance from the radar to the storm, which affects the resolution of the observations. Radar also provides an excellent methodology to obtain a proxy representation of hail swath data which has seen increasingly wide application around the world (e.g. Cintineo et al., 2012; Lukach et al., 2017; Nisi et al., 2016; Ortega, 2018; Puskeiler et al., 2016; Soderholm et al., 2017a). Given the extending length of climatologies of this kind, it is likely that the radar-derived occurrence will play an important role in defining climatological frequency in the years to come, and in providing a climate quality record that is independent of the problematic surface observations.

Satellite-derived techniques have evolved to also address the limitations of in situ observations (e.g., Bedka et al., 2010; Bedka, Murillo, et al., 2018; Punge et al., 2017). However, these techniques remain a proxy measurement for hail that is not necessarily well correlated with observed hail at the surface, though appears to often capture the more intense storms (Cecil & Blankenship, 2012; Ferraro et al., 2015; Bedka et al., 2018). While the potential for these techniques to assist in operational nowcasting is clear, there is also a role to play in providing global estimates of hail frequency (e.g. Bang & Cecil, 2019; Cecil & Blankenship, 2012; Mroz et al., 2017; Ni, Liu, et al., 2017), either using updraft characteristics or combining these with environmental parameters (e.g., Bedka, Allen, et al., 2018; Punge et al., 2017). However, the relatively short longevity of some of these observation platforms and continual updates of sensors mean that, while satellites can provide a picture of estimated occurrence, their potential for application as a long-term record of hail observations is limited.

Driven by the lack of direct surface observations, forecast parameters for hail are not specifically optimized and have not taken the latest evolutions in our physical understanding of hail into account. This is particularly the case for hail size. Forecast parameters primarily center around some combination of thermodynamic instability and vertical wind shear, though the ideal choice for this type of relationship remains unclear (e.g. Johnson & Sugden, 2014; Kunz et al., 2017). There remains a significant need for large data set analysis to explore forecast parameters for hail and hail size and identify regional differences between their formative environments. Applications of machine learning to this problem appear to be a promising avenue, provided a sufficiently large reliable sample of hail observations can be developed in order to leverage the statistical power of these techniques (e.g. Czernecki et al., 2019; Gagne et al., 2017; Gagne et al., 2019; McGovern et al., 2017).

Much of the underlying climatology that drives our understanding of when and where hailstorms occur over the Unites States centers around the early studies of Stanley Changnon (e.g. Changnon, 1977; Changnon, 1999; Changnon & Changnon, 1997; Changnon & Changnon, 2000), with only relatively limited climatologies of these events in the years since (Allen et al., 2015a; Allen & Tippett, 2015; Cintineo et al., 2012; Doswell et al., 2005). Over Europe, many of the climatologies to date have been regional (e.g. Mohr, Kunz, & Keuler, 2015; Sánchez, Marcos, et al., 2009), though more recent studies have pushed toward continental scale analyses (e.g. Mohr, Kunz, & Geyer, 2015; Rädler et al., 2018). Similar country-centric or regional analyses have also demonstrated occurrence over China (e.g. Zhang et al., 2017)s, Australia (e.g. Soderholm et al., 2017a), and South America (e.g. Martins et al., 2017). While interest internationally is growing, there is a need to better understand the global distribution of hailstorms, and a need to use environmental proxies and or remote sensing methods to establish this underlying frequency and expectations, building on recent work by Prein and Holland (2018) and Ni, Liu, et al. (2017). This understanding is necessary to appreciate the potential risks associated with hail, and provide underpinning for studies of the role of climate variability in modulating hail frequency, and the potential implications of a changing climate (Allen, 2018). While work has begun to address these questions (Brimelow et al., 2017; Mahoney et al., 2012; Púčik et al., 2017; Trapp et al., 2019), there is an increasing need to understand how this change will influence the hail experienced worldwide.

Finally, we note that a greater synergy is needed that ties the progress being made by the research and operational communities to the insurance industry. Hail can have remarkable impacts both in terms of losses and impacts to society, and yet research has not always been directed toward answering the fundamental questions needed to inform business decisions. Understanding how these threats exist presently, or potentially evolve into the future in terms of societal impact is also a necessary direction, similar to work that has been done for tornadoes (Strader et al., 2017). In addition to providing this context, there is also room for enhancements to mitigate the impacts of hail, for example, by using advancements in hail forecasting and nowcasting to alert insured individuals of an impending threat in order to promote sheltering their vehicle, thereby reducing loss. Even a small mitigative improvement like this when applied to a large population center would stand to substantially diminish potential losses.

Acknowledgments
This material is based upon work supported by the National Science Foundation under Grant AGS-1855054 (J. Allen and M. Kumjian). Q. Zhang was supported by the Chinese National Science Foundation (Grant 41330421). P. Groenemeijer's contribution was carried out within the project ARCS, funded by the German Federal Ministry of Education and Research (BMBF) under Grant 01LP1525A and by Munich Re. H. J. Punge is supported by the Willis Research Network. We thank A. Rädler for her permission to include Figure 18, and Skylar Williams (CIMMS/NSSL) for her contribution of the MESH composite climatology (Figure 16, data used are available from https://doi.org/10.7910/DVN/TOUBMM). The authors are grateful to the respective authors who contributed figures that provide the context for this review. Data used in Figures 3–5 are available from the Institute for Home and Business Safety (https://ibhs.org/risk-research/hail/). Data and code to reproduce Figure 10 are available online (https://doi.org/10.7910/DVN/BBJN5O). Data for Figure 11 are sourced from the European Severe Weather Dataset (ESWD) available online (https://eswd.eu). Data for Figure 15 are available directly online (https://www.ncdc.noaa.gov/nexradinv/index.jsp). We are grateful to the authors who consented to the inclusion of figures from published work, and all relevant copyrights are described for the relevant figures.

References

Abshaev, M. T., Malkarova, A. M., Borisova, N. A. (2009). Zoning of the territory by hail, *Tech. Rep. RD 52.37.722-2009*, Federal Service for Hydrometeorology and environmental monitoring (ROSHYDROMET), Nalchik, (in Russian).

Achenbach, E. (1972). Experiments on the flow past spheres at very high Reynolds Numbers. *Journal of Fluid Mechanics*, *54*(3), 565–575. https://doi.org/10.1017/S0022112072000874

Achenbach, E. (1974). The effects of surface roughness and tunnel blockage on the flow past spheres. *Journal of Fluid Mechanics*, *65*(1), 113–125. https://doi.org/10.1017/S0022112074001285

Adams-Selin, R. D., & Ziegler, C. L. (2016). Forecasting hail using a one-dimensional hail growth model within WRF. *Monthly Weather Review*, *144*(12), 4919–4939. https://doi.org/10.1175/MWR-D-16-0027.1

Admirat, P., Goyer, G. G., Wojtiw, L., Carte, E. A., Roos, D., & Lozowki, E. P. (1985). A comparative study of hailstorms in Switzerland, Canada and South Africa. *International Journal of Climatology*, *5*(1), 35–51. https://doi.org/10.1002/joc.3370050104

Allen, J. T. (2018). Climate change and severe thunderstorms. In Dr. Harold Brooks (Ed.), *Oxford Research Encyclopedia of Climate Science* (pp. 1–67). Retrieved from https://doi.org/10.1093/acrefore/9780190228620.013

Allen, J. T. (2019). Replication Data for: Allen et al. (2019) - Understanding hail in the Earth System - Reviews of Geophysics - Figure 10 - Canadian Hail Dataset 1979-2010, *Harvard Dataverse*, available at https://doi.org/10.7910/DVN/BBJN5O

Allen, J. T., & Allen, E. R. (2016). A review of severe thunderstorms in Australia. *Atmospheric Research*, *178*, 347–366.

Allen, J. T., Giammanco, I. M., Kumjian, M. R. , Punge, H. J., Zhang, Q., Groenemeijer, P. , et al. (2019). Replication Data for: Allen et al. (2019) Understanding Hail in the Earth System - Reviews of Geophysics - Figure 16 - MRMS derived Maximum Value of MESH, *Harvard Dataverse*, available at https://doi.org/10.7910/DVN/TOUBMM

Allen, J. T., & Karoly, D. J. (2014). A climatology of Australian severe thunderstorm environments 1979–2011: Inter-annual variability and ENSO influence. *International Journal of Climatology*, *34*(1), 81–97. https://doi.org/10.1002/joc.3667

Allen, J. T., Karoly, D. J., & Mills, G. A. (2011). A severe thunderstorm climatology for Australia and associated thunderstorm environments. *Australian Meteorological and Oceanographic Journal*, *61*(3), 143–158. https://doi.org/10.22499/2.6103.001

Allen, J. T., & Tippett, M. K. (2015). The characteristics of United States hail reports: 1955-2014. *Electronic Journal of Severe Storms Meteorology*, *10*, 1–31.

Allen, J. T., Tippett, M. K., Kaheil, Y., Sobel, A. H., Lepore, C., Nong, S., & Muehlbauer, A. (2017). An extreme value model for United States hail size. *Monthly Weather Review*, *145*(11), 4501–4519. https://doi.org/10.1175/MWR-D-17-0119.1

Allen, J. T., Tippett, M. K., & Sobel, A. H. (2015a). An empirical model relating U.S. monthly hail occurrence to large-scale meteorological environment. *JAMES*, *7*(1), 226–243.

Allen, J. T., Tippett, M. K., & Sobel, A. H. (2015b). Influence of the El Niño/Southern Oscillation on tornado and hail frequency in the United States. *Nature Geoscience*, *8*(4), 278–283. https://doi.org/10.1038/ngeo2385

Amburn, S. A., & Wolf, P. W. (1997). VIL density as a hail indicator, *Wea. Forecast*, *12*(3), 473–478. https://doi.org/10.1175/1520-0434(1997)012<0473:VDAAHI>2.0.CO;2

American Meteorological Society (2017). Hail. Glossary of meteorology. Available online at: http://glossary.ametsoc.org/wiki/hail.

Andreae, M., & Rosenfeld, D. (2008). Aerosol–cloud–precipitation interactions. Part 1. The nature and sources of cloud-active aerosols. *Earth Science Reviews*, *89*(1-2), 13–41. https://doi.org/10.1016/j.earscirev.2008.03.001

Aran, M., Pena, J., & Torà, M. (2011). Atmospheric circulation patterns associated with hail events in Lleida (Catalonia). *Atmospheric Research*, *100*(4), 428–438. https://doi.org/10.1016/j.atmosres.2010.10.029

Arias, C., E. Ramiro, et al. (2010). Recopilación histórica y análisis climatológico de eventos de granizada ocurridos sobre bogotá y su relación con el cambio climático global/historical data collection and climatological analysis of hailstorms events occurring over bogota and its relation to global climate change (PhD Thesis). Bogot, Columbia: Universidad Nacional de Colombia.

Atlas, D., & Wexler, R. (1963). Back-scatter by oblate ice spheroids. *Journal of the Atmospheric Sciences*, *20*(1), 48–61. https://doi.org/10.1175/1520-0469(1963)020<0048:BSBOIS>2.0.CO;2

Aydin, K., Seliga, T. A., & Balaji, V. (1986). Remote sensing of hail with a dual linear polarization radar. *Journal of Climate and Applied Meteorology*, *25*(10), 1475–1484. https://doi.org/10.1175/1520-0450(1986)025<1475:RSOHWA>2.0.CO;2

Aydin, K., Seliga, T. A., & Bringi, V. N. (1984). Differential radar scattering properties of model hail and mixed-phase hydrometeors. *Radio Science*, *19*(1), 58–66. https://doi.org/10.1029/RS019i001p00058

Balakrishnan, N., & Zrnić, D. S. (1990). Use of polarization to characterize precipitation and discriminate large hail. *Journal of the Atmospheric Sciences*, *47*(13), 1525–1540. https://doi.org/10.1175/1520-0469(1990)047<1525:UOPTCP>2.0.CO;2

Bang, S. D., & Cecil, D. J. (2019). Constructing a multifrequency passive microwave hail retrieval and climatology in the GPM domain. *Journal of Applied Meteorology and Climatology*, *58*(9), 1889–1904. https://doi.org/10.1175/JAMC-D-19-0042.1

Barge, B., & Isaac, G. (1973). The shape of Alberta hailstones. *Journal de Recherches Atmospheriques*, *7*(1), 11–20.

Barras, H., Hering, A., Martynov, A., Noti, P.-A., Germann, U., & Martius, O. (2019). Experiences with >50,000 crowd-sourced hail reports in Switzerland. *Bulletin of the American Meteorological Society*, *100*(8), 1429–1440. https://doi.org/10.1175/BAMS-D-18-0090.1

Barrett, B. S., & Gensini, V. A. (2013). Variability of central United States April–May tornado day likelihood by phase of the Madden-Julian Oscillation. *Geophysical Research Letters*, *40*, 2790–2795. https://doi.org/10.1002/grl.50522

Barrett, B. S., & Henley, B. N. (2015). Intraseasonal variability of hail in the contiguous United States: Relationship to the Madden–Julian Oscillation. *Monthly Weather Review*, *143*(4), 1086–1103. https://doi.org/10.1175/MWR-D-14-00257.1

Barth, E. J. (1962). *Asphalt: Science and Technology* (p. 700). New York, New York: Gordon and Breach Scientific Publishers.

Basara, J. B., Cheresnick, D. R., Mitchell, D., & Illston, B. G. (2007). An analysis of severe hail swaths in the southern plains of the United States. *Transactions in GIS*, *11*(4), 531–554. https://doi.org/10.1111/j.1467-9671.2007.01059.x

Bedka, K., Allen, J., Punge, H., & Kunz, M. (2018). A long-term overshooting convective cloud top detection database over Australia derived from MTSAT Japanese advanced meteorological imager observ. *Journal of Applied Meteorology and Climatology*, *57*(4), 937–951. https://doi.org/10.1175/JAMC-D-17-0056.1

Bedka, K., Brunner, J., Dworak, R., Feltz, W., Otkin, J., & Greenwald, T. (2010). Objective satellite-based detection of overshooting tops using infrared window channel brightness temperature gradients. *Journal of Applied Meteorology and Climatology*, *49*(2), 181–202. https://doi.org/10.1175/2009JAMC2286.1

Bedka, K., Murillo, E., Homeyer, C. R., Scarino, B., & Mersiovsky, H. (2018). The above anvil cirrus plume: An important severe weather indicator in visible and infrared satellite imagery. *Weather and Forecasting*, *33*(5), 1159–1181. https://doi.org/10.1175/WAF-D-18-0040.1

Bell, J. R., & Molthan, A. L. (2016). Evaluation of approaches to identifying hail damage to crop vegetation using satellite imagery. *J. Oper. Meteor.*, *4*(11).

Berthet, C., Dessens, J., & Sanchez, J. (2011). Regional and yearly variations of hail frequency and intensity in France. *Atmospheric Research*, *100*(4), 391–400. https://doi.org/10.1016/j.atmosres.2010.10.008

Berthet, C., Wesolek, E., Dessens, J., & Sanchez, J. (2013). Extreme hail day climatology in southwestern France. *Atmospheric Research*, *123*, 139–150. https://doi.org/10.1016/j.atmosres.2012.10.007

Bilhelm, E.-G., & Relf, E.-F. (1937). The dynamics of large hailstones. *Quarterly Journal of the Royal Meteorological Society*, *88*, 117–135.

Billet, J., DeLisi, M., & Smith, B. G. (1997). Use of regression techniques to predict hail size and the probability of large hail. *Weather and Forecasting*, *12*(1), 154–164. https://doi.org/10.1175/1520-0434(1997)012<0154:UORTTP>2.0.CO;2

Blair, S., Cavanaugh, D. E., Laflin, J., Leighton, J., Sanders, K. (2014). High-resolution hail observations: Implications for NWS warning operations and climatological data., in *26th Conf. on Weather Analysis and Forecasting, Atlanta, GA*. Boston, MA: Amer. Meteor. Soc.

Blair, S. F., Deroche, D. R., Boustead, J. M., Leighton, J. W., Barjenbruch, B. L., & Gargan, W. P. (2011). A radar-based assessment of the detectability of giant hail. *Electronic Journal of Severe Storms Meteorology*, *6*(7).

Blair, S. F., Laflin, J. M., Cavanaugh, D. E., Sanders, K. J., Currens, S. R., Pullin, J. I., et al. (2017). High-resolution hail observations: Implications for NWS warning operations. *Weather and Forecasting*, *32*(3), 1101–1119. https://doi.org/10.1175/WAF-D-16-0203.1

Blair, S. F., & Leighton, J. W. (2012). Creating high-resolution hail datasets using social media and post-storm ground surveys. *Electronic Journal Oper. Meteor*, *13*(3), 32–45.

Blamey, R., Middleton, C., Lennard, C., & Reason, C. (2017). A climatology of potential severe convective environments across South Africa. *Climate Dynamics*, *49*(5-6), 2161–2178. https://doi.org/10.1007/s00382-016-3434-7

Bohren, C. F., & Battan, L. J. (1982). Radar backscattering of microwaves by spongy ice spheres. *Journal of the Atmospheric Sciences*, *39*(11), 2623–2628. https://doi.org/10.1175/1520-0469(1982)039<2623:RBOMBS>2.0.CO;2

BOM (2017). Bureau of Meteorology Severe Thunderstorm Archive. Retrieved from http://www.bom.gov.au/australia/stormarchive/ Accessed: 25th November 2015.

Brimelow, J. (2018). Hail and hailstorms. *Oxford Research Encyclopedia of Climate Science*. https://doi.org/10.1093/acrefore/9780190228620.013.666

Brimelow, J. C., Burrows, W. R., & Hanesiak, J. M. (2017). The changing hail threat over North America in response to anthropogenic climate change. *Nature Climate Change*, *7*(7), 516–522. https://doi.org/10.1038/nclimate3321

Brimelow, J. C., Reuter, G. W., Goodson, R., & Krauss, T. W. (2006). Spatial forecasts of maximum hail size using prognostic model soundings and HAILCAST. *Weather and Forecasting*, *21*(2), 206–219. https://doi.org/10.1175/WAF915.1

Brimelow, J. C., Reuter, G. W., & Poolman, E. R. (2002). Modeling maximum hail size in Alberta thunderstorms. *Weather and Forecasting*, *17*(5), 1048–1062. https://doi.org/10.1175/1520-0434(2002)017<1048:MMHSIA>2.0.CO;2

Bringi, V. N., & Chandrasekar, V. (2001). *Polarimetric Doppler weather radar* (1st ed., p. 636). Cambridge, UK: Cambridge University Press, DOI: https://doi.org/10.1017/CBO9780511541094.

Bringi, V. N., Liu, L., Kennedy, P. C., Chandrasekar, V., & Rutledge, S. A. (1996). Dual multiparameter radar observations of intense convective storms: The 24 June 1992 case study. *Meteorology and Atmospheric Physics*, *59*(1-2), 3–31. https://doi.org/10.1007/BF01031999

Bringi, V. N., Seliga, T. A., & Aydin, K. (1984). Hail detection with a differential reflectivity radar. *Science*, *225*(4667), 1145–1147. https://doi.org/10.1126/science.225.4667.1145

Brock, F. V., Crawford, K. C., Elliot, R. L., Cuperus, G. W., Stadler, S. J., Johnson, H. L., & Elits, M. D. (1995). The Oklahoma mesonet: A technical review. *Journal of Atmospheric and Oceanic Technology*, *12*(1), 5–19. https://doi.org/10.1175/1520-0426(1995)012<0005:TOMATO>2.0.CO;2

Brooks, H. E. (2013). Severe thunderstorms and climate change. *Atmospheric Research*, *123*, 129–138. https://doi.org/10.1016/j.atmosres.2012.04.002

Brooks, H. E., Lee, J. W., & Craven, J. P. (2003). The spatial distribution of severe thunderstorm and tornado environments from global reanalysis data. *Atmospheric Research*, *67-68*, 73–94. https://doi.org/10.1016/S0169-8095(03)00045-0

Brown, T., & Giammanco, I. (2013). IBHS multi-faceted hail research program. *RCI*, *31*, 5–8.

Brown, T. M., Pogorzelski, W. H., & Giammanco, I. M. (2015). Evaluating hail damage using property insurance claims data. *Weather and Climate Extremes*, *7*(3), 197–210. https://doi.org/10.1175/WCAS-D-15-0011.1

Browning, K. (1963). The growth of large hail within a steady updraught. *Quarterly Journal of the Royal Meteorological Society*, *89*(382), 490–506. https://doi.org/10.1002/qj.49708938206

Browning, K. (1977). The structure and mechanisms of hailstorms. In *Hail: A Review of Hail Science and Hail Suppression* (pp. 1–47). Boston, MA: American Meteorological Society. https://doi.org/10.1007/978-1-935704-30-0_1

Browning, K., & Foote, G. (1976). Airflow and hail growth in supercell storms and some implications for hail suppression. *Quarterly Journal of the Royal Meteorological Society*, *102*(433), 499–533. https://doi.org/10.1002/qj.49710243303

Browning, K. A. (1964). Airflow and precipitation trajectories with severe local storms which travel to the right of the winds. *Journal of the Atmospheric Sciences*, *21*(6), 634–639. https://doi.org/10.1175/1520-0469(1964)021<0634:AAPTWS>2.0.CO;2

Browning, K. A. (1966). The lobe structure of giant hailstones. *Quarterly Journal of the Royal Meteorological Society*, *92*(391), 1–14. https://doi.org/10.1002/qj.49709239102

Browning, K. A., & Beimers, J. G. (1967). The oblateness of large hailstones. *Journal of Applied Meteorology*, *6*(6), 1075–1081. https://doi.org/10.1175/1520-0450(1967)006<1075:TOOLH>2.0.CO;2

Burcea, S., Cică, R., & Bojariu, R. (2016). Hail climatology and trends in Romania: 1961–2014. *Monthly Weather Review*, *144*(11), 4289–4299. https://doi.org/10.1175/MWR-D-16-0126.1

Bussmann, S., Willmot, K., Hewitt, E., Hoemier, N., & Kubicek, A. (2017). Ground-based hail, rain, and wind sensor networks operating in real-time, in *Special Symposium on Meteorological Observations and Instrumentation, 97th American Meteorological Society Meeting*, Amer. Meteor. Soc., Seatle, WA.

Carbone, R., Atlas, D., Eccles, P., Fetter, R., & Mueller, E. (1973). Dual-wavelength radar hail detection. *Bulletin of the American Meteorological Society*, *54*(9), 921–924. https://doi.org/10.1175/1520-0477(1973)054<0921:DWRHD>2.0.CO;2

Carrió, G. G., Cotton, W. R., & Loftus, A. (2014). On the response of hailstorms to enhanced CCN concentrations. *Atmospheric Research*, *143*, 342–350. https://doi.org/10.1016/j.atmosres.2014.03.002

Carte, A., & Kidder, R. (1966). Transvaal hailstones. *Quarterly Journal of the Royal Meteorological Society*, *92*(393), 382–391. https://doi.org/10.1002/qj.49709239307

Cazac, V., Daradur, M., Leah, T., & Pandey, R. (2017). Effects of hail suppression operational programs on hail frequency and environment in Moldova. *Present Environment and Sustainable Development*, *11*(1), 141–150. https://doi.org/10.1515/pesd-2017-0013

Cecil, D. J. (2009). Passive microwave brightness temperatures as proxies for hailstorms. *Journal of Applied Meteorology and Climatology*, *48*(6), 1281–1286. https://doi.org/10.1175/2009JAMC2125.1

Cecil, D. J., & Blankenship, C. B. (2012). Toward a global climatology of severe hailstorms as estimated by satellite passive microwave imagers, *J. Journal Climate*, *25*(2), 687–703. https://doi.org/10.1175/JCLI-D-11-00130.1

Changnon, D., & Changnon, S. A. (1997). Surrogate data to estimate crop-hail loss. *Journal of Applied Meteorology*, *36*(9), 1202–1210. https://doi.org/10.1175/1520-0450(1997)036<1202:SDTECH>2.0.CO;2

Changnon, D., Changnon, S. A., & Changnon, S. S. (2002). A method for estimating crop losses from hail in uninsured periods and regions. *Journal of Applied Meteorology*, *40*(1), 84–91.

Changnon, S. A. (1966). Note on recording hail incidences. *Journal of Applied Meteorology*, *5*(6), 899–901. https://doi.org/10.1175/1520-0450(1966)005<0899:NORHI>2.0.CO;2

Changnon, S. A. (1977). The scales of hail. *Journal of Applied Meteorology*, *16*(6), 626–648. https://doi.org/10.1175/1520-0450(1977)016<0626:TSOH>2.0.CO;2

Changnon, S. A. (1999). Data and approaches for determining hail risk in the contiguous United States. *Journal of Applied Meteorology*, *38*(12), 1730–1739. https://doi.org/10.1175/1520-0450(1999)038<1730:DAAFDH>2.0.CO;2

Changnon, S. A., & Changnon, D. (2000). Long-term fluctuations in hail incidences in the United States. *Journal of Climate*, *13*(3), 658–664. https://doi.org/10.1175/1520-0442(2000)013<0658:LTFIHI>2.0.CO;2

Cheng, L., English, M., & Wong, R. (1985). Hailstone size distributions and their relationship to storm thermodynamics. *Journal of Climate and Applied Meteorology*, *24*(10), 1059–1067. https://doi.org/10.1175/1520-0450(1985)024<1059:HSDATR>2.0.CO;2

China Meteorological Administration (2003). *Handbook of surface meteorological observation (in Chinese)* (p. 151). Beijing, China: China Meteorological Press.

Cintineo, J. L., Smith, T. M., Lakshmanan, V., Brooks, H. E., & Ortega, K. L. (2012). An objective high-resolution hail climatology of the contiguous United States. *Weather and Forecasting*, *27*(5), 1235–1248. https://doi.org/10.1175/WAF-D-11-00151.1

Cober, S. G., & List, R. (1993). Measurements of the heat and mass transfer parameters characterizing conical graupel growth. *Journal of the Atmospheric Sciences*, *50*(11), 1591–1609. https://doi.org/10.1175/1520-0469(1993)050<1591:MOTHAM>2.0.CO;2

Conway, J. W., & Zrnić, D. S. (1993). A study of embryo production and hail growth using dual-Doppler and multiparameter radars. *Monthly Weather Review*, *121*(9), 2511–2528. https://doi.org/10.1175/1520-0493(1993)121<2511:ASOEPA>2.0.CO;2

Cook, A. R., Leslie, L. M., Parsons, D. B., & Schaefer, J. T. (2017). The impact of the El Niño Southern Oscillation (ENSO) on winter and early spring US tornado outbreaks. *Journal of Applied Meteorology and Climatology*, *56*(9), 2455–2478. https://doi.org/10.1175/JAMC-D-16-0249.1

Cook, A. R., & Schaefer, J. T. (2008). The relation of El Niño–Southern Oscillation (ENSO) to winter tornado outbreaks. *Monthly Weather Review*, *136*(8), 3121–3137. https://doi.org/10.1175/2007MWR2171.1

Cox, M., & Armstrong, P. R. (1981). A statistical model for the incidence of large hailstones on solar collectors. *Solar Energy*, *26*(2), 97–111. https://doi.org/10.1016/0038-092X(81)90072-4

Creel, S., Segura, C., Quaas, R., Guevara, E., Sanchez, T., Ortiz, G., & Pimentel, C. (2001). *Diagnóstico de peligros e identificación de riesgos de desastres en México,* CENAPRED (Centro Nacional de Prevención de Desastres), (Primera ed.). México: Centro Nacional de Prevencion de Desastres.

Czernecki, B., Taszarek, M., Marosz, M., Półrolniczak, M., Kolendowicz, L., Wyszogrodzki, A., & Szturc, J. (2019). Application of machine learning to large hail prediction-the importance of radar reflectivity, lightning occurrence and convective parameters derived from ERA5. *Atmospheric Research*, *227*, 249–262. https://doi.org/10.1016/j.atmosres.2019.05.010

Dee, D. P., Uppala, S., Simmons, A., Berrisford, P., Poli, P., Kobayashi, S., et al. et al. (2011). The ERA-Interim reanalysis: Configuration and performance of the data assimilation system. *Quarterly Journal of the Royal Meteorological Society*, *137*(656), 553–597. https://doi.org/10.1002/qj.828

Delobbe, L., & Holleman, I. (2006). Uncertainties in radar echo top heights used for hail detection. *Meteorological Applications*, *13*(04), 361–374. https://doi.org/10.1017/S1350482706002374

Dennis, A., Schock, C. A., & Koscielski, A. (1970). Characteristics of hailstorms in western South Dakota. *Journal of Applied Meteorology*, *9*(1), 127–135. https://doi.org/10.1175/1520-0450(1970)009<0127:COHOWS>2.0.CO;2

Dennis, E. J., & Kumjian, M. R. (2017). The impact of vertical wind shear on hail growth in simulated supercells. *Journal of the Atmospheric Sciences*, *74*(3), 641–663. https://doi.org/10.1175/JAS-D-16-0066.1

Depue, T. K., Kennedy, P. C., & Rutledge, S. A. (2007). Performance of the hail differential reflectivity (h_{DR}) polarimetric radar hail indicator. *Journal of Applied Meteorology and Climatology*, *46*(8), 1290–1301. https://doi.org/10.1175/JAM2529.1

Dessens, J., Berthet, C., & Sanchez, J. L. (2015). Change in hailstone size distributions with an increase in the melting level height. *Atmospheric Research*, *158-159*, 245–253. https://doi.org/10.1016/j.atmosres.2014.07.004

Dessens, J., Sánchez, J., Berthet, C., Hermida, L., & Merino, A. (2016). Hail prevention by ground-based silver iodide generators: Results of historical and modern field projects. *Atmospheric Research*, *170*, 98–111. https://doi.org/10.1016/j.atmosres.2015.11.008

Detwiler, A., Scannell, J., Kliche, D., & Williams, S. (2012). Creating the long-term T-28 instrumented research aircraft data archive. *Bulletin of the American Meteorological Society*, *93*(12), 1817–1820. https://doi.org/10.1175/BAMS-D-11-00066.1

Diffenbaugh, N. S., Scherer, M., & Trapp, R. J. (2013). Robust increases in severe thunderstorm environments in response to greenhouse forcing. *Proceedings of National Academy Science (USA)*, *101*, 16,361–16,366.

Donavon, R. A., & Jungbluth, K. A. (2007). Evaluation of a technique for radar identification of large hail across the Upper Midwest and Central Plains of the United States. *Weather and Forecasting*, *22*(2), 244–254. https://doi.org/10.1175/WAF1008.1

Doswell, C. (1982). Thermodynamic analysis procedures at the national severe storms forecast center, in *Conference on Weather Forecasting and Analysis, 9 th, Seattle, WA* (pp. 304–309). Boston, MA: American Meteorological Society.

Doswell, C. A. III, Brooks, H. E., & Kay, M. P. (2005). Climatological estimates of daily local nontornadic severe thunderstorm probability for the United States. *Weather and Forecasting*, *20*(4), 577–595. https://doi.org/10.1175/WAF866.1

Doswell, C. A. III, Brooks, H. E., & Maddox, R. A. (1996). Flash flood forecasting: An ingredients-based methodology. *Weather and Forecasting*, *11*(4), 560–581. https://doi.org/10.1175/1520-0434(1996)011<0560:FFFAIB>2.0.CO;2

Dotzek, N., Groenemeijer, P., Feuerstein, B., & Holzer, A. M. (2009). Overview of ESSL's severe convective storms research using the European Severe Weather Database ESWD. *Atmospheric Research*, *93*(1-3), 575–586. https://doi.org/10.1016/j.atmosres.2008.10.020

Doviak, R. J., & Zrnić, D. S. (1993). *Doppler radar and weather observations*, (2nd ed.p. 562). Academic Press.

Dyson, L., & Pienaar, N. (2017). A hail climatology for South Africa, in European Conference on Severe Storms, Pula, Croatia, 18-22 Sept, 2017. Wessling, Germany and South Africa: European Severe Storms Laboratory (via Copernicus).

Eccel, E., Cau, P., Riemann-Campe, K., & Biasioli, F. (2012). Quantitative hail monitoring in an alpine area: 35-year climatology and links with atmospheric variables. *International Journal of Climatology*, *32*(4), 503–517. https://doi.org/10.1002/joc.2291

Edwards, R., & Thompson, R. L. (1998). Nationwide comparisons of hail size with WSR-88D vertically integrated liquid water and derived thermodynamics sounding data. *Weather and Forecasting*, *13*(2), 277–285. https://doi.org/10.1175/1520-0434(1998)013<0277:NCOHSW>2.0.CO;2

Elmore, K. L., Flamig, Z. L., Lakshmanan, V., Kaney, B. T., Farmer, V., Reeves, H. D., & Rothfusz, L. P. (2014). MPING: Crowd-sourcing weather reports for research. *Bulletin of the American Meteorological Society*, *95*(9), 1335–1342. https://doi.org/10.1175/BAMS-D-13-00014.1

Etkin, D., & Brun, S. E. (1999). A note on Canada's hail climatology: 1977-1993. *International Journal of Climatology*, *19*(12), 1357–1373. https://doi.org/10.1002/(SICI)1097-0088(199910)19:12<1357::AID-JOC422>3.0.CO;2-B

Fabry, F. (2015). *Radar Meteorology Principles and Practice* (1st ed., p. 256). Cambridge, UK: Cambridge University Press. https://doi.org/10.1017/CBO9781107707405

Fan, J., Leung, L. R., Rosenfeld, D., Chen, Q., Li, Z., Zhang, J., & Yan, H. (2013). Microphysical effects determine macrophysical response for aerosol impacts on deep convective clouds. *Proceedings of National Academy Science (USA)*, *110*(48), E4581–E4590. https://doi.org/10.1073/pnas.1316830110

Fan, J., Wang, Y., Rosenfeld, D., & Liu, X. (2016). Review of aerosol–cloud interactions: Mechanisms, significance, and challenges. *Journal of the Atmospheric Sciences*, *73*(11), 4221–4252. https://doi.org/10.1175/JAS-D-16-0037.1

Fan, J., Yuan, T., Comstock, J. M., Ghan, S., Khain, S., Leung, L. R., et al. (2009). Dominant role by vertical wind shear in regulating aerosol effects on deep convective clouds. *Journal of Geophysical Research*, *114*(D22), D22,206. https://doi.org/10.1029/2009JD012352

Farley, R. D., Chen, H., Orville, H. D., & Hjelmfelt, M. R. (2004). Numerical simulation of hail formation in the 28 June 1989 Bismarck thunderstorm: Part ii, cloud seeding results. *Atmospheric Research*, *71*(1-2), 81–113. https://doi.org/10.1016/j.atmosres.2004.03.006

Fawbush, E. J., & Miller, R. C. (1953). A method for forecasting hailstone size at the Earth's surface. *Bulletin of the American Meteorological Society*, *34*(6), 235–244. https://doi.org/10.1175/1520-0477-34.6.235

Federer, B., Thalmann, B., & Jouzel, J. (1982). Stable isotropes in hailstones: Part II: Embryo and hailstone growth in different storms. *Journal of the Atmospheric Sciences*, *39*(6), 1336–1355. https://doi.org/10.1175/1520-0469(1982)039<1336:SIIHPI>2.0.CO;2

Federer, B., Waldvogel, A., Schmid, W., Schiesser, H. H., Hampel, F., Schweingruber, M., et al. (1986). Main Results of Grossversuch IV. *Journal of Applied Meteorology*, *25*(7), 917–957. https://doi.org/10.1175/1520-0450(1986)025<0917:MROGI>2.0.CO;2

Ferraro, R., Beauchamp, J., Cecil, D., & Heymsfield, G. (2015). A prototype hail detection algorithm and hail climatology developed with the advanced microwave sounding unit (AMSU). *Atmospheric Research*, *163*(Supplement C), 24–35. https://doi.org/10.1016/j.atmosres.2014.08.010

Field, P. R., Heymsfield, A. J., Detwiler, A. G., & Wilkinson, J. M. (2019). Normalized hail particle size distributions from the T-28 storm-penetrating aircraft. *Journal of Applied Meteorology and Climatology*, *58*(2), 231–245. https://doi.org/10.1175/JAMC-D-18-0118.1

Flossmann, A. I., M. J. Manton, A. Abshaev, R. Bruintjet, M. Murakami, T. Prabhakaran, and Z. Yao (2018), Peer review report on global precipitation enhancement activities, *Tech. rep*.

Fluck, E. (2018), Hail potential over Western Europe, Ph.D. thesis, Institute of Meteorology and Climate Research, Karlsruhe Institute of Technology (KIT), 140 pp.

FM Approvals (2005), Specification test standard for impact resistance testing of rigid roofing materials by impact with freezer ice balls, *Tech. rep*. West Gloucester, Rhode Island: FM Global, West Gloucester, Rhode Island.

Foote, G. B. (1984). A study of hail growth utilizing observed storm conditions. *Journal of Climate and Applied Meteorology*, *23*(1), 84–101. https://doi.org/10.1175/1520-0450(1984)023<0084:ASOHGU>2.0.CO;2

Foote, G. B., & Knight, C. (1977). *Hail: A review of hail science and hail suppression* (Vol. 16, p. 272). Boston, MA: American Meteorological Society.

Foote, G. B., & Knight, C. A. (1979). Results of a randomized hail supression experiment in northeast Colorado. Part I: Design and conduct of the experiment. *Journal of Applied Meteorology*, *18*.

Foster, D. S., & Bates, F. C. (1956). A hail size forecasting technique. *Bulletin of the American Meteorological Society*, *135–141*.

Fraile, R., Berthet, C., Dessens, J., & Sánchez, J. L. (2003). Return periods of severe hailfalls computed from hailpad data. *Atmospheric Research*, *67-68*(Supplement C), 189–202. https://doi.org/10.1016/S0169-8095(03)00051-6

Fraile, R., Castro, A., & Sánchez, J. (1992). Analysis of hailstone size distributions from a hailpad network. *Atmospheric Research*, *28*(3-4), 311–326.

Frisby, E. M., & Sansom, H. (1967). Hail incidence in the tropics. *Journal of Applied Meteorology*, *6*(2), 339–354. https://doi.org/10.1175/1520-0450(1967)006<0339:HIITT>2.0.CO;2

Gagne, D. J., Haupt, S. E., Nychka, D. W., & Thompson, G. (2019). Interpretable deep learning for spatial analysis of severe hailstorms. *Monthly Weather Review*, *147*(8), 2827–2845. https://doi.org/10.1175/MWR-D-18-0316.1

Gagne, D. J., McGovern, A., Haupt, S. E., Sobash, R. A., Williams, J. K., & Xue, M. (2017). Storm-based probabilistic hail forecasting with machine learning applied to convection-allowing ensembles. *Weather and Forecasting*, *32*(5), 1819–1840. https://doi.org/10.1175/WAF-D-17-0010.1

Gallo, B. T., Clark, A. J., Jirak, I., Kain, J. S., Weiss, S. J., Coniglio, M., et al. (2017). Breaking new ground in severe weather prediction: The 2015 NOAA/Hazardous Weather Testbed spring forecasting experiment. *Weather and Forecasting*, *32*(4), 1541–1568. https://doi.org/10.1175/WAF-D-16-0178.1

Gallo, K., Schumacher, P., Boustead, J., & Ferguson, A. (2019). Validation of satellite observations of storm damage to cropland with digital photographs. *Weather and Forecasting*, *34*(2), 435–446. https://doi.org/10.1175/WAF-D-18-0059.1

García-Ortega, E., Hermida, L., Hierro, R., Merino, A., Gascón, E., Fernández-González, S., et al. (2014). Anomalies, trends and variability in atmospheric fields related to hailstorms in north-eastern Spain. *International Journal of Climatology*, *34*(11), 3251–3263. https://doi.org/10.1002/joc.3910

García-Ortega, E., López, L., & Sánchez, J. (2011). Atmospheric patterns associated with hailstorm days in the Ebro Valley, Spain. *Atmospheric Research*, *100*(4), 401–427. https://doi.org/10.1016/j.atmosres.2010.08.023

Gavrilov, M. B., Marković, S. B., Zorn, M., Komac, B., Lukić, T., Milošević, M., & Janićević, S. (2013). Is hail suppression useful in Serbia? General review and new results. *Acta Geographica Slovenica*, *53*(1), 165–179. https://doi.org/10.3986/AGS53302

Gensini, V. A., & Allen, J. T. (2018). US hail frequency and the Global Wind Oscillation. *Geophysical Research Letters*, *45*, 1611–1620. https://doi.org/10.1002/2017GL076822

Gensini, V. A., & Ashley, W. L. (2011). Climatology of potentially severe convective environments from the North American Regional Reanalysis. *Electronic Journal of Severe Storms Meteorology*, *6*, 1–40.

Gensini, V. A., & Marinaro, A. (2016). Tornado frequency in the United States related to global relative angular momentum. *Monthly Weather Review*, *144*(2), 801–810. https://doi.org/10.1175/MWR-D-15-0289.1

Gensini, V. A., & Mote, T. L. (2014). Estimations of hazardous convective weather in the United States using dynamical downscaling. *Journal of Climate*, *27*(17), 6581–6589. https://doi.org/10.1175/JCLI-D-13-00777.1

Gensini, V. A., Ramseyer, C., & Mote, T. L. (2014). Future convective environments using NARCCAP. *International Journal of Climatology*, *34*(5), 1699–1705. https://doi.org/10.1002/joc.3769

Giaiotti, D., Nordio, S., & Stel, F. (2003). The climatology of hail in the plain of Friuli Venezia Giulia. *Atmospheric Research*, *67-68*, 247–259. https://doi.org/10.1016/S0169-8095(03)00084-X

Giammanco, I. M., Brown, T. M., Grant, R. G., Dewey, D. L., Hodel, J. D., & Stumpf, R. A. (2015). Evaluating the hardness characteristics of hail through compressive strength measurements. *Journal of Atmospheric and Oceanic Technology*, *32*(11), 2100–2113. https://doi.org/10.1175/JTECH-D-15-0081.1

Giammanco, I. M., Maiden, B. R., Estes, H. E., & Brown-Giammanco, T. M. (2017). Using 3d laser scanning technology to create digital models of hailstones. *Bulletin of the American Meteorological Society*, *98*(7), 1341–1347. https://doi.org/10.1175/BAMS-D-15-00314.1

Gokhale, N. R. (1975). *Hailstorms and hailstone growth*. Albany, NY: SUNY Press.

Goudenhoofdt, E., & Delobbe, L. (2013). Statistical characteristics of convective storms in Belgium derived from volumetric weather radar observations. *Journal of Applied Meteorology and Climatology*, *52*(4), 918–934. https://doi.org/10.1175/JAMC-D-12-079.1

Goyer, G. (1970), The testing of airborne infrared detection systems for mapping hailswaths and measuring hailfall coverage at the ground. The joint hail research project-summer 1969, summary report (Tech. Rep.). Boulder, CO: NCAR Internal Report.

Grams, J. S., Thompson, R. L., Snively, D. V., Prentice, J. A., Hodges, G. M., & Reames, L. J. (2012). A climatology and comparison of parameters for significant tornado events in the United States. *Weather and Forecasting*, *27*(1), 106–123. https://doi.org/10.1175/WAF-D-11-00008.1

Grant, L. D., & van den Heever, S. C. (2014). Microphysical and dynamical characteristics of low-precipitation and classic supercells. *Journal of the Atmospheric Sciences*, *71*(7), 2604–2624. https://doi.org/10.1175/JAS-D-13-0261.1

Greenfeld, S. H. (1969). Hail resistance of roofing products, *Tech. rep*., National Bureau of Standards, August 1969. Washington DC: US Department of Commerce.

Griffiths, D., Colquhoun, J., Batt, K., & Casinader, T. (1993). Severe thunderstorms in New South Wales: Climatology and means of assessing the impact of climate change. *Climatic Change*, *25*(3-4), 369–388. https://doi.org/10.1007/BF01098382

Groenemeijer, P., Púčik, T., Holzer, A. M., Antonescu, B., Riemann-Campe, K., Schultz, D. M., et al. (2017). Severe convective storms in Europe: Ten years of research and education at the European Severe Storms Laboratory. *Bulletin of the American Meteorological Society*, *98*(12), 2641–2651. https://doi.org/10.1175/BAMS-D-16-0067.1

Groenemeijer, P. H., & van Delden, A. (2007). Sounding-derived parameters associated with large hail and tornadoes in the Netherlands. *Atmospheric Research*, *83*(2-4), 473–487. https://doi.org/10.1016/j.atmosres.2005.08.006

Gunturi, P., & Tippett,M. K. (2017). Managing severe thunderstorm risk: Impact of ENSO on U.S. tornado and hail frequencies (Tech. Rep.). Minneapolis, MN, USA: Willis Re.

Hamberg, H. (1919). *Fréquence de la grêle en Suède 1865–1917*. Almqvist & Wiksells boktryckeri-a.-b. [In French]

Heinselman, P. L., & Ryzhkov, A. V. (2006). Validation of polarimetric hail detection. *Weather and Forecasting*, *21*(5), 839–850. https://doi.org/10.1175/WAF956.1

Herman, B. M., & Battan, L. J. (1961). Calculations of Mie back-scattering from melting ice spheres. *Journal of Meteorology*, *18*(4), 468–478. https://doi.org/10.1175/1520-0469(1961)018<0468:COMBSF>2.0.CO;2

Hermida, L., López, L., Merino, A., Berthet, C., García-Ortega, E., Sánchez, J. L., & Dessens, J. (2015). Hailfall in southwest France: Relationship with precipitation, trends and wavelet analysis. *Atmospheric Research*, *156*, 174–188. https://doi.org/10.1016/j.atmosres.2015.01.005

Heymsfield, A., Szakáll, M., Jost, A., Giammanco, I., & Wright, R. (2018). A comprehensive observational study of graupel and hail terminal velocity, mass flux, and kinetic energy. *Journal of the Atmospheric Sciences*, *75*(11), 3861–3885. https://doi.org/10.1175/JAS-D-18-0035.1

Heymsfield, A. J. (1982). A comparative study of the rates of development of potential graupel and hail embryos in High Plains storms. *Journal of the Atmospheric Sciences*, *39*(12), 2867–2897. https://doi.org/10.1175/1520-0469(1982)039<2867:ACSOTR>2.0.CO;2

Heymsfield, A. J. (1983). Case-study of a hailstorm in Colorado, Part IV: Graupel and hail growth mechanisms deduced through particle trajectory calculations. *Journal of the Atmospheric Sciences*, *40*(6), 1482–1509. https://doi.org/10.1175/1520-0469(1983)040<1482:CSOAHI>2.0.CO;2

Heymsfield, A. J., Giammanco, I. M., & Wright, R. (2014). Terminal velocities and kinetic energies of natural hailstones. *Geophysical Research Letters*, *41*, 8666–8672. https://doi.org/10.1002/2014GL062324

Heymsfield, A. J., & Musil, D. J. (1982). Case study of a hailstorm in Colorado. Part II: Particle growth processes at mid-levels deduced from in-situ measurements. *Journal of the Atmospheric Sciences*, *39*(12), 2847–2866. https://doi.org/10.1175/1520-0469(1982)039<2847:CSOAHI>2.0.CO;2

Heymsfield, A. J., & Wright, R. (2014). Graupel and hail terminal velocities: Does a supercritical Reynolds Number apply. *Journal of the Atmospheric Sciences*, *71*(9), 3392–3403. https://doi.org/10.1175/JAS-D-14-0034.1

Hohl, R., Schiesser, H.-H., & Aller, D. (2002). Hailfall: The relationship between radar-derived hail kinetic energy and hail damage to buildings. *Atmospheric Research*, *63*(3-4), 177–207. https://doi.org/10.1016/S0169-8095(02)00059-5

Hohl, R., Schiesser, H.-H., & Knepper, I. (2002). The use of weather radars to estimate hail damage to automobiles: An exploratory study in switzerland. *Atmospheric Research*, *61*(3), 215–238. https://doi.org/10.1016/S0169-8095(01)00134-X

Holleman, I. (2001). Hail detection using single-polarization radar. Scientific report WR-2001-01 (Tech. Rep.). Amsterdam, NE: Royal Netherlands
Meteorological Institute (KNMI), 74 S.

Holleman, I., Wessels, H. R. A., Onvlee, J. R. A., & Barlag, S. J. M. (2000). Development of a hail-detection-product. *Physics and Chemistry of the Earth B*, *25*(10-12), 1293–1297. https://doi.org/10.1016/S1464-1909(00)00197-0

Holzer, A. M., P. Groenemeijer, K. Riemann-Campe, and B. Antonescu (2017), Experience after 1 year of EWOB, in *European Conference on Severe Storms, Pula, Croatia, 18-22 Sept, 2017*.

Hoogewind, K. A., Baldwin, M. E., & Trapp, R. J. (2017). The impact of climate change on hazardous convective weather in the united states: Insight from high-resolution dynamical downscaling. *Journal of Climate*, *30*(24), 10081–10100. https://doi.org/10.1175/JCLI-D-16-0885.1

Hubbert, J. C., & Bringi, V. N. (2000). The effects of three-body scattering on differential reflectivity signatures. *Journal of Atmospheric and Oceanic Technology*, *17*(1), 51–61. https://doi.org/10.1175/1520-0426(2000)017<0051:TEOTBS>2.0.CO;2

Hubbert, J. C., Bringi, V. N., Carey, L. D., & Bolen, S. (1998). CSU-CHILL polarimetric radar measurements from a severe hail storm in eastern Colorado. *Journal of Applied Meteorology*, *37*(8), 749–775. https://doi.org/10.1175/1520-0450(1998)037<0749:CCPRMF>2.0.CO;2

Huntrieser, H., Schiesser, H. H., Schmid, W., & Waldvogl, A. (1997). Comparison of traditional and newly developed thunderstorm indices for Switzerland. *Weather and Forecasting*, *12*(1), 108–125. https://doi.org/10.1175/1520-0434(1997)012<0108:COTAND>2.0.CO;2

Huuskonen, A., Saltikoff, E., & Holleman, I. (2014). The operational weather radar network in Europe. *Bulletin of the American Meteorological Society*, *95*(6), 897–907. https://doi.org/10.1175/BAMS-D-12-00216.1

Jameson, A. R., & Heymsfield, A. (1980). Hail growth mechanisms in a Colorado hailstorm. Part I: Dual-wavelength radar observations. *Journal of the Atmospheric Sciences*, *37*(8), 1763–1778. https://doi.org/10.1175/1520-0469(1980)037<1763:HGMIAC>2.0.CO;2

Jameson, A. R., & Srivastava, R. (1978). Dual-wavelength Doppler radar observations of hail at vertical incidence. *Journal of Applied Meteorology*, *17*(11), 1694–1703. https://doi.org/10.1175/1520-0450(1978)017<1694:DWDROO>2.0.CO;2

Jamli, J. (2014). Physical analysis of hail fall risk in Iran and the consequent damages on agricultural crops. *Atmospheric Climate Science*, *4*, 919–930.

Jewell, R., & Brimelow, J. (2009). Evaluation of Alberta hail growth model using severe hail proximity soundings from the United States. *Weather and Forecasting*, *24*(6), 1592–1609. https://doi.org/10.1175/2009WAF2222230.1

Jiang, Z., Kumjian, M. R., Schrom, R. S., Giammanco, I., Brown-Giammanco, T., Estes, H., et al. (2018). Comparisons of electromagnetic scattering properties of real hailstones and spheroids. *Journal of Applied Meteorology and Climatology*, *58*, 93–112.

Jin, H.-G., Lee, H., Lkhamjav, J., & Baik, J.-J. (2017). A hail climatology in South Korea. *Atmospheric Research*, *188*, 90–99. https://doi.org/10.1016/j.atmosres.2016.12.013

Johnson, A. W., & Sugden, K. E. (2014). Evaluation of sounding-derived thermodynamic and wind-related parameters associated with large hail events. *Electronic Journal of Severe Storms Meteorology*, *9*(5).

Johnson, G. N., & Smith, P. L. Jr. (1980). Meteorological instrumentation system on the T-28 thunderstorm research aircraft. *Bulletin of the American Meteorological Society*, *61*(9), 972–979. https://doi.org/10.1175/1520-0477(1980)061<0972:MISOTT>2.0.CO;2

Johnson, J. T., MacKeen, P. L., Witt, A., Mitchell, E. D. W., Stumpf, G. J., Eilts, M. D., & Thomas, K. W. (1998). The storm cell identification and tracking algorithm: An enhanced WSR-88D algorithm. *Weather and Forecasting*, *13*(2), 263–276. https://doi.org/10.1175/1520-0434(1998)013<0263:TSCIAT>2.0.CO;2

Junghänel, T., Brendel, C., Winterrath, T., & Walter, A. (2016). Towards a radar-and observation-based hail climatology for Germany. *Meteorologische Zeitschrift*, *25*(4), 435–445.
Kahraman, A., Tilev-Tanriover, Ş., Kadioglu, M., Schultz, D. M., & Markowski, P. M. (2016). Severe hail climatology of Turkey. *Monthly Weather Review*, *144*(1), 337–346. https://doi.org/10.1175/MWR-D-15-0337.1
Kalina, E. A., Friedrich, K., Motta, B. C., Deierling, W., Stano, G. T., & Rydell, N. N. (2016). Colorado plowable hailstorms: Synoptic weather, radar, and lightning characteristics. *Weather and Forecasting*, *31*(2), 663–693. https://doi.org/10.1175/WAF-D-15-0037.1
Kaltenboeck, R., & Ryzhkov, A. V. (2013). Comparison of polarimetric signatures of hail at S and C bands for different hail sizes. *Atmospheric Research*, *123*, 323–336. https://doi.org/10.1016/j.atmosres.2012.05.013
Kapsch, M.-L., Kunz, M., Vitolo, R., & Economou, T. (2012a). Long-term trends of hail-related weather types in an ensemble of regional climate models using a Bayesian approach. *Journal of Geophysical Research*, *117*, D15107.
Kapsch, M.-L., Kunz, M., Vitolo, R., & Economou, T. (2012b). Long-term trends of hail-related weather types in an ensemble of regional climate models using a Bayesian approach. *Journal of Geophysical Research – Atmospheres*, *117*, 1984–2012.
Karlinski, F. (1867-1875), Wykaz miejsc nawiedzonych gradem, *Tech. Rep*. 2 (1867) - 10 (1875), [in Polish].
Kelly, D. L., Schaefer, J. T., & Doswell, C. A. III (1985). Climatology of nontornadic severe thunderstorm events in the United States. *Monthly Weather Review*, *113*(11), 1997–2014. https://doi.org/10.1175/1520-0493(1985)113<1997:CONSTE>2.0.CO;2
Kennedy, P. C., Rutledge, S. A., Petersen, W. A., & Bringi, V. N. (2001). Polarimetric radar observations of hail formation. *Journal of Applied Meteorology*, *40*(8), 1347–1366. https://doi.org/10.1175/1520-0450(2001)040<1347:PROOHF>2.0.CO;2
Khain, A., Rosenfeld, D., Pokrovsky, A., Blahak, U., & Ryzhkov, A. (2011). The role of CCN in precipitation and hail in a mid-latitude storm as seen in simulations using a spectral (bin) microphysics model in a 2D dynamic frame. *Atmospheric Research*, *99*(1), 129–146. https://doi.org/10.1016/j.atmosres.2010.09.015
Kim, H., & Kedward, K.-T. (2000). Modeling hail ice impacts and predicting impact damage initiation in composite structures. *AIAA*, *38*(7), 1278–1288. https://doi.org/10.2514/2.1099
Kitzmiller, D. H., McGovern, W. E., & Saffle, R. F. (1995). The WSR-88D severe weather potential algorithm. *Weather and Forecasting*, *10*(1), 141–159. https://doi.org/10.1175/1520-0434(1995)010<0141:TWSWPA>2.0.CO;2
Knight, C. A. (1968). On the mechanism of spongy hailstone growth. *Journal of the Atmospheric Sciences*, *25*(3), 440–444. https://doi.org/10.1175/1520-0469(1968)025<0440:OTMOSH>2.0.CO;2
Knight, C. A. (1982). The cooperative convective precipitation experiment (CCOPE), 18 May–7 August 1981. *Bulletin of the American Meteorological Society*, *63*(4), 386–398. https://doi.org/10.1175/1520-0477(1982)063<0386:TCCPEM>2.0.CO;2
Knight, C. A., Ehhalt, D. H., Roper, N., & Knight, N. C. (1975). Radial and tangential variation of deuterium in hailstones. *Journal of the Atmospheric Sciences*, *32*(10), 1990–2000. https://doi.org/10.1175/1520-0469(1975)032<1990:RATVOD>2.0.CO;2
Knight, C. A., Foote, G. B., & Summers, P. W. (1979). Results of a randomized hail suppression experiment in northeast colorado. Part IX: Overall discussion and summary in the context of physical research. *Journal of Applied Meteorology*, *18*(12), 1629–1639. https://doi.org/10.1175/1520-0450(1979)018<1629:ROARHS>2.0.CO;2
Knight, C. A., & Knight, N. C. (1970a). Hailstone embryos. *Journal of the Atmospheric Sciences*, *27*(4), 659–666. https://doi.org/10.1175/1520-0469(1970)027<0659:HE>2.0.CO;2
Knight, C. A., & Knight, N. C. (1970b). Lobe structures of hailstones. *Journal of the Atmospheric Sciences*, *27*(4), 667–671. https://doi.org/10.1175/1520-0469(1970)027<0667:LSOH>2.0.CO;2
Knight, C. A., & Knight, N. C. (1979). Results of a randomized hail suppression experiment in northeast Colorado: Part V: Hailstone embryo types. *Journal of Applied Meteorology*, *18*(12), 1583–1588. https://doi.org/10.1175/1520-0450(1979)018<1583:ROARHS>2.0.CO;2
Knight, C. A., & Knight, N. C. (2001). Hailstorms. *Severe Convective Storms, Meteorological Monographs*, *28*, 223–248.
Knight, C. A., & Knight, N. C. (2005). Very large hailstones from Aurora, Nebraska. *Bulletin of the American Meteorological Society*, *86*(12), 1773–1782. https://doi.org/10.1175/BAMS-86-12-1773
Knight, C. A., Schlatter, P. T., & Schlatter, T. W. (2008). An unusual hailstorm on 24 June 2006 in Boulder, Colorado. Part II: Low-density growth of hail. *Monthly Weather Review*, *136*(8), 2833–2848. https://doi.org/10.1175/2008MWR2338.1
Knight, C. A., & Squires, P. (1982). *Hailstorms of the central high plains: The National Hail Research Experiment* (Vol. 1, p. 282). Boulder, CO: University Press of Colorado.
Knight, N. C. (1981). The climatology of hailstone embryos. *Journal of Applied Meteorology*, *20*(7), 750–755. https://doi.org/10.1175/1520-0450(1981)020<0750:TCOHE>2.0.CO;2
Knight, N. C. (1986). Hailstone shape factor and its relation to radar interpretation of hail. *Journal of Climate and Applied Meteorology*, *25*(12), 1956–1958. https://doi.org/10.1175/1520-0450(1986)025<1956:HSFAIR>2.0.CO;2
Kolkowska, K., & Lorenc, H. (2012). Kleski żywiołowe a bezpieczeństwo wewnetrzne kraju - TOM III, chap. Ryzyko występowania gradu w Polsce, Monografie IMGW-PIB, The Institute of Meteorology and Water Management, Państwowy Instytut Badawczy, WARSZAWA pp. 80–97. [In Polish]
Koonz, J. D. (1991). The effects of hail on residential roofing products, third International Symposium on Roofing Technology, National Roofing Contractors Association and National Institute for Standards and Technology, 17-19 April 1991, Gaithersburg, Maryland.
Kumjian, M. R. (2013a). Principles and applications of dual-polarization weather radar. Part I: Description of the polarimetric radar variables. *Journal Operational Meteorology*, *1*(19), 226–242. https://doi.org/10.15191/nwajom.2013.0119
Kumjian, M. R. (2013b). Principles and applications of dual-polarization weather radar. Part II: Warm and cold season applications. *Journal Operational Meteorology*, *1*(20), 243–264. https://doi.org/10.15191/nwajom.2013.0120
Kumjian, M. R. (2013c). Principles and applications of dual-polarization weather radar. Part III: Artifacts. *Journal Operational Meteorology*, *1*(21), 265–274. https://doi.org/10.15191/nwajom.2013.0121
Kumjian, M. R. (2018). Weather radars. In C. Andronache (Ed.), *Remote Sensing of Clouds and Precipitation* (pp. 1–48). Berlin, Germany: Springer. https://doi.org/10.1007/978-3-319-72583-3_2
Kumjian, M. R., Khain, A. P., BenMoshe, N., Ilotoviz, E., Ryzhkov, A. V., & Phillips, V. T. J. (2014). The anatomy and physics of Z_{DR} columns: Investigating a polarimetric radar signature with a spectral bin microphysical model. *Journal of Applied Meteorology and Climatology*, *53*(7), 1820–1843. https://doi.org/10.1175/JAMC-D-13-0354.1
Kumjian, M. R., & Lebo, Z. J. (2016). Large accumulations of small hail, in *28th Conf. on Severe Local Storms*, 8A.4, Amer. Meteor. Soc., Portland, OR.
Kumjian, M. R., Lebo, Z. J., & Ward, A. M. (2019). Storms producing large accumulations of small hail. *Journal of Applied Meteorology and Climatology*, *58*(2), 341–364. https://doi.org/10.1175/JAMC-D-18-0073.1
Kumjian, M. R., Richardson, Y. P., Meyer, T., Kosiba, K. A., & Wurman, J. (2018). Resonance scattering effects in wet hail observed with a dual-X-band-frequency, dual-polarization Doppler on Wheels on radar. *Journal of Applied Meteorology and Climatology*, *57*(12), 2713–2731. https://doi.org/10.1175/JAMC-D-17-0362.1

Kumjian, M. R., & Ryzhkov, A. V. (2008). Polarimetric signatures in supercell thunderstorms. *Journal of Applied Meteorology and Climatology*, *47*(7), 1940–1961. https://doi.org/10.1175/2007JAMC1874.1

Kumjian, M. R., Ryzhkov, A. V., Melnikov, V. M., & Schuur, T. J. (2010). Rapid-scan super-resolution observations of a cyclic supercell with a dual-polarization WSR-88D. *Monthly Weather Review*, *138*(10), 3762–3786. https://doi.org/10.1175/2010MWR3322.1

Kunz, M. (2007). The skill of convective parameters and indices to predict isolated and severe thunderstorms. *Natural Hazards and Earth System Sciences*, *7*(2), 327–342. https://doi.org/10.5194/nhess-7-327-2007

Kunz, M., Fluck, E., Baumstark, S., Wandel, J., Ritz, S., Schemm, S., & Schmidberger, M. (2017). Hail frequency in central Europe estimated from 2D radar data and the relation to atmospheric characteristics, 9th European Conference on Severe Storms (ECSS), 18–22 Sept. 2017, Pula, Croatia. Wessling, Germany: European Severe Storms Laboratory (via Copernicus).

Kunz, M., & Kugel, P. (2015). Detection of hail signatures from 3D C-Band radar reflectivity. *Atmospheric Research*, *153*, 565–577. https://doi.org/10.1016/j.atmosres.2014.09.010

Kunz, M., & Puskeiler, M. (2010). High-resolution assessment of the hail hazard over complex terrain from radar and insurance data. *Meteorologische Zeitschrift*, *19*(5), 427–439. https://doi.org/10.1127/0941-2948/2010/0452

Kunz, M., Sander, J., & Kottmeier, C. (2009). Recent trends of thunderstorm and hailstorm frequency and their relation to atmospheric characteristics in southwest Germany. *International Journal of Climatology*, *29*(15), 2283–2297. https://doi.org/10.1002/joc.1865

Labriola, J., Snook, N., Jung, Y., & Xue, M. (2019). Explicit ensemble prediction of hail in 19 May 2013 Oklahoma City thunderstorms and analysis of hail growth processes with several multi-moment microphysics schemes. *Monthly Weather Review*, *147*(4), 1193–1213. https://doi.org/10.1175/MWR-D-18-0266.1

Lakshmanan, V., Smith, T., Hondl, K., Stumpf, G. J., & Witt, A. (2006). A real-time, three-dimensional, rapidly updating, heterogeneous radar merger technique for reflectivity, velocity, and derived products. *Weather and Forecasting*, *21*(5), 802–823. https://doi.org/10.1175/WAF942.1

Lakshmanan, V., Smith, T., Stumpf, G., & Hondl, K. (2007). The warning decision support system-integrated information. *Weather and Forecasting*, *22*(3), 596–612. https://doi.org/10.1175/WAF1009.1

Lamb, D., & Verlinde, J. (2011). *Physics and chemistry of clouds* (1st ed., p. 584). Cambridge, UK: Cambridge University Press.

Lane, J., Youngquist, R. C., Haskell, W. D., & Cox, R. B. (2006). A hail size distribution impact transducer. *The Journal of the Acoustical Society of America*, *119*, 47–53.

Latrach, M. M. (2013). *La grêle en Tunisie: Diagnostic et gestion d'un risque agricole émergent, Thesis*. Université Paul Valéry - Montpellier III.

Laurie, J. A. P. (1960). Hail and its effects on buildings, *Tech. rep*., Council for Scientific and Industrial Research, Pretoria, South Africa.

Le Roux, N., & Olivier, J. (1996). Modelling hail frequency using a generalized additive interactive technique. *South African Geographical Journal*, *78*(1), 7–12. https://doi.org/10.1080/03736245.1996.9713601

Lebo, Z. J. (2014). The sensitivity of a numerically simulated idealized squall line to the vertical distribution of aerosols. *Journal of the Atmospheric Sciences*, *71*(12), 4581–4596. https://doi.org/10.1175/JAS-D-14-0068.1

Lebo, Z. J. (2018). A numerical investigation of the potential effects of aerosol-induced warming and updraft width and slope on updraft intensity in deep convective clouds. *Journal of the Atmospheric Sciences*, *75*(2), 535–554. https://doi.org/10.1175/JAS-D-16-0368.1

Lebo, Z. J., & Morrison, H. (2014). Dynamical effects of aerosol perturbations on simulated idealized squall lines. *Monthly Weather Review*, *142*(3), 991–1009. https://doi.org/10.1175/MWR-D-13-00156.1

Lebo, Z. J., Morrison, H., & Seinfeld, J. H. (2012). Are simulated aerosol-induced effects on deep convective clouds strongly dependent on saturation adjustment? *Atmospheric Chemistry and Physics*, *12*(20), 9941–9964. https://doi.org/10.5194/acp-12-9941-2012

Lee, S.-K., Atlas, R., Enfield, D., Wang, C., & Liu, H. (2012). Is there an optimal ENSO pattern that enhances large-scale atmospheric processes conducive to tornado outbreaks in the United States? *Journal of Climate*, *26*, 1626–1642.

Lee, S.-K., Wittenberg, A. T., Enfield, D. B., Weaver, S. J., Wang, C., & Atlas, R. (2016). US regional tornado outbreaks and their links to spring ENSO phases and North Atlantic SST variability. *Environmental Research Letters*, *11*(4), 044008. https://doi.org/10.1088/1748-9326/11/4/044008

Lemon, L. R. (1998). The radar "three-body scatter spike": An operational large-hail signature. *Weather and Forecasting*, *13*(2), 327–340. https://doi.org/10.1175/1520-0434(1998)013<0327:TRTBSS>2.0.CO;2

Lepore, C., Tippett, M. K., & Allen, J. T. (2017). ENSO-based probabilistic forecasts of March–May US tornado and hail activity. *Geophysical Research Letters*, *44*, 9093–9101. https://doi.org/10.1002/2017GL074781

Lesins, G. B., & List, R. (1986). Sponginess and drop shedding of gyrating hailstones in a pressure-controlled icing wind tunnel. *Journal of the Atmospheric Sciences*, *43*(23), 2813–2825. https://doi.org/10.1175/1520-0469(1986)043<2813:SADSOG>2.0.CO;2

Li, M., Zhang, Q., & Zhang, F. (2016). Hail day frequency trends and associated atmospheric circulation patterns over China during 1960–2012. *Journal of Climate*, *29*(19), 7027–7044. https://doi.org/10.1175/JCLI-D-15-0500.1

Li, X., Zhang, Q., & Xue, H. (2017). The role of initial cloud condensation nuclei concentration in hail using the wrf nssl 2-moment microphysics scheme. *Advances in Atmospheric Sciences*, *34*(9), 1106–1120. https://doi.org/10.1007/s00376-017-6237-9

Li, X., Zhang, Q., Zhu, T., Li, Z., Lin, J., & Zou, T. (2018). Water-soluble ions in hailstones in northern and southwestern China. *Science Bulletin*, *63*(18), 1177–1179. https://doi.org/10.1016/j.scib.2018.07.021

Li, X., Zhang, Q., Zou, T., Lin, J., Kong, H., & Ren, Z. (2018). Climatology of hail frequency and size in China, 1980–2015. *Journal of Applied Meteorology and Climatology*, *57*(4), 875–887. https://doi.org/10.1175/JAMC-D-17-0208.1

Lindley, T. T., & Lemon, L. R. (2007). Preliminary observations of weak three-body scatter spikes associated with low-end severe hail. *Electronic Journal of Severe Storms Meteorology*, *2*(3), 1–15.

List, R. (1959). Wachstum von eis-wassergemischen im hagelversuchskanal. *Helv. Phys. Acta (in German)*, *32*, 293–296.

List, R., & de Quervain, M. (1953). Zur struktur von hagelkörnern. *Z. Agnew. Math. Phys.*, *4*, 492–496.

List, R., Rentsch, U. W., Byram, E. P., & Lozowski, A. C. (1973). On the aerodynamics of spheroidal hail stone models. *Journal of the Atmospheric Sciences*, *30*, 653–661.

Liu, Q., & Tang, M. (1966). Climatological characteristics of hail in China. *Acta Geographica Sinica*, *32*, 48–65.

Liu, X., & Niu, S. (2010). Numerical simulation of macro-and micro-structures of intense convective clouds with a spectral bin microphysics model. *Advances in Atmospheric Sciences*, *27*(5), 1078–1088. https://doi.org/10.1007/s00376-010-8088-5

Lkhamjav, J., Jin, H.-G., Lee, H., & Baik, J.-J. (2017). A hail climatology in Mongolia. *Asia-Pacific Journal of Atmospheric Sciences*, *53*(4), 501–509.

Loftus, A., & Cotton, W. (2014). Examination of CCN impacts on hail in a simulated supercell storm with triple-moment hail bulk microphysics. *Atmospheric Research*, *147*, 183–204.

Ludlam, F. H. (1958). The hail problem. *Nubila*, *1*, 13–96.

Lukach, M., Foresti, L., Giot, O., & Delobbe, L. (2017). Estimating the occurrence and severity of hail based on 10 years of observations from weather radar in belgium. *Meteorological Applications*, *24*(2), 250–259. https://doi.org/10.1002/met.1623

Macklin, W. (1977). The characteristics of natural hailstones and their interpretation. In *Hail: A Review of Hail Science and Hail Suppression* (pp. 65–91). Boston, MA: American Meteorological Society. https://doi.org/10.1007/978-1-935704-30-0_3

Madonna, E., Ginsbourger, D., & Martius, O. (2018). A poisson regression approach to model monthly hail occurrence in northern Switzerland using large-scale environmental variables. *Atmospheric Research*, *203*, 261–274. https://doi.org/10.1016/j.atmosres.2017.11.024

Mahmood, R., and co authors (2017), Mesonets: Mesoscale weather and climate observations for the United States. *Bulletin of the American Meteorological Society*, *98*, 1349–1361, 7, DOI: https://doi.org/10.1175/BAMS-D-15-00258.1.

Mahoney, K., Alexander, M. A., Thompson, G., Barsugli, J. J., & Scott, J. D. (2012). Changes in hail and flood risk in high-resolution simulations over Colorado's mountains. *Nature Climate Change*, *2*(2), 125–131. https://doi.org/10.1038/nclimate1344

Makitov, V., Inyukhin, V., Kalov, H., & Kalov, R. (2017). Radar research of hailstorm formation and development over the central part of northern Caucasus (Russia). organization and main results of the regional hail suppression projects. *Natural Hazards*, *88*(S1), 253–272. https://doi.org/10.1007/s11069-016-2433-7

Manross, K. L., K. L. Ortega, and A. E. Pietrycha (2010), Examining radar "sidelobe spikes" for severe hail identification, in 25th Conf. on Severe Local Storms, p. P4.12, Amer. Meteor. Soc., Denver, CO.

Manzato, A. (2005). The use of sounding-derived indices for a neural network short-term thunderstorm forecast. *Weather and Forecasting*, *20*(6), 896–917. https://doi.org/10.1175/WAF898.1

Manzato, A. (2012). Hail in northeast Italy: Climatology and bivariate analysis with the sounding-derived indices. *Journal of Applied Meteorology and Climatology*, *51*(3), 449–467. https://doi.org/10.1175/JAMC-D-10-05012.1

Martins, J. A., Brand, V. S., Capucim, M. N., Felix, R. R., Martins, L. D., Freitas, E. D., et al. (2017). Climatology of destructive hailstorms in Brazil. *Atmospheric Research*, *184*(Supplement C), 126–138. https://doi.org/10.1016/j.atmosres.2016.10.012

Martius, O., Hering, A., Kunz, M., Manzato, A., Mohr, S., Nisi, L., & Trefalt, S. (2018). Challenges and recent advances in hail research. *Bulletin of the American Meteorological Society*, *99*(3), ES51–ES54. https://doi.org/10.1175/BAMS-D-17-0207.1

Marwitz, J. D. (1972). The structure and motion of severe hailstorms. Part I: Supercell storms. *Journal of Meteorology*, *11*(1), 166–179. https://doi.org/10.1175/1520-0450(1972)011<0166:TSAMOS>2.0.CO;2

Mather, G., Terblanche, D., Steffens, F., & Fletcher, L. (1997). Results of the South African cloud-seeding experiments using hygroscopic flares. *Journal of Applied Meteorology*, *36*(11), 1433–1447. https://doi.org/10.1175/1520-0450(1997)036<1433:ROTSAC>2.0.CO;2

Matson, R. J., & Huggins, A. W. (1980). The direct measurement of the sizes, shapes and kinematics of falling hailstones. *Journal of the Atmospheric Sciences*, *37*(5), 1107–1125. https://doi.org/10.1175/1520-0469(1980)037<1107:TDMOTS>2.0.CO;2

McCaul, E. W. Jr., & Cohen, C. (2002). The impact on simulated storm structure and intensity of variations in the mixed layer and moist layer depths. *Monthly Weather Review*, *130*(7), 1722–1748. https://doi.org/10.1175/1520-0493(2002)130<1722:TIOSSS>2.0.CO;2

McDonald, J. (1963). The saturation adjustment in numerical modelling of fog. *Journal of the Atmospheric Sciences*, *20*(5), 476–478. https://doi.org/10.1175/1520-0469(1963)020<0476:TSAINM>2.0.CO;2

McGovern, A., Elmore, K. L., Gagne, D. J., Haupt, S. E., Karstens, C. D., Lagerquist, R., et al. (2017). Using artificial intelligence to improve real-time decision-making for high-impact weather. *Bulletin of the American Meteorological Society*, *98*(10), 2073–2090. https://doi.org/10.1175/BAMS-D-16-0123.1

McMaster, H. (2001). Hailstorm risk assessment in rural New South Wales. *Natural Hazards*, *24*(2), 187–196. https://doi.org/10.1023/A:1011820206279

Melcón, P., Merino, A., Sánchez, J. L., López, L., & Hermida, L. (2016). Satellite remote sensing of hailstorms in France. *Atmospheric Research*, *182*, 221–231. https://doi.org/10.1016/j.atmosres.2016.08.001

Melnikov, V. M., Lee, R. R., & Langlieb, N. J. (2010). Hail reflectivity signatures from two adjacent WSR-88Ds: Carrier frequency and calibration issues, in 26th Conf. on Interactive Information and Processing Systems for Meteorology, Oceanography, and Hydrology, p. 8.5, Amer. Meteor. Soc., Atlanta, GA.

Melnikov, V. M., Zrnić, D. S., Burgess, D., & Mansell, E. (2014). Observations of hail cores of tornadic thunderstorms with three polarimetric radars, in 30th Conf. on Environmental Information Processing Techniques, 11, Amer. Meteor. Soc., Atlanta, GA.

Merino, A., López, L., Sánchez, J., García-Ortega, E., Cattani, E., & Levizzani, V. (2014). Daytime identification of summer hailstorm cells from MSG data. *Natural Hazards and Earth System Sciences*, *14*(4), 1017–1033. https://doi.org/10.5194/nhess-14-1017-2014

Merino, A., Wu, X., Gascón, E., Berthet, C., García-Ortega, E., & Dessens, J. (2014). Hailstorms in southwestern France: Incidence and atmospheric characterization. *Atmospheric Research*, *140*, 61–75.

Mezher, R. N., Doyle, M., & Barros, V. (2012). Climatology of hail in Argentina. *Atmospheric Research*, *114*, 70–82.

Michaelides, S., Karacostas, T., Sánchez, J. L., Retalis, A., Pytharoulis, I., Homar, V., et al. et al. (2018). Reviews and perspectives of high impact atmospheric processes in the Mediterranean. *Atmospheric Research*, *208*, 4–44. https://doi.org/10.1016/j.atmosres.2017.11.022

Miglietta, M. M., Mazon, J., Motola, V., & Pasini, A. (2017). Effect of a positive sea surface temperature anomaly on a Mediterranean tornadic supercell. *Scientific Reports*, *7*(1), 12828. https://doi.org/10.1038/s41598-017-13170-0

Miller, L. J., & Fankhauser, J. C. (1983). Radar echo structure, air motion and hail formation in a large stationary multicellular thunderstorm. *Journal of the Atmospheric Sciences*, *40*(10), 2399–2418. https://doi.org/10.1175/1520-0469(1983)040<2399:RESAMA>2.0.CO;2

Miller, R. C. (1972). Notes on analysis and severe-storm forecasting procedures of the Air Force Global Weather Central (Tech. Rep.). Air Weather Service (MAC), United States Air Force, Scott Air Force Base, Illinois, USA. 190 pp.

Millikan, C. B., & Klein, A. L. (1933). The effect of turbulence: An investigation of maximum lift coefficient and turbulence in flight. *Aircraft Engineering*, *5*(8), 169–174. https://doi.org/10.1108/eb029703

Mills, G., & Colquhoun, J. (1998). Objective prediction of severe thunderstorm environments: Preliminary results linking a decision tree with an operational regional NWP model. *Weather and Forecasting*, *13*(4), 1078–1092. https://doi.org/10.1175/1520-0434(1998)013<1078:OPOSTE>2.0.CO;2

Mohr, S., & Kunz, M. (2013). Recent trends and variabilities of convective parameters relevant for hail events in Germany and Europe. *Atmospheric Research*, *123*, 211–228. https://doi.org/10.1016/j.atmosres.2012.05.016

Mohr, S., Kunz, M., & Geyer, B. (2015). Hail potential in Europe based on a regional climate model hindcast. *Geophysical Research Letters*, *42*, 10,904–10,912. https://doi.org/10.1002/2015GL067118

Mohr, S., Kunz, M., & Keuler, K. (2015). Development and application of a logistic model to estimate the past and future hail potential in Germany. *Journal of Geophysical: Research*, *120*, 3939–3956.

Molina, M. J., Timmer, R. P., & Allen, J. T. (2016). Importance of the Gulf of Mexico as a climate driver for U.S. severe thunderstorm activity. *Geophysical Research Letters*, *43*, 12,295–12,304. https://doi.org/10.1002/2016GL071603

Moore, J. T., & Pino, J. P. (1990). An interactive method for estimating maximum hailstone size from forecast soundings. *Weather and Forecasting*, *5*(3), 508–525. https://doi.org/10.1175/1520-0434(1990)005<0508:AIMFEM>2.0.CO;2

Morgan, G. M. (1972). On the growth of large hail. *Monthly Weather Review*, *100*(3), 196–205. https://doi.org/10.1175/1520-0493(1972)100<0196:OTGOLH>2.3.CO;2

Morgan, G. M. (1973). A General Description of the Hail Problem in the Po Valley of Northern Italy. *Journal of Applied Meteorology*, *12*(2), 338–353. https://doi.org/10.1175/1520-0450(1973)012<0338:AGDOTH>2.0.CO;2

Morrison, H. C. (2016a). Impacts of updraft size and dimensionality on the perturbation pressure and vertical velocity in cumulus convection. Part I: Simple, generalized analytic solutions. *Journal of the Atmospheric Sciences*, *73*(4), 1441–1454. https://doi.org/10.1175/JAS-D-15-0040.1

Morrison, H. C. (2016b). Impacts of updraft size and dimensionality on the perturbation pressure and vertical velocity in cumulus convection. Part II: Comparison of theoretical and numerical solutions and fully dynamical simulations. *Journal of the Atmospheric Sciences*, *73*(4), 1455–1480. https://doi.org/10.1175/JAS-D-15-0041.1

Morrison, S. J. (1999). Long-term effects of hail impact on asphalt shingles—An interim report. In *North American Conference on Roofing Technology, 16-17 Sept. 1999* (pp. 30–39). Toronto, Ontario, Canada: National Roofing Contractors Association.

Mroz, K., Battaglia, A., Lang, T. J., Cecil, D. J., Tanelli, S., & Tridon, F. (2017). Hail-detection algorithm for the GPM core observatory satellite sensors. *Journal of Applied Meteorology and Climatology*, *56*(7), 1939–1957. https://doi.org/10.1175/JAMC-D-16-0368.1

Munich R. E. (2017). *TOPICS Geo Natural Catastrophes 2017*, Munich RE.

Murillo, E. M., & Homeyer, C. R. (2019). Severe hail fall and hailstorm detection using remote sensing observations. *Journal of Applied Meteorology and Climatology*, *58*(5), 947–970. https://doi.org/10.1175/JAMC-D-18-0247.1

Musil, D. J., Heymsfield, A. J., & Smith, P. L. (1986). Microphysical characteristics of a well-developed weak echo region in a High Plains supercell thunderstorm. *Journal of Climate and Applied Meteorology*, *25*(7), 1037–1051. https://doi.org/10.1175/1520-0450(1986)025<1037:MCOAWD>2.0.CO;2

Nelson, S. P. (1983). The influence of storm flow structure on hail growth. *Journal of the Atmospheric Sciences*, *40*(8), 1965–1983. https://doi.org/10.1175/1520-0469(1983)040<1965:TIOSFS>2.0.CO;2

Ni, X., Liu, C., Cecil, D. J., & Zhang, Q. (2017). On the detection of hail using satellite passive microwave radiometers and precipitation radar. *Journal of Applied Meteorology and Climatology*, *56*(10), 2693–2709. https://doi.org/10.1175/JAMC-D-17-0065.1

Ni, X., Zhang, Q., Liu, C., Li, X., Zou, T., Lin, J., et al. (2017). Decreased hail size in China since 1980. *Scientific Reports*, *7*(1), 10913. https://doi.org/10.1038/s41598-017-11395-7

Niall, S., & Walsh, K. (2005). The impact of climate change on hailstorms in southeastern Australia. *International Journal of Climatology*, *25*(14), 1933–1952. https://doi.org/10.1002/joc.1233

Nisi, L., Martius, O., Hering, A., Kunz, M., & Germann, U. (2016). Spatial and temporal distribution of hailstorms in the Alpine region: A long-term, high resolution, radar-based analysis. *Quarterly Journal of the Royal Meteorological Society*, *697*, 1590–1604.

Nizamuddin, S. (1993). Hail occurrences in India. *Weather*, *48*(3), 90–92. https://doi.org/10.1002/j.1477-8696.1993.tb05847.x

Noll, S., Elmore, K. L., & Kingfield, D. M. (2018). General hail occurrence frequency in convective storms using mPING data, in *19th Sym. on Meteorol. Observation and Instrumentation, Austin, TX, Amer. Meteor. Soc*. Boston, MA; American Meteorology Society.

Noon, R. K. (2000). *Forensic engineering investigation*, (p. 488). Boca Raton, Florida: CRC Press. https://doi.org/10.1201/9781420041415

Noppel, H., Blahak, U., Seifert, A., & Beheng, K. D. (2010). Simulations of a hailstorm and the impact of ccn using an advanced two-moment cloud microphysical scheme. *Atmospheric Research*, *96*(2), 286–301.

Ortega, K. L. (2015). A radar-based storm climatology for the contiguous United States for improved severe weather climatologies and warnings, in 31st Conf. on Environmental Interactive Processing Systems, Phoenix, AZ. Boston, MA: American Meteorological Society.

Ortega, K. L. (2018). Evaluating multi-radar, multi-sensor products for surface hailfall diagnosis. *Electronic Journal of Severe Storms Meteorology*, *13*(1), 1–36.

Ortega, K. L., Krause, J. M., & Ryzhkov, A. V. (2016). Polarimetric radar characteristics of melting hail. Part III: Validation of the algorithm for hail size discrimination. *Journal of Applied Meteorology and Climatology*, *55*, 829–848.

Ortega, K. L., Smith, T. M., Manross, K. L., Scharfenberg, K. A., Witt, A., Kolodziej, A. G., & Gourley, J. J. (2009). The severe hazards analysis and verification experiment. *Bulletin of the American Meteorological Society*, *90*(10), 1519–1530. https://doi.org/10.1175/2009BAMS2815.1

Picca, J. C., & Ryzhkov, A. V. (2012). A dual-wavelength polarimetric analysis of the 16 May 2010 Oklahoma City extreme hailstorm. *Monthly Weather Review*, *140*(4), 1385–1403. https://doi.org/10.1175/MWR-D-11-00112.1

Piper, D., & Kunz, M. (2017). Spatiotemporal variability of lightning activity in Europe and the relation to the North Atlantic Oscillation teleconnection pattern. *Natural Hazards and Earth System Sciences*, *17*(8), 1319–1336. https://doi.org/10.5194/nhess-17-1319-2017

Pocakal, D. (2011). Hailpad data analysis for the continental part of Croatia. *Meteorologische Zeitschrift*, *20*(4), 441–447. https://doi.org/10.1127/0941-2948/2011/0263

Prein, A. F., & Holland, G. J. (2018). Global estimates of damaging hail hazard. *Weather and Climate Extremes*, *22*, 10–23. https://doi.org/10.1016/j.wace.2018.10.004

Prohaska, K. (1902). Über Gewitter und Hagelschläge in Steiermark, Kärnten und Oberkrain. *Mitteilungen des Naturwissenschaftlichen Vereins für Steiermark*, *38*, 49–84, [in German].

Pruppacher, H. R., & Klett, J. D. (1997). *Microphysics of clouds and precipitation* (2nd ed., p. 954). Springer: Was Kluwer Academic Publishers.

Púčik, T., Groenemeijer, P., Rädler, A. T., Tijssen, L., Nikulin, G., Prein, A. F., et al. (2017). Future changes in European severe convection environments in a regional climate model ensemble. *Journal of Climate*, *30*(17), 6771–6794. https://doi.org/10.1175/JCLI-D-16-0777.1

Púčik, T., Groenemeijer, P., Róva, D., & Kolář, M. (2015). Proximity soundings of severe and non-severe thunderstorms in central Europe. *Monthly Weather Review*, *143*(12), 4805–4821. https://doi.org/10.1175/MWR-D-15-0104.1

Punge, H., & Kunz, M. (2016). Hail observations and hailstorm characteristics in Europe: A review. *Atmospheric Research*, *176*, 159–184.

Punge, H. J., Bedka, K. M., Kunz, M., & Reinbold, A. (2017). Hail frequency estimation across Europe based on a combination of overshooting top detections and the ERA-INTERIM reanalysis. *Atmospheric Research*, *198*, 34–43. https://doi.org/10.1016/j.atmosres.2017.07.025

Punge, H. J., Bedka, K. M., Kunz, M., & Werner, A. (2014). A new physically based stochastic event catalog for hail in Europe. *Natural Hazards*, *73*(3), 1625–1645. https://doi.org/10.1007/s11069-014-1161-0

Puskeiler, M., Kunz, M., & Schmidberger, M. (2016). Hail statistics for Germany derived from single-polarization radar data. *Atmospheric Research*, *178-179*(Supplement C), 459–470. https://doi.org/10.1016/j.atmosres.2016.04.014

Pyle, D. M. (2006). Severe convective storm risk in the eastern Cape Province of South Africa (PhD thesis). Grahamstown, South Africa: Rhodes University.

Rädler, A. T., Groenemeijer, P., Faust, E., & Sausen, R. (2018). Detecting severe weather trends using an additive regressive convective hazard model (ARCHAMO). *Journal of Applied Meteorology and Climatology*, *57*(3), 569–587. https://doi.org/10.1175/JAMC-D-17-0132.1

Rasmussen, E. N., & Blanchard, D. O. (1998). A baseline climatology of sounding-derived supercell and tornado forecast parameters. *Weather and Forecasting*, *13*(4), 1148–1164. https://doi.org/10.1175/1520-0434(1998)013<1148:ABCOSD>2.0.CO;2

Rasmussen, E. N., & Straka, J. M. (1998). Variations in supercell morphology. Part I: Observations of the role of upper-level storm-relative flow. *Monthly Weather Review*, *126*(9), 2406–2421. https://doi.org/10.1175/1520-0493(1998)126<2406:VISMPI>2.0.CO;2

Rasmussen, K. L., Zuluaga, M. D., & Houze, R. A. (2014). Severe convection and lightning in subtropical South America. *Geophysical Research Letters*, *41*, 7359–7366. https://doi.org/10.1002/2014GL061767

Rasmussen, R. M., & Heymsfield, A. J. (1987a). Melting and shedding of graupel and hail. Part I: Model physics. *Journal of the Atmospheric Sciences*, *44*(19), 2754–2763. https://doi.org/10.1175/1520-0469(1987)044<2754:MASOGA>2.0.CO;2

Rasmussen, R. M., & Heymsfield, A. J. (1987b). Melting and shedding of graupel and hail. Part II: Sensitivity study. *Journal of the Atmospheric Sciences*, *44*(19), 2764–2782. https://doi.org/10.1175/1520-0469(1987)044<2764:MASOGA>2.0.CO;2

Reges, H. W., Doesken, N., Turner, J., Newman, N., Bergantino, A., & Schwalbe, Z. (2016). CoCoRaHS: The evolution and accomplishments of a volunteer rain gauge network. *Bulletin of the American Meteorological Society*, *97*(10), 1831–1846. https://doi.org/10.1175/BAMS-D-14-00213.1

Rinehart, R. E., & Tuttle, J. D. (1982). Antenna beam patterns and dual-wavelength processing. *Journal of Applied Meteorology*, *21*(12), 1865–1880. https://doi.org/10.1175/1520-0450(1982)021<1865:ABPADW>2.0.CO;2

Robinson, E. D., Trapp, R. J., & Baldwin, M. E. (2013). The geospatial and temporal distributions of severe thunderstorms from high-resolution dynamical downscaling. *Journal of Applied Meteorology and Climatology*, *52*(9), 2147–2161. https://doi.org/10.1175/JAMC-D-12-0131.1

Romppainen-Martius, O., Kunz, M., Nisi, L. D., & Hering, A. (2015). Conference report 1st European Hail Workshop. *Meteorologische Zeitschrift*, *24*(4), 441–442. https://doi.org/10.1127/metz/2015/0667

Rosenfeld, D., Lohmann, U., Raga, G. B., O'Dowd, C. D., Kulmala, M., Fuzzi, S., et al. (2008). Flood or drought: How do aerosols affect precipitation? *Science*, *321*(5894), 1309–1313. https://doi.org/10.1126/science.1160606

Rosseau, D., Ortega, K. L., Reinhart, A. E., & Obermeier, H. (2017). A multi-radar, multi-sensor-based hail climatology for the conus: 2000-2011, in *Special Symposium on Severe Local Storms,* Seattle, WA, Amer. Meteor. Soc.

Russell, H. (1893). Hail storms. *Nature*, *47*, 573–574.

Ryzhkov, A. V., Kumjian, M. R., Ganson, S. M., & Khain, A. P. (2013). Polarimetric radar characteristics of melting hail. Part I: Theoretical simulations using spectral microphysical modeling. *Journal of Applied Meteorology and Climatology*, *52*(12), 2849–2870. https://doi.org/10.1175/JAMC-D-13-073.1

Ryzhkov, A. V., Kumjian, M. R., Ganson, S. M., & Zhang, P. (2013). Polarimetric radar characteristics of melting hail. Part II: Practical implications. *Journal of Applied Meteorology and Climatology*, *52*(12), 2871–2886. https://doi.org/10.1175/JAMC-D-13-074.1

Samenow, J. (2015). Corn stalk encased in ice hailed down from tornado-producing Texas thunderstorm. Washington DC: The Washington Post.

Sánchez, J., Fraile, R., De La Madrid, J., De La Fuente, M., Rodríguez, P., & Castro, A. (1996). Crop damage: The hail size factor. *Journal of Applied Meteorology*, *35*(9), 1535–1541. https://doi.org/10.1175/1520-0450(1996)035<1535:CDTHSF>2.0.CO;2

Sanchez, J., Merino, A., Melcón, P., García-Ortega, E., Fernández-González, S., Berthet, C., & Dessens, J. (2017). Are meteorological conditions favoring hail precipitation change in Southern Europe? Analysis of the period 1948–2015. *Atmospheric Research*, *198*, 1–10. https://doi.org/10.1016/j.atmosres.2017.08.003

Sánchez, J. L., Gil-Robles, B., Dessens, J., Martin, E., Lopez, L., Marcos, J. L., et al. (2009). Characterization of hailstone size spectra in hailpad networks in France, Spain, and Argentina. *Atmospheric Research*, *93*, 641–654.

Sánchez, J. L., J. L. Marcos, J. Dessens, L. López, C. Bustos, and E. García-Ortega (2009), Assessing sounding-derived parameters as storm predictors in different latitudes. *Atmospheric Research*, *93*(1-3), 446–456, DOI: https://doi.org/10.1016/j.atmosres.2008.11.006.

Sand, W., & Schleusener, R. (1974). Development of an armored T-28 aircraft for probing hailstorms. *Bulletin of the American Meteorological Society*, *55*(9), 1115–1122. https://doi.org/10.1175/1520-0477(1974)055<1115:DOAATA>2.0.CO;2

Sand, W. R. (1976). Observations in hailstorms using the T-28 aircraft system. *Journal of Applied Meteorology*, *15*(6), 641–650. https://doi.org/10.1175/1520-0450(1976)015<0641:OIHUTT>2.0.CO;2

Sander, J., Eichner, J., Faust, E., & Steuer, M. (2013). Rising variability in thunderstorm-related US losses as a reflection of changes in large-scale thunderstorm forcing. *Weather and Climate Extremes*, *5*(4), 317–331. https://doi.org/10.1175/WCAS-D-12-00023.1

Sanderson, M. G., Hand, W. H., Groenemeijer, P., Boorman, P. M., Webb, J. D. C., & McColl, L. J. (2015). Projected changes in hailstorms during the 21st century over the UK. *International Journal of Climatology*, *35*(1), 15–24. https://doi.org/10.1002/joc.3958

Sansom, H. (1966). The use of explosive rockets to suppress hail in Kenya. *Weather*, *21*(3), 86–91. https://doi.org/10.1002/j.1477-8696.1966.tb05193.x

Schaefer, J. T., & Edwards, R. (1999). The SPC Tornado/Severe Thunderstorm Database. In *Preprints, 11th Conf. Applied Climatology*, (pp. 215–220). Dallas, TX: Amer. Meteor. Soc.

Schemm, S., Nisi, L., Martinov, A., Leuenberger, D., & Martius, O. (2016). On the link between cold fronts and hail in Switzerland. *Atmospheric Science Letters*, *17*(5), 315–325. https://doi.org/10.1002/asl.660

Schemm, S., Rudeva, I., & Simmonds, I. (2014). Extratropical fronts in the lower troposphere–global perspectives obtained from two automated methods. *Quarterly Journal of the Royal Meteorological Society*, *141*, 1686–1698.

Schmid, P., et al. (1967). On "Grossversuch III", a randomized hail suppression experiment in Switzerland, in *Proceedings of the Fifth Berkeley Symposium on Mathematical Statistics and Probability, Volume 5: Weather Modification*. University of California Press Berkeley and Los Angeles, CA.

Schroeder, J. L., Burgett, W. S., Haynie, K. B., Sonmez, I., Skwira, G. D., Doggett, A. L., & Lipe, J. W. (2005). The west Texas mesonet: A technical review. *Journal of Atmospheric and Oceanic Technology*, *22*(2), 211–222. https://doi.org/10.1175/JTECH-1690.1

Schulson, E. M., & Duval, P. (2009). *Creep and fracture of ice* (p. 416). Cambridge, UK: Cambridge University Press.

Schumann, T. (1938). The theory of hailstone formation. *Quarterly Journal of the Royal Meteorological Society*, *64*, 3–21.

Schuster, S., Blong, R., Leigh, R., & McAneney, K. (2005). Characteristics of the 14 April 1999 Sydney hailstorm based on ground observations, weather radar, insurance data and emergency calls. *Natural Hazards and Earth System Sciences*, *5*(5), 613–620. https://doi.org/10.5194/nhess-5-613-2005

Schuster, S. S., Blong, R. J., & McAneney, K. J. (2006). Relationship between radar-derived hail kinetic energy and damage to insured buildings for severe hailstorms in Eastern Australia. *Atmospheric Research*, *81*(3), 215–235. https://doi.org/10.1016/j.atmosres.2005.12.003

Schuster, S. S., Blong, R. J., & Speer, M. S. (2005). A hail climatology of the greater Sydney area and New South Wales, Australia. *International Journal of Climatology*, *25*(12), 1633–1650. https://doi.org/10.1002/joc.1199

Seimon, A., Allen, J. T., Seimon, T. A., Talbot, S. J., & Hoadley, D. K. (2016). Crowdsourcing the El Reno 2013 tornado: A new approach for collation and display of storm chaser imagery for scientific applications. *Bulletin of the American Meteorological Society*, *97*(11), 2069–2084. https://doi.org/10.1175/BAMS-D-15-00174.1

Silva, V. Q. (2011), Design of protective covers against natural hazards, Master's thesis. Auburn, AL: Auburn University.

Simeonov, P. (1996). An overview of crop hail damage and evaluation of hail suppression efficiency in Bulgaria. *Journal of Applied Meteorology*, *35*(9), 1574–1581. https://doi.org/10.1175/1520-0450(1996)035<1574:AOOCHD>2.0.CO;2

Skripniková, K., & Řezáčová, D. (2014). Radar-based hail detection. *Atmospheric Research*, *144*, 175–185. https://doi.org/10.1016/j.atmosres.2013.06.002

Smith, B. T., Thompson, R. L., Grams, J. S., Broyles, C., & Brooks, H. E. (2012). Convective modes for significant severe thunderstorms in the contiguous United States. Part I: Storm classification and climatology. *Weather and Forecasting*, *27*(5), 1114–1135. https://doi.org/10.1175/WAF-D-11-00115.1

Smith, T. M., Lakshmanan, V., Stumpf, G. J., Ortega, K. L., Hondl, K., Cooper, K., et al. (2016). Multi-radar multi-sensor (MRMS) severe weather and aviation products: Initial operating capabilities. *Bulletin of the American Meteorological Society*, *97*(9), 1617–1630. https://doi.org/10.1175/BAMS-D-14-00173.1

Soderholm, J., McGowan, H., Richter, H., Walsh, K., Weckwerth, T., & Coleman, M. (2016). The coastal convective interactions experiment (CCIE): Understanding the role of sea breezes for hailstorm hotspots in eastern Australia. *Bulletin of the American Meteorological Society*, *97*(9), 1687–1698. https://doi.org/10.1175/BAMS-D-14-00212.1

Soderholm, J., McGowan, H., Richter, H., Walsh, K., Weckwerth, T., & Coleman, M. (2017a). An 18-year climatology of hailstorm trends and related drivers across southeast Queensland, Australia, *Quart*. *Journal of the Royal Meteorological Society*, *143*(703), 1123–1135. https://doi.org/10.1002/qj.2995

Soderholm, J. S., McGowan, H. A., Richter, H., Walsh, K., Wedd, T., & Weckwerth, T. M. (2017b). Diurnal preconditioning of subtropical coastal convective storm environments. *Monthly Weather Review*, *145*(9), 3839–3859. https://doi.org/10.1175/MWR-D-16-0330.1

Souter, R. K., and J. B. Emerson (1952), Summary of available hail literature and the effect of hail on aircraft in flight, *Tech. rep*., NATIONAL AERONAUTICS AND SPACE ADMINISTRATION WASHINGTON DC.

Squires, P., & Knight, C. A. (1982). *Hailstorms of the Central High Plains: Case studies of the National Hail Research Experiment* (Vol. 2). Colorado: University Press of.

Strader, S. M., Ashley, W. S., Pingel, T. J., & Krmenec, A. J. (2017). Observed and projected changes in United States tornado exposure. *Weather and Climate Extremes*, *9*(2), 109–123. https://doi.org/10.1175/WCAS-D-16-0041.1

Stržinar, G., & Skok, G. (2018). Comparison and optimization of radar-based hail detection algorithms in Slovenia. *Atmospheric Research*, *203*, 275–285. https://doi.org/10.1016/j.atmosres.2018.01.005

Suwala, K., & Bednorz, E. (2013). Climatology of hail in central Europe. *Quaestiones Geographicae*, *32*(3), 99–110. https://doi.org/10.2478/quageo-2013-0025

Svabik, O. (1989). Review of meteorological aspects on hail defense activities in Austria. *Theoretical and Applied Climatology*, *40*(4), 247–254. https://doi.org/10.1007/BF00865975

Svabik, O., Meyer, V., Tüchler, L., & Zenkl, G. (2013). *Hail risk areas in Austria, on the basis of reports 1971–2011 and weather radar images 2002–2011, in* 7th European Conference on Severe Storms, (p. 2). Finland: Helsinki.

Swift, J. M. (2013). Simulated hail ice mechanical properties and failure mechanisms at quasi-static strain rates, Master's thesis. Seattle, Washington: University of Washington.

Taszarek, M., Allen, J., Púčik, T., Groenemeijer, P., Czernecki, B., Kolendowicz, L., et al. (2019). A climatology of thunderstorms across Europe from a synthesis of multiple data sources. *Journal of Climate*, *32*(6), 1813–1837. https://doi.org/10.1175/JCLI-D-18-0372.1

Tessendorf, S. A., Miller, L. J., Wiens, K. C., & Rutledge, S. A. (2005). The 29 June 2000 supercell observed during STEPS. Part I: Kinematics and microphysics. *Journal of the Atmospheric Sciences*, *62*(12), 4127–4150. https://doi.org/10.1175/JAS3585.1

Thams, J. C. (1966). *Die Ergebnisse des Großversuches III zur Bekämpfung des Hagels im Tessin in den Jahren 1957-1963*, na.

Thompson, R. L., Edwards, R., Hart, J. A., Elmore, K. L., & Markowski, P. (2003). Close proximity soundings within supercell environments obtained from the Rapid Update Cycle. *Weather and Forecasting*, *18*(6), 1243–1261. https://doi.org/10.1175/1520-0434(2003)018<1243:CPSWSE>2.0.CO;2

Tippett, M. K. (2018). Robustness of relations between the MJO and US tornado occurrence. *Monthly Weather Review*, *2018*.

Tippett, M. K., Allen, J. T., Gensini, V. A., & Brooks, H. E. (2015). Climate and hazardous convective weather. *Current Climate Change Report*, *1*(2), 60–73. https://doi.org/10.1007/s40641-015-0006-6

Trapp, R. J., & Hoogewind, K. A. (2016). The realization of extreme tornadic storm events under future anthropogenic climate change. *Journal Climate*, *29*(14), 5251–5265. https://doi.org/10.1175/JCLI-D-15-0623.1

Trapp, R. J., Hoogewind, K. A., & Lasher-Trapp, S. (2019). Future changes in hail occurrence in the United States determined through convection-permitting dynamical downscaling. *Journal of Climate*, *2019*.

Tuovinen, J., Punkka, A., Rauhala, J., Hohti, H., & Schultz, D. M. (2009). Climatology of severe hail in Finland: 1930-2006. *Monthly Weather Review*, *137*(7), 2238–2249. https://doi.org/10.1175/2008MWR2707.1

Tuovinen, J.-P., Rauhala, J., & Schultz, D. M. (2015). Significant-hail-producing storms in Finland: Convective-storm environment and mode. *Weather and Forecasting*, *30*(4), 1064–1076. https://doi.org/10.1175/WAF-D-14-00159.1

Tuttle, J. D., Bringi, V. N., Orville, H. D., & Kopp, F. J. (1989). Multiparameter radar study of a microburst: Comparison with model results. *Journal of the Atmospheric Sciences*, *46*(5), 601–620. https://doi.org/10.1175/1520-0469(1989)046<0601:MRSOAM>2.0.CO;2

Tuttle, J. D., & Rinehart, R. E. (1983). Attenuation correction in dual-wavelength analyses. *Journal of Climate and Applied Meteorology*, *22*(11), 1914–1921. https://doi.org/10.1175/1520-0450(1983)022<1914:ACIDWA>2.0.CO;2

Underwriters Laboratory (2012). UL2218: Standard for impact resistance of prepared roof covering materials, *Tech. rep*, Underwritter Laboratory, Northbrook, Illinois.

Vali, G., DeMott, P., Möhler, O., & Whale, T. (2015). Technical note: A proposal for ice nucleation terminology. *Atmospheric Chemistry and Physics*, *15*(18), 10–263.

Vinet, F. (2001). Climatology of hail in France. *Atmospheric Research*, *56*(1-4), 309–323. https://doi.org/10.1016/S0169-8095(00)00082-X

Waldvogel, A., Federer, B., Schmid, W., & Mezeix, J. (1978). The kinetic energy of hailfalls. Part II: Radar and hailpads. *Journal of Applied Meteorology*, *17*(11), 1680–1693. https://doi.org/10.1175/1520-0450(1978)017<1680:TKEOHP>2.0.CO;2

Wapler, K., Hengstebeck, T., & Groenemeijer, P. (2016). Mesocyclones in central Europe as seen by radar. *Atmospheric Research*, *168*, 112–120. https://doi.org/10.1016/j.atmosres.2015.08.023

Weaver, S. J., Baxter, S., & Kumar, A. (2012). Climatic role of North American low-level jets on U.S. regional tornado activity. *Journal of Climate*, *25*(19), 6666–6683. https://doi.org/10.1175/JCLI-D-11-00568.1

Weickmann, H. (1953). Observational data on the formation of precipitation in cumulonimbus clouds. In *Thunderstorm Electricity* (pp. 66–138). Chicago, IL: University of Chicago Press.

Weisman, M. L., & Klemp, J. B. (1982). The dependence of numerically simulated convective storms on vertical wind shear and buoyancy. *Monthly Weather Review*, *110*(6), 504–520. https://doi.org/10.1175/1520-0493(1982)110<0504:TDONSC>2.0.CO;2

Wieringa, J., & Holleman, I. (2006). If cannons cannot fight hail, what else? *Meteorologische Zeitschrift*, *15*(6), 659–669. https://doi.org/10.1127/0941-2948/2006/0147

Willis, J. T., Browning, K. A., & Atlas, D. (1967). Wind tunnel tests of simulated spherical hailstones with variable roughness. *Journal of Atmospheric Science*, *24*, 58–62.

Wilson, J. W., & Reum, D. (1988). The flare echo: Reflectivity and velocity signature. *Journal of Atmospheric and Oceanic Technology*, *5*(2), 197–205. https://doi.org/10.1175/1520-0426(1988)005<0197:TFERAV>2.0.CO;2

Witt, A., Burgess, D. W., Seimon, A., Allen, J. T., Snyder, J. C., & Bluestein, H. B. (2018). Rapid-scan radar observations of an Oklahoma tornadic hailstorm producing giant hail. *Weather and Forecasting*, *33*(5), 1263–1282. https://doi.org/10.1175/WAF-D-18-0003.1

Witt, A., Eilts, N. D., Stumpf, G. J., Johnson, J. T., Mitchell, E. D., & Thomas, K. W. (1998). An enhanced hail detection algorithm for the WSR-88D. *Weather and Forecasting*, *13*(2), 286–303. https://doi.org/10.1175/1520-0434(1998)013<0286:AEHDAF>2.0.CO;2

Witt, A., & Nelson, S. P. (1991). The use of single-Doppler radar for estimating maximum hailstone size. *Journal of Applied Meteorology*, *30*(4), 425–431. https://doi.org/10.1175/1520-0450(1991)030<0425:TUOSDR>2.0.CO;2

Xie, B., Zhang, Q., & Wang, Y. (2008). Trends in hail in China during 1960–2005. *Geophysical Research Letters*, *35*, L13801. https://doi.org/10.1029/2008GL034067

Xu, J.-L. (1983). Some hail research in China. *Bulletin of the American Meteorological Society*, *64*(2), 124–132. https://doi.org/10.1175/1520-0477(1983)064<0124:SHRIC>2.0.CO;2

Yamane, Y., Hayashi, T., Dewan, A. M., & Akter, F. (2010). Severe local convective storms in Bangladesh: Part I. Climatology. *Atmospheric Research*, *95*(4), 400–406.

Yang, H.-L., Xiao, H., & Hong, Y.-C. (2011). A numerical study of aerosol effects on cloud microphysical processes of hailstorm clouds. *Atmospheric Research*, *102*(4), 432–443. https://doi.org/10.1016/j.atmosres.2011.09.007

Yeo, C. S. (2005). Severe thunderstorms in the brisbane region and a relationship to the El Niño Southern Oscillation. *Australian Meteorological Magazine*, *54*(3), 197.

Yeo, S., Leigh, R., Kuhne, I., et al. (1999). The April 1999 Sydney hailstorm. *Australian Journal of Emergency Management, The*, *14*(4), 23.

Zhang, C., Zhang, Q., & Wang, Y. (2008). Climatology of hail in China: 1961–2005. *Journal of Applied Meteorology and Climatology*, *47*(3), 795–804. https://doi.org/10.1175/2007JAMC1603.1

Zhang, Q., Ni, X., & Zhang, F. (2017). Decreasing trend in severe weather occurrence over China during the past 50 years. *Scientific Reports*, *7*(1), 42,310. https://doi.org/10.1038/srep42310

Ziegler, C. L., Ray, P. S., & Knight, N. C. (1983). Hail growth in an Oklahoma multicell storm. *Journal of the Atmospheric Sciences*, *40*(7), 1768–1791. https://doi.org/10.1175/1520-0469(1983)040<1768:HGIAOM>2.0.CO;2

Zrnić, D. S. (1987). Three-body scattering produces precipitation signature of special diagnostic value. *Radio Science*, *22*(1), 76–86. https://doi.org/10.1029/RS022i001p00076

Zrnić, D. S., Zhang, G., Melnikov, V., & Andrić, J. (2010). Three-body scattering and hail size. *Journal of Applied Meteorology and Climatology*, *49*(4), 687–700. https://doi.org/10.1175/2009JAMC2300.1